Titre: Title:	3D Stochastic Inversion and Joint Inversion of Potential Fields for Multi Scale Parameters
Auteur: Author:	Pejman Shamsipour
Date:	2011
Type:	Mémoire ou thèse / Dissertation or Thesis
Référence: Citation:	Shamsipour, P. (2011). 3D Stochastic Inversion and Joint Inversion of Potential Fields for Multi Scale Parameters [Thèse de doctorat, École Polytechnique de Montréal]. PolyPublie. https://publications.polymtl.ca/657/

UNIVERSITÉ DE MONTRÉAL

3D STOCHASTIC INVERSION AND JOINT INVERSION OF POTENTIAL FIELDS FOR MULTI SCALE PARAMETERS

PEJMAN SHAMSIPOUR
DÉPARTEMENT DES GÉNIES CIVIL, GÉOLOGIQUE ET DES MINES
ÉCOLE POLYTECHNIQUE DE MONTRÉAL

THÈSE PRÉSENTÉE EN VUE DE L'OBTENTION
DU DIPLÔME DE PHILOSOPHIÆ DOCTOR
(GÉNIE MINÉRAL)
AOÛT 2011

UNIVERSITÉ DE MONTRÉAL

ÉCOLE POLYTECHNIQUE DE MONTRÉAL

Cette thèse intitulée :

3D STOCHASTIC INVERSION AND JOINT INVERSION OF POTENTIAL FIELDS FOR MULTI SCALE PARAMETERS

présentée par : SHAMSIPOUR Pejman

en vue de l'obtention du diplôme de : Philosophiæ Doctor

a été dûment acceptée par le jury d'examen constitué de :

M. JI Shaocheng, Ph.D., président

M. CHOUTEAU Michel, Ph.D., membre et directeur de recherche

M. MARCOTTE Denis, Ph.D., membre et codirecteur de recherche

M. MARESCHAL Jean-Claude, Ph.D., membre

M. FARQUHARSON Colin, Ph.D., membre

To Farnaz

ACKNOWLEDGMENTS

I would like to express my gratitude to all those who gave me the possibility to complete my thesis. Foremost, I would like to express my thanks to my supervisor, professor Michel Chouteau, for giving me the opportunity to work in his group, for his support and encouragement throughout my research not only as a professor but also as a close friend. Without his guidance and teaching, I would not be able to complete this research.

I wish to express sincere thanks to professor Denis Marcotte, my co-supervisor, who is the best reference for me in Geostatistics forever. Throughout my article-writing period, he provided encouragement, good teaching, good company, and lots of good ideas.

I would like to thank all members of my PhD defence : professor Colin Farquharson, Jean Claude Mareschal and Shaocheng Ji for their supportive efforts, valuable comments and all the time they spent to read this thesis.

I wish to thank all members of Matagami project team especially Michel Allard (from Xstrata zinc company) and Pierre Keating for their guidances and supports.

I also want to thank all current and previous members of applied geophysics laboratory of *École polytechnique de Montréal* for their helps and comments. Especially, I would like to thank my friends Abderrezak Bouchedda, Bernard Giroux and Jeremie Gaucher.

I wish to thank Kasra Alishahhi and Omid Naghshineh who have encouraged me to learn and love Mathematics. I also thank Farzad, Kamran and Ibrahim for helping me get through the difficult times, and for all the emotional supports, camaraderie, entertainment, and caring they provided.

My thanks also go to my beloved **mother, Parvaneh,** and my **father, Hassan**. I only hope I have made their trials and support worthwhile. I hope this thesis would fulfil part of my father's wishes for me.

RÉSUMÉ

Dans cette thèse nous présentons le développement de nouvelles méthodes d'inversion pour l'interprétation des champs de potentiel (données gravimétriques et magnétiques). Les méthodes gravimétrique et magnétique sont parmi les plus utilisées et les plus économiques pour l'exploration pétrolière et minière. Les nouvelles méthodes tiennent compte du problème récurrent de la non-unicité des inversions avec ces types de données. La thèse comprend trois articles (un quatrième article est présenté en annexe), qui ont été publiés, ou soumis, dans des revues scientifiques réputées.

Le but de cette thèse est d'introduire de nouvelles méthodes d'inversion en 3D basées sur des approches géostatistiques pour : 1) l'inversion des données du potentiel magnétique, 2) l'inversion multi-échelle utilisant des données de surface et des forages et 3) l'inversion conjointe (gravité et magnétisme) de données géophysiques de champs de potentiel.

Nous présentons d'abord une méthode d'inversion stochastique des données magnétiques basée sur une approche géostatistique (cokrigeage) permettant d'estimer les susceptibilités dans un modèle 3D découpé en blocs. Nous évaluons l'incertitude sur le modèle de paramètres en utilisant des simulations géostatistiques conditionnelles (aux données observées) obtenues par post-conditionnement par cokrigeage. Les champs magnétiques correspondant aux champs de susceptibilités obtenus par ces inversions reproduisent chacun les données observées si l'on admet l'absence de bruit sur les données. En présence de bruit, ils reproduisent les données à un niveau compatible avec l'importance du bruit tel que décrit par l'effet de pépite des modèles de covariance. Afin d'atténuer la tendance naturelle de la structure estimée à se retrouver près de la surface, une pondération en fonction de la profondeur est proposée et incluse dans le système de cokrigeage. Nous montrons toutefois les difficultés pratiques de cette approche par pondération en fonction de la profondeur.

Ensuite, nous introduisons l'algorithme pour l'inversion multi-échelles. La méthode comprend quatre étapes principales : i. krigeage des densités des blocs du modèle à partir des

densités mesurées en forage, ii. sélection des blocs à utiliser comme contraintes en fonction d'un seuil appliqué à la variance de krigeage, iii. inversion des données observées de gravité tenant compte des densités des blocs sélectionnés comme contraintes, et iv. estimation des paramètres sur de petits prismes utilisant les valeurs inversés sur les blocs et les données de densité en forage. Deux modes d'application sont présentés : l'estimation et la simulation conditionnelle.

Enfin, une nouvelle méthode d'inversion 3D stochastique basée sur le cokrigeage et la simulation conditionnelle est développée pour l'inversion conjointe des champs de potentiel magnétique et gravimétrique. La méthode intègre pleinement les relations physiques entre les propriétés (densité et susceptibilité magnétique) et les observations indirectes (gravité et champ magnétique total). Ainsi, lorsque les données sont considérées comme sans bruit, les champs inversés reproduisent exactement les données observées des deux champs de potentiel. Un modèle linéaire de coregionalization (LCM) est utilisé pour décrire les covariances et covariances croisées entre toutes ces variables.

Dans chaque cas, deux modèles synthétiques sont utilisés pour bien comprendre le comportement des méthodes : un modèle déterministe compact et un modèle stochastique. Ces modèles synthétiques montrent la capacité des méthodes d'inverser les données de surface et de forage simultanément et à différentes échelles, tout en reproduisant les données observées. Ils montrent aussi l'importance essentielle des données de forage pour bien localiser les anomalies en profondeur. Les données de la mine Persévérance (Québec, Canada) sont utilisées pour tester les 3 méthodes décrites. Les données comportent des mesures en surface du champ magnétique total et du champ gravimétrique ainsi que des mesures de densité en forage. L'étude démontre la capacité de l'inversion conjointe à utiliser efficacement l'information du champ magnétique pour l'estimation de la densité. Les champs de susceptibilité magnétique et de densité obtenus par inversion reconnaissent bien deux des trois dépôts de sulfures connus sur le site. Ils fournissent des informations utiles pour mieux comprendre la géologie des sulfures massifs présents dans le domaine d'étude.

ABSTRACT

In this thesis we present the development of new techniques for the interpretation of potential field (gravity and magnetic data), which are the most widespread economic geophysical methods used for oil and mineral exploration. These new techniques help to address the long-standing issue with the interpretation of potential fields, namely the intrinsic non-uniqueness inversion of these types of data. The thesis takes the form of three papers (four including Appendix), which have been published, or soon to be published, in respected international journals. The purpose of the thesis is to introduce new methods based on 3D stochastical approaches for:
1) Inversion of potential field data (magnetic), 2) Multiscale Inversion using surface and borehole data and 3) Joint inversion of geophysical potential field data.

We first present a stochastic inversion method based on a geostatistical approach to recover 3D susceptibility models from magnetic data. The aim of applying geostatistics is to provide quantitative descriptions of natural variables distributed in space or in time and space. We evaluate the uncertainty on the parameter model by using geostatistical unconditional simulations. The realizations are post-conditioned by cokriging to observation data. In order to avoid the natural tendency of the estimated structure to lay near the surface, depth weighting is included in the cokriging system.

Then, we introduce algorithm for multiscale inversion, the presented algorithm has the capability of inverting data on multiple supports. The method involves four main steps :i. upscaling of borehole parameters (It could be density or susceptibility) to block parameters, ii. selection of block to use as constraints based on a threshold on kriging variance, iii. inversion of observation data with selected block densities as constraints, and iv. downscaling of inverted parameters to small prisms. Two modes of application are presented : estimation and simulation.

Finally, a novel stochastic joint inversion method based on cokriging is applied to esti-

mate density and magnetic susceptibility distributions from gravity and total magnetic field data. The method fully integrates the physical relations between the properties (density and magnetic susceptibility) and the indirect observations (gravity and total magnetic field). As a consequence, when the data are considered noise-free, the inverted fields exactly reproduce the observed data. The required density and magnetic susceptibility auto- and cross covariance are assumed to follow a linear model of coregionalization (LCM).

In all the methods presented in this thesis, compact and stochastic synthetic models are investigated. The results show the ability of the methods to invert surface and borehole data simultaneously on multiple scale parameters. A case study using ground measurements of total magnetic field and gravity data at the Perseverance mine (Quebec, Canada) is selected and tested with the 3 approaches presented. The recovered 3D susceptibility and density model provides beneficial information that can be used to analyze the geology of massive sulfides for the domain under study.

TABLE OF CONTENTS

LIST OF TABLES

LIST OF FIGURES

LIST OF APPENDICES

LIST OF ABBREVIATIONS AND SYMBOLS

$FFT\text{-}MA$	fast Fourier transform moving average
CGA	conjugate gradient algorithm
LCM	linear coregionalization model
SVD	singular value decomposition
LU	Cholesky decomposition
MAE	mean absolute error
VMS	volcanogenic massive sulfide
Λ	diagonal matrix of eigenvalues
ρ	density (kg/m^3)
ρ^*	estimated density (kg/m^3)
χ	susceptibility SI
χ^*	estimated susceptibility
g	gravity ($mGal$)
T	magnetic field (nT)
e	error
γ	Newton's gravitational constant : $6.67 \times 10^{11} (N.m/kg^2)$
G	matrix of kernels (sensitivity matrix)
C	covariance function
C_0	nugget effect
C_m	magnetic constant $10 : ^{-7}$ (henry.meter^{-1} (SI units))
$Z(x)$	random function
$\gamma(h)$	variogram
σ^2	variance
σ_k^2	cokriging variance
$E[.]$	expectation function

λ, μ, η	cokriging coefficients
gr	density gradient
F	index matrix of known densities or susceptibilities
H	index matrix of known density gradients
$\vec{H}$	Earth's magnetic field
W	Weighting matrix
n_x, n_y, n_z	number of prisms in x, y, z directions
a	variogram range
$MCMC$	Markov chain Monte Carlo

CHAPITRE 1

INTRODUCTION

One of the significant current topics in geophysics is the inverse problem. Inversion of geophysical data is often an ill-posed problem, which means that solutions might not depend continuously on the data. Although a solution that satisfies the observed data can easily be found, there is still the problem of non-uniqueness which is caused by the nature of the physics and the under-determination of the problem. Generally, in inverse problems, we want to describe the measured data d by finding model parameters m characterizing some physical process which reduces to solving the system,

$$Gm + e = d, \qquad \text{Linear systems} \tag{1.1}$$

$$G(m) + e = d, \qquad \text{Non-linear systems} \tag{1.2}$$

where G is a forward mapping operator that maps the model parameters m into observations d and e is the error in the measured data. This general system is shown in Figure 1.1.

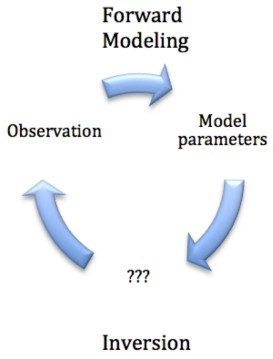

Figure 1.1 General schematic diagram of the inversion problem.

In 3D potential field inversion, there are different ways that the model parameters can be defined. One flexible way is to describe the model by a grid of prismatic cells. The subsurface is divided into prisms of known sizes and positions. The parameter contrasts are supposed constant within each cell. The parameters to estimate are the cell parameters shown schematically in Figure 1.2.

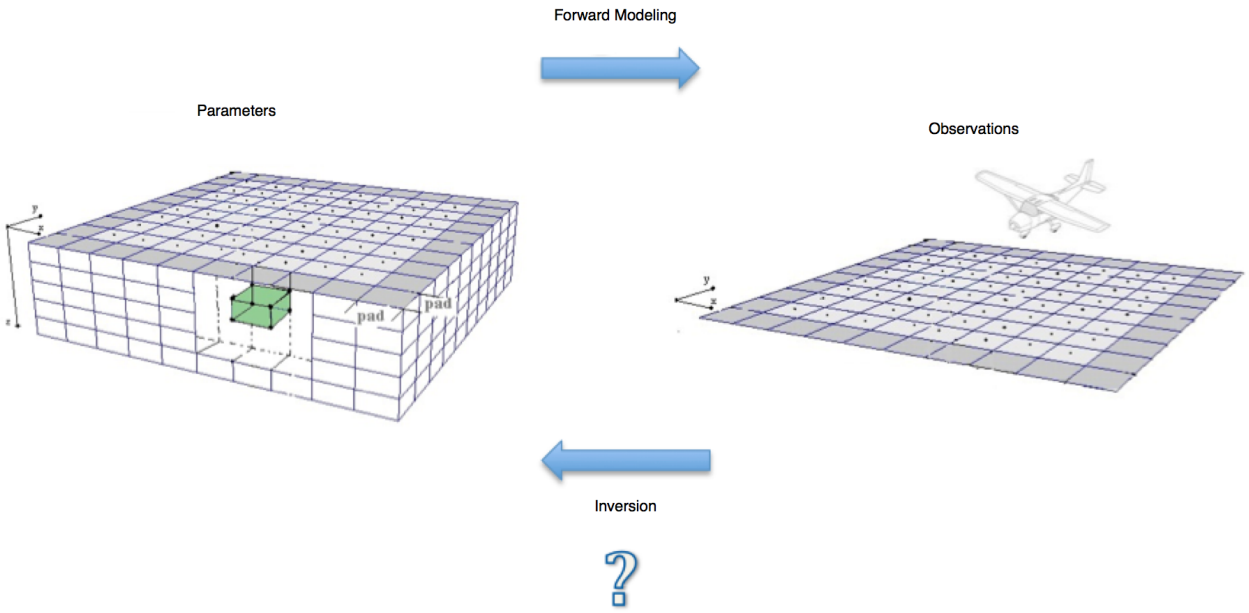

Figure 1.2 Schematic diagram of the inversion problem assuming prismatic cells to represent the model parameters.

In the next sections, we explain two other important concerns, scaling and jointing, arise while inverting data. Scaling and Jointing data are two demanding tasks for most earth scientists.

Multiscale :

In inversion of geophysical data, one often needs to integrate a large diversity of data with

different support volumes which convey information at different scales. In mineral exploration, it is crucial to use fine scale support data such as parameters coming from drill cores to constrain the subsurface structures. Any mapping of parameters should include all relevant information from different supports. Change of the support refers to a group of geostatistical tools that allow the user to predict the behavior of smaller units from larger block estimates and vice versa. This problem of changing support is illustrated in Figure 1.3 schematically.

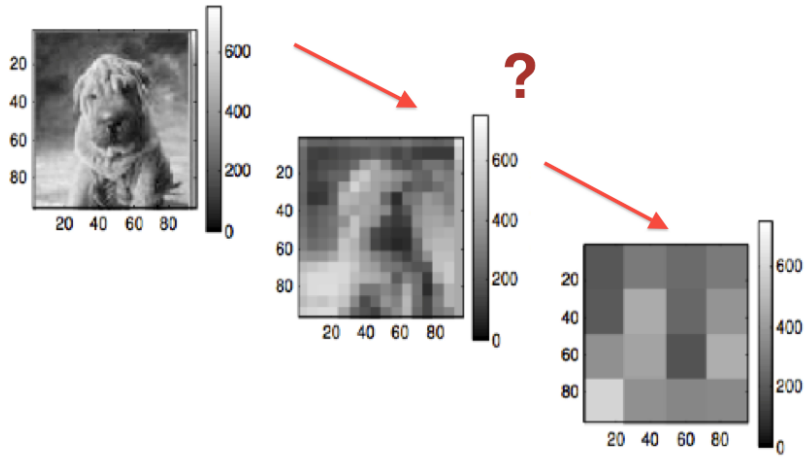

Figure 1.3 The problem of changing support.

Joint inversion :

Interpretation of geophysical data needs to bring together different types of information to make the proposed model geologically more realistic. Multiple data sets can reduce ambiguity and non-uniqueness present in separate geophysical data inversions. Potential fields surveys (gravity and magnetic) are suitable candidates for the joint inversion as they are among the most economical methods in geophysics. Moreover, the gravity and magnetic fields are closely related fields, yet complementary. Most often, the magnetic minerals are dense minerals so they cause also gravimetric anomalies. However, many dense rocks are not magnetic. Also, magnetic field data display higher frequency variations than gravity data, so they are often more effective than gravity at resolving shallow or complex structures.

1.1 Objectives

The purpose of this thesis is to introduce and develop new methods based on 3D stochastical approaches for :

- Inversion of potential field data (magnetic and gravity),
- Multiscale Inversion,
- Joint inversion of geophysical potential field data.

1.2 Theoretical framework

A 3D stochastic inversion method based on geostatistical approaches (cokriging and cosimulation) is presented for three-dimensional inversion of potential field data. This method has been applied on potential field data for multiple scale parameters using borehole and surface observation data. We also propose a new method, based on cokriging for the joint inversion of geophysical data.

Cokriging is a method of estimation that minimizes the error variance by applying cross-correlation between several variables. In this study, the estimates are derived using observation data as the secondary variable and the parameters as the primary variable. In the proposed method, the linearity between observation data and parameters allows us to obtain a covariance matrix of parameters using observed data, i.e, we adjust the parameter covariance matrix by fitting experimental and theoretical observation covariance matrices.

Cosimulation : Stochastic inversion based on cokriging gives a smooth estimate of the density distribution. Using geostatistical simulation algorithms, we can explore various reasonable solutions showing the kind of variability that can be expected from the parameter covariance model. Then we do post-conditioning with the cokriging of parameters obtained from the observed data.

Scaling : In order to integrate parameter data of different scales, we must consider different supports simultaneously in our inversion method. The major assumption is that the initial parameter information is at the "quasi" point support level and block data are calculated as averages of the point support. Suppose that we require a block estimate, in other words an estimate of the average value of the parameter within a certain area. In order to find this estimate, we use the known block kriging method described in Appendix B.

In addition to the observation data, the point parameters measured along boreholes need to be accounted for in the inversion process. Note that the inversion is done on large blocks whereas the measured parameters are on point support. To incorporate the point information, one idea is to krige blocks from point parameters using standard block kriging. Then, the most precise block estimates are considered as constraints in the inversion. After inversion, the parameters of all large blocks are known. Then, we can use downscaling to find the parameter distribution for smaller prisms. Indeed, the downscaling must also incorporate the known borehole point parameter values.

Joint inversion : In order to recover more realistic parameters from geophysical data, we need to incorporate different types of available information in the inversion process. Using multiple data sets (joint inversion) can reduce ambiguity and non-uniqueness of separate geophysical data inversions. The method presented in this thesis exploits the complementary nature of the two potential fields (gravity and magnetic) to provide joint inversions with geologically more accurate parameters compared to separate inversions of each field. For this purpose, a 3D stochastic inversion approach based on cokriging is used.

It should be noted that the basic theory of stochastical inversion methods (cokriging and cosimulation) are given in Appendix A. This appendix includes an article previously published by the author.

1.3 Thesis plan

This thesis has been organized and divided into seven chapters. *Chapter 1* includes a brief overview of the thesis (introduction) such as theoretical framework, problems, hypotheses, purpose of the study, objectives, etc.

Chapter 2 presents a literature review encompassing the major topics of the thesis.

Chapeter 3 clarifies the organization of the thesis which is based on three articles. In this chapter, we give a brief summary of the most important items in each article.

Chpater 4 contains an article published in the Journal of Applied Geophysics with the title of "3D stochastic inversion of magnetic data".

Chpater 5 contains an article published in Geophysical Prospecting with the title of "Stochastic inversion of a gravity field on multiple scale parameters using surface and borehole data".

Chpater 6 contains an article submitted to the Journal of Applied Geophysics with the title of " 3D stochastic joint inversion of gravity and magnetic data ".

Chpater 7 presents conclusions and discussions of the thesis. In this chapter, we also suggest some future works.

CHAPITRE 2

LITERATURE REVIEW

We divide this chapter into three sections. In the first part, we present the literature review of 3D stochastic inversion of potential field (magnetic and gravity). In the second part, we review the works on integrating multi-scale parameter information into three dimensional stochastic gravity inversion. In the last section, we attempt to fully review the works on joint inversion.

2.1 3D stochastic potential field inversion

Inverse problems seek to retrieve the model parameters from measured data using a linear or nonlinear forward mapping operator. By defining the potential field using potential theorem (Blakely, 1995), there are no assumptions about the shape of the sources or distribution of parameters. Many equivalent parameter distributions below the surface will reproduce the known field at the surface (theoretical ambiguity) even when the surface field is known at every point. Besides, when the number of parameters is larger than the number of observations at the ground surface, the system does not provide enough information to determine uniquely all model parameters. In this situation, the problem is said to be underdetermined. As a result, although a solution that satisfies the observed data can easily be found, a problem of non-uniqueness still exists which is caused by the nature of the physics and the underdetermination of the problem. The non-uniqueness of solutions is further increased when one considers data uncertainty.

Many strategies can be used to deal with the non-uniqueness problem in potential field inversion. They all involve some kind of constraints or regularization (Gallardo-Delgado *et al.*, 2003) to limit the resulting solution space. Green (1975) used an appropriate weighting matrix to fix some of the parameters when geological or density information are available. Last et

Kubik (1983) sought a compact solution with a minimum volume constraint. Smoothness or roughness of parameter distribution which controls gradients of parameters in spatial directions are used in magnetic inversion by Pilkington (1997). Li et Oldenburg (1996) proposed a generalized 3D inversion of magnetic data. Their solutions are based on minimization of a global objective function composed of the model objective function and data misfit. They counteract the decreasing sensitivities of cells with depth by weighting them with an inverse function of depth. Li et Oldenburg (1998) also applied depth weighting approach to gravity inversion. Another 3D inversion technique allowing definition of depth resolution is proposed by Fedi et Rapolla (1999). Prior information in the form of parameter covariances can be included (Tarantola et Valette, 1982). Montagner et Jobert (1988) used exponential covariance functions in which the rate of exponential decay determines the correlation length of the parameters.

Geostatistical methods in geophysical inversion were applied by Asli *et al.* (2000), Gloaguen *et al.* (2005, 2007), Giroux *et al.* (2007), Hansen *et al.* (2006), Hansen et Mosegaard (2008) and Gomez-Hernandez *et al.* (2004). Bosch et McGaughey (2001) and Bosch *et al.* (2006) also applied geostatistical constraints to gravity inversion using Monte Carlo techniques. In fact, linear stochastic inversion was first described by Franklin (1970) and then popularized by Tarantola et Valette (1982). Chasseriau et Chouteau (2003) have done 3D inversion of gravity data using an a priori model of covariance. However, their method involved nonlinear constraints on density so they used an iterative approach (Tarantola et Valette, 1982). Asli *et al.* (2000) cokriged gravity anomalies to obtain cell densities. They showed how the covariance model can be adjusted to observed gravity data using some prior information to guide the choice of the model.

We assess uncertainty of inversions by using geostatistical conditional simulations. Simulations allow to identify stable features of the inverted fields. Simulations are also essential to estimate non-linear functions of the inverted fields like, for example, the maximum density gradient. Such quantities could indicate favourable exploration targets. Simulations allow to

estimate values and locations of high density gradients. There exist many efficient algorithms (Chilès et Delfiner, 1999) to simulate spatially structured models such as the Fast Fourier Transform Moving Average simulation (FFT-MA) (Le Ravalec *et al.*, 2000). In a Gaussian framework, the simulations obtained are then post-conditioned to the observed data by using cokriging (Journel et Huijbregts, 1978). We show that parameter simulation ensures exact reproduction of potential field data, when observed without error, for any choice of the covariance model. This is due to the linear relationship between parameters and potential field data. This property applies also for the case of non-linear averaging that can be approximated by a power average (Journel, 1999). In geophysics, Gloaguen *et al.* (2005) and Hansen *et al.* (2006) applied geostatistical simulation to inversion of radar data. Shamsipour *et al.* (2010b) proposed geostatistical techniques of cokriging and conditional simulation for the three-dimensional inversion of gravity data including geological constraints. Shamsipour *et al.* (2010a) applied this approach to inversion of gravity data obtained at ground surface and in boreholes.

2.1.1 Forward modeling

The purpose of forward modeling is to compute the potential field (T or g) at the surface due to a susceptibility or density distribution in the sub-surface (χ or ρ). The most common method of evaluating the observations from the parameters is to break down the 3D domain into geometrically simple bodies having constant density or susceptibility. In our case, and for the sake of simplicity, the domain studied is divided into a finite number of rectangular prisms .

The magnetic field of a rectangular prism was first presented by Bhattacharyya (1964). Closed form solutions for forward modeling were first presented by Bhattacharyya (1964), later simplified in Rao et Babu (1991) into a form more suitable for fast computer implementation. We use the formulation of Rao et Babu (1991) to compute total field magnetic values resulting from individual prisms.

2.2 Multiscale inversion

Shamsipour *et al.* (2010b) proposed geostatistical techniques of cokriging and conditional simulation for the three-dimensional inversion of gravity data including geological constraints. They assumed all densities were known on a block support. However, in inversion of gravity data, one often needs to integrate a large diversity of data with different support volumes which convey information at different scales. In mineral exploration, it is crucial to use fine scale support data such as densities coming from drill cores to constrain the subsurface structures. Any mapping of densities should include all relevant information from different supports. Liu et journel (2009) proposed a method for integration of coarse and fine scale data built on a combination of kriging using both point and block data with direct sequential simulation or error simulation.

The major assumption is that the initial parameter information is at the point support level and block data are calculated as averages of the point support. In order to find an estimate of the average value of the parameter in a block, we use the block kriging method (Chilès et Delfiner, 1999). In this thesis, we extend the geostatistical algorithm proposed for gravity inversion by Shamsipour *et al.* (2010b) to multiscale inversion. Contrary to Shamsipour *et al.* (2010b), here the basic density covariance model is assumed to be known on the point scale rather than the block scale.

2.3 Joint inversion

3D joint inversion of magnetic and gravity data was first described in the work by Zeyen et Pous (1993). They applied a priori information to reduce ambiguity of potential field inversion and interpolation. Gallardo-Delgado *et al.* (2003) proposed the method based on optimization to minimize the joint data misfit. The stochastic formulation for joint inversion is presented by Bosch *et al.* (2006). The approach is based on lithology discrimination and classification. This method allows for joint inversion of gravity, magnetic and other priori information to provide a model for major layers and properties inside layers. Gravity and

magnetic data were inverted also jointly by Pilkington (2006) in terms of a model consisting of an interface separating two layers having a constant density and magnetization contrast. In Fregoso et Gallardo (2009), the authors propose using cross gradient for 3D inversion of gravity and magnetic data. Most of the proposed methods directly and indirectly adapt the Tarantola et Valette (1982) techniques to generalize the minimization problem under the Baysian framework.

In this thesis, we propose a stochastic joint inversion method based on cokriging to estimate density and magnetic susceptibility distributions from gravity and total magnetic field data.

CHAPITRE 3

THESIS ORGANIZATION

This thesis is based on three articles. The organization of the thesis follows the structure proposed by Ecole polytechnique de Montreal for an article based thesis. In this chapter, we describe the articles which will be presented in the next chapters and we point out the most important items in each article. The articles are explained and arranged in chronological order. The objective of each article is explicitly stated.

3.1 First Article (Chapter 4)

Title : *3D stochastic inversion of magnetic data*

Article history : Received by Editor 31 August 2010, Accepted 9 February 2011, Available online 23 February 2011, Journal of applied geophysics.

Authors : Pejman Shamsipour, Michel Chouteau and Denis Marcotte.

Summary : A stochastic inversion method based on a geostatistical approach is presented to recover 3D susceptibility models from magnetic data. Cokriging, the method which is used in this paper, is a method of estimation that minimizes the theoretical estimation error variance by using auto- and cross-correlations of several variables. The covariances for total field, susceptibility and total field-susceptibility are estimated using the observed data. Then, the susceptibility is cokriged or simulated as the primary variable. In order to avoid the natural tendency of the estimated structure to lay near the surface, depth weighting is included in the cokriging system. The algorithm assumes there is no remanent magnetization and the observation data represent only induced magnetization effects. The method is applied on different synthetic models to demonstrate its suitability for 3D inversion of magnetic data. A case study using ground measurements of total field at the Perseverance mine (Quebec, Canada) is presented. The recovered 3D susceptibility model provides beneficial information

that can be used to analyze the geology of massive sulfide for the domain under study.

The most important points of this article are :

- Introduction of a 3D stochastic method for magnetic inversion.
- Investigation of the method using synthetic and real data.
- Consideration of both surface and borehole data.
- Application and examination of conditional simulation.
- Addition of Depth weighting matrix in cokriging system.
- Discussion on the potential use of sparse matrix.

3.2 Second Article (Chapter 5)

Title : *Stochastic inversion of a gravity field on multiple scale parameters using surface and borehole data*

Article history : Submitted 30 November 2010, Accepted 18 April 2011, Published online 5 July 2011, Journal of geophysics prospecting.

Authors : Pejman Shamsipour, Denis Marcotte, Michel Chouteau and Michel Allard .

Summary : A 3D stochastic inversion method based on a geostatistical approach is presented for three-dimensional inversion of gravity on multiple scale parameters using borehole density and gravity and surface gravity. The algorithm has the capability of inverting data on multiple supports. The method involves four main steps :

i. upscaling of borehole densities to block densities,

ii. selection of block densities to use as constraints,

iii. inversion of gravity data with selected block densities as constraints,

and iv. downscaling of inverted densities to small prisms.

Two modes of application are presented : estimation and simulation. The method is first applied to a synthetic stochastic model. The results show the ability of the method to invert surface and borehole data simultaneously on multiple scale parameters. The results show the usefulness of borehole data to improve depth resolution. Finally, a case study using gravity measurements collected in the area of the Perseverance mine (Quebec, Canada) is presented.

The recovered 3D density model identifies well three known deposits and it provides beneficial information to analyze the geology of massive sulfide for the domain under study.

The most important points of this article :

- Introducing a 3D stochastic method for upscaling and downscaling
- Presenting two algorithms :
  - Inversion with constraints and downscaling
  - Conditional simulation of densities and downscaling
- Investigating the method using synthetic and real data
- The method can be easily extended to account for blocks of various sizes.
- The algorithm is flexible as it allows all combinations of conditioning point and block density support data simultaneously.

3.3 Third Article (Chapter 6)

Title : *3D stochastic joint inversion of gravity and magnetic data*

Article history : Submitted 15 July 2011, Currently under review, Journal of applied geophysics.

Authors : Pejman Shamsipour, Denis Marcotte, Michel Chouteau.

Summary :A novel stochastic joint inversion method based on cokriging is applied to estimate density and magnetic susceptibility distributions from gravity and total magnetic field data. The method fully integrates the physical relations between the properties (density and magnetic susceptibility) and the indirect observations (gravity and total magnetic field). As a consequence, when the data are considered noise-free, the inverted fields exactly reproduce the observed data. The required density and magnetic susceptibility auto- and cross covariance are assumed to follow a linear model of coregionalization (LCM). The parameters of the LCM are estimated from v-v plot fitting of the gravity and total magnetic experimental covariances. The model is tested on two synthetic cases and one real data set, the Perseverance mine (Quebec, Canada). Joint inversions are compared to separate inversions. The

joint inversions better recover the known models in the synthetic cases. With the real data set, better definition and location of the mineralized lenses is achieved by joint inversion. The benefit of joint inversion is especially noticeable when the two data sources are not collocated, therefore informing different parts of the study area.

The most important points of this article :

- Introducing a 3D stochastic method for joint inversion.
- Investigating the method using synthetic and real data.
- The method can be easily used for any other two linear geophysical methods.
- One of the advantages of the inversion by cokriging is that the magnetic field and the gravity field do not need to be caused by the exact same source.

3.4 Links between the papers

The first article presents the necessary equations for stochastic inversion of magnetic data. The second article indicates the possibility of using multiscale parameters in stochastic inversion. It is applied on gravity data but the same approach could be used also for magnetic data. Finally, the last article joins both gravity and magnetic information for more reliable stochastic inversions. Although all information is on the same support, generalization using the approach described in the second article is possible (future work) to do a joint inversion with data both on multiscale.

CHAPITRE 4

Article 1 : 3D STOCHASTIC INVERSION OF MAGNETIC DATA

Article history : Received by Editor 31 August 2010, Accepted 9 February 2011, Available online 23 February 2011, Journal of applied geophysics.
Authors : Pejman Shamsipour, Michel Chouteau and Denis Marcotte.

4.1 Abstract

A stochastic inversion method based on a geostatistical approach is presented to recover 3D susceptibility models from magnetic data. The aim of applying geostatistics is to provide quantitative descriptions of natural variables distributed in space or in time and space. Cokriging, the method which is used in this paper, is a method of estimation that minimizes the theoretical estimation error variance by using auto- and cross-correlations of several variables. The covariances for total field, susceptibility and total field-susceptibility are estimated using the observed data. Then, the susceptibility is cokriged or simulated as the primary variable. In order to avoid the natural tendency of the estimated structure to lay near the surface, depth weighting is included in the cokriging system. The algorithm assumes there is no remanent magnetization and the observation data represent only induced magnetization effects. The method is applied on different synthetic models to demonstrate its suitability for 3D inversion of magnetic data. A case study using ground measurements of total field at the Perseverance mine (Quebec, Canada) is presented. The recovered 3D susceptibility model provides beneficial information that can be used to analyze the geology of massive sulfide for the domain under study.

4.2 Introduction

Inverse problems seek to retrieve the model parameters from measured data using a linear or nonlinear forward mapping operator. In magnetic inversion, nonuniqueness of solution is a problem as, from the mathematical properties of potential fields, many subsurface distributions of magnetization can produce exactly the same response. Imposing simple constraints on admissible solutions based on geologic knowledge helps in guiding the inversions and obtaining more robust results.

Li et Oldenburg (1996) proposed a generalized 3D inversion of magnetic data. Their solutions are based on minimization of a global objective function composed of the model objective function and data misfit. They counteract the decreasing sensitivities of cells with depth by weighting them with an inverse function of depth. In magnetic inversion, Pilkington (1997) applied the smoothness or roughness of susceptibility distribution to control gradients of parameters in different spatial directions. Linear stochastic inversion was originally introduced by Franklin (1970) and then simplified and popularized in geophysics by Tarantola et Valette (1982). Geostatistical methods in geophysical inversion were applied by Asli *et al.* (2000), Gloaguen *et al.* (2005, 2007), Giroux *et al.* (2007), Hansen *et al.* (2006), and Gomez-Hernandez *et al.* (2004). Bosch et McGaughey (2001) and Bosch *et al.* (2006) also used Monte Carlo techniques in gravity inversion for generating a posterior probability density function describing acceptable models. Chasseriau et Chouteau (2003) advocate 3D inversion of gravity data using an a priori model of covariance. Shamsipour *et al.* (2010b) proposed geostatistical techniques of cokriging and conditional simulation for the three-dimensional inversion of gravity data including geological constraints. The conditional simulations allow identification of stable features of the inverted fields. Shamsipour *et al.* (2010a) applied this approach to inversion from gravity data obtained at ground surface and in boreholes.

We adapt to magnetic data inversion the geostatistical algorithm proposed for gravity inversion by Asli *et al.* (2000) and extended by Shamsipour *et al.* (2010b). We show the capibility of the method to use the depth weighting matrix approach of Li et Oldenburg (1996).

We evaluate the uncertainty on the susceptibility model by using geostatistical unconditional simulations obtained using the Fast Fourier Transform Moving Average simulation method (FFT-MA) Le Ravalec *et al.* (2000). The realizations are post-conditioned by cokriging (Journel et Huijbregts, 1978) to total magnetic field data. We show that in absence of observation errors susceptibility simulation ensures exact reproduction of total field data for any choice of the covariance model and for all realizations.

The method is tested on two synthetic models : a model consisting of two magnetic prisms buried in a nonmagnetic background and a stochastic distribution of susceptibilities. Borehole information, both susceptibility and total magnetic field, is added as constraints to the cokriging system. The results show the ability of the method to integrate complex a priori information. In addition, the survey data collected over the Perseverance and Equinox deposits of the Matagami mining camp (Quebec, Canada) are considered as a case study. To the authors' knowledge, this is the first time that cokriging and conditional simulations are applied to 3D magnetic data inversion.

4.3 Methodology

4.3.1 Forward modeling

The purpose of forward modeling is to compute the magnetic field T at the surface due to a susceptibility distribution in the sub-surface χ. The magnetization vector $\vec{m}$ can be obtained as a vector sum :

$$\vec{m} = \chi\vec{H} + \vec{m}_r \tag{4.1}$$

where $\vec{H}$ is earth's magnetic field and $\vec{m}_r$ is the remanent component. If we assume no remanence, the magnetization $\vec{m}$ is in the direction of the earth's field and can be obtained simply as : $\overrightarrow{m} = \chi\vec{H}$. Analogous to gravity equations, total component of the magnetic field can be expressed as Blakely (1995) :

$$\vec{T} = -C_m \nabla \int_R \vec{m}.\nabla(\frac{1}{r})dv \tag{4.2}$$

where the constant C_m is 10^{-7} (henry.meter^{-1} (SI units)), r is distance and R indicates the volume occupied by causative source. The most common method of the above equation is to break the 3D domain down into geometrically simple bodies having constant susceptibilities. In our case, and for the sake of simplicity, the domain studied is divided into a finite number of rectangular prisms of uniform susceptibilities. It should be noted this classic method can consume memory space for a fine domain discretization. The magnetic field of a rectangular prism was first presented by Bhattacharyya (1964) starting with Eq. (4.2). By his definition, the total field anomaly caused at point (x_0, y_0, z_0) by prism j is given by Fregoso et Gallardo (2009) :

$$T_{0,j} = C_m(l \quad m \quad n) \begin{bmatrix} -\tan^{-1}\left(\frac{yz}{xr}\right) & \ln(r+z) & \ln(r+y) \\ \ln(r+z) & -\tan^{-1}\left(\frac{xz}{yr}\right) & \ln(r+x) \\ \ln(r+y) & \ln(r+x) & -\tan^{-1}\left(\frac{xy}{zr}\right) \end{bmatrix} \Bigg|_{\Delta x_1}^{\Delta x_2} \Bigg|_{\Delta y_1}^{\Delta y_2} \Bigg|_{\Delta z_1}^{\Delta z_2} \begin{bmatrix} m_x \\ m_y \\ m_z \end{bmatrix} \tag{4.3}$$

where $\Delta x_i = x_i - x_0$, $\Delta y_i = y_i - y_0$ and $\Delta z_i = z_i - z_0$ and x_i, y_i, z_i for $i = 1, 2$ represent the eight vertices of the prism. Also, $(l \quad m \quad n)$ are the direction cosines of the geomagnetic field. The bars on the right hand side of Equation (3) indicate the summation is to be taken on the eight vertex of the prisms, according to : , $f(x,y,z)\Big|_{\Delta x_1}^{\Delta x_2}\Big|_{\Delta y_1}^{\Delta y_2}\Big|_{\Delta z_1}^{\Delta z_2} = \sum_{i=1}^{2}\sum_{j=1}^{2}\sum_{k=1}^{2}(-1)^i(-1)^j(-1)^k f(\Delta x_i, \Delta y_i, \Delta z_i)$. Closed form solutions for forward modeling were first presented by Bhattacharyya (1964), later simplified in Rao et Babu (1991) into a form more suitable for fast computer implementation. We use the formulation of Rao et Babu (1991) to compute total field magnetic values resulting from individual prisms. The response at the observation point (x_0, y_0, z_0) of all the prisms making up the body, is the sum of the

contribution of each prism :

$$T_0 = \sum_{j=1}^{m} T_{0,j} \tag{4.4}$$

Considering that there are n total field observations and m rectangular prisms, the preceding relationship can also be written in the matrix form :

$$T_{n\times 1} = G_{n\times m}\chi_{m\times 1} \tag{4.5}$$

with G, the matrix of the geometric terms (or kernel matrix).

4.3.2 Cokriging

Cokriging (Myers, 1982) (Chilès et Delfiner, 1999) is a geostatistical tool that utilizes the spatial correlation between the secondary variables and a primary variable to interpolate or extrapolate primary variable at unsampled locations. The cokriging method provides weights to data so as to minimize the theoretical estimation variance (the cokriging variance). In this approach, the primary variable is susceptibility ($\boldsymbol{\chi}$, estimated by $\boldsymbol{\chi}^*$) and the secondary variable is total magnetic field ($\boldsymbol{T}$). Assuming spatial homogeneity of the mean for the susceptibility and total magnetic field i.e., $E[\boldsymbol{\chi}] = E[\boldsymbol{T}] = 0$, the estimation variances appear on the diagonal of the following matrix (Myers, 1982) :

$$E((\boldsymbol{\chi} - \boldsymbol{\chi}^*)(\boldsymbol{\chi} - \boldsymbol{\chi}^*)^T) = \boldsymbol{C}_{\chi\chi} - 2\boldsymbol{C}_{\chi T}^T\boldsymbol{\Lambda} + \boldsymbol{\Lambda}^T\boldsymbol{C}_{TT}\boldsymbol{\Lambda}. \tag{4.6}$$

where $\boldsymbol{\chi}$ and $\boldsymbol{T}$ are random variables and $\boldsymbol{\chi}^*$ is the estimated susceptibility defined on the rectangular prism support. $\boldsymbol{C}_{TT}$ is the total magnetic field covariance matrix, $\boldsymbol{C}_{\chi\chi}$ is the susceptibility covariance matrix, $\boldsymbol{C}_{T\chi}$ is the cross covariance between total magnetic field and susceptibility and $\boldsymbol{\Lambda}$ is the vector of weighting coefficients. Minimization of the above estimation variance with respect to Λ yields the simple cokriging solution :

$$\boldsymbol{C}_{TT}\boldsymbol{\Lambda} = \boldsymbol{C}_{T\chi} \tag{4.7}$$

From Eq. (4.7), the estimates of susceptibilities are obtained from the total magnetic field data using the optimal weights :

$$\boldsymbol{\chi}^* = \boldsymbol{\Lambda}^T \boldsymbol{T} \tag{4.8}$$

The vector of cokriging variances is obtained from :

$$\boldsymbol{\sigma}_{ck} = diag(\boldsymbol{C}_{\chi\chi} - \boldsymbol{\Lambda}^T \boldsymbol{C}_{T\chi}) \tag{4.9}$$

The off-diagonal elements give the covariances between estimation errors.

4.3.3 Inversion by cokriging

From Eq. (4.5), susceptibility and total magnetic field covariance matrices are linearly related :

$$\boldsymbol{C}_{TT} = \boldsymbol{G}\boldsymbol{C}_{\chi\chi}\boldsymbol{G}^T + \boldsymbol{C}_0 \tag{4.10}$$

where $\boldsymbol{C}_0$ is the total magnetic field observation error covariance matrix. This matrix is usually considered diagonal often with a constant value. We also know :

$$\boldsymbol{C}_{T\chi} = \boldsymbol{G}\boldsymbol{C}_{\chi\chi} \tag{4.11}$$

In case of $C_0 = 0$ (no error on observation), we have the following property :

$$\boldsymbol{T}^* = \boldsymbol{G}\boldsymbol{\chi}^* = \boldsymbol{G}\boldsymbol{\Lambda}^T\boldsymbol{T} = \boldsymbol{G}(\boldsymbol{C}_{TT}^{-1}\boldsymbol{C}_{T\chi})^T\boldsymbol{T} = \boldsymbol{G}(\boldsymbol{G}\boldsymbol{C}_{\chi\chi})^T(\boldsymbol{G}\boldsymbol{C}_{\chi\chi}\boldsymbol{G}^T)^{-1}\boldsymbol{T} = \boldsymbol{T} \tag{4.12}$$

It shows that the total magnetic field anomaly of the cokriged susceptibility is equal to the observed total magnetic field anomaly.

The model covariance is obtained using the V-V plot method (Shamsipour *et al.*, 2010b). In this method we adjust iteratively the parameter covariance matrix $\boldsymbol{C}_{\chi\chi}$ such that non-linear regression between experimental cross-products $\boldsymbol{T}\boldsymbol{T}$ and theoretical ($\boldsymbol{C}_{TT}$) data covariance matrices have a good correlation. In essence, the V-V plot approach follows exactly the steps

for variogram computation instead that the initial binning is done on the theoretical structural distance (obtained from the theoretical magnetic field covariance (or variogram) computed with Eq. (4.10)) instead of the classical euclidean distance used in variogram computation. Details of the V-V plot approach are given in Gloaguen *et al.* (2005) and Shamsipour *et al.* (2010b). When the model covariance function is obtained, the model parameters (susceptibilities) is cokriged using the total magnetic field data and any available known model data. Including constraints is simple in this algorithm. Suppose that we know susceptibilities $\boldsymbol{\chi}_F$ of some cells. The estimate for susceptibilities is obtained using a similar cokriging system as before, but now we expand the matrix for new variables. The estimation variance is minimized with respect to the weights $\boldsymbol{\Lambda}$, $\boldsymbol{\Gamma}$. The simple cokriging system is given by :

$$\begin{bmatrix} \boldsymbol{C}_{T,T} & \boldsymbol{C}_{T,\chi_F} \\ \boldsymbol{C}_{\chi_F,T} & \boldsymbol{C}_{\chi_F,\chi_F} \end{bmatrix} \begin{bmatrix} \boldsymbol{\Lambda} \\ \boldsymbol{\Gamma} \end{bmatrix} = \begin{bmatrix} \boldsymbol{C}_{T,\chi} \\ \boldsymbol{C}_{\chi_F,\chi} \end{bmatrix} \tag{4.13}$$

$$\boldsymbol{\chi}^* = \boldsymbol{\Lambda}^T \boldsymbol{T} + \boldsymbol{\Gamma}^T \boldsymbol{\chi}_F \tag{4.14}$$

The vector of cokriging variances is obtained from :

$$\boldsymbol{\sigma}_{ck} = diag(\boldsymbol{C}_{\chi\chi} - \tilde{\boldsymbol{\Lambda}}^T \tilde{\boldsymbol{C}}_{T\chi}) \tag{4.15}$$

where : $\tilde{\boldsymbol{\Lambda}}^T = [\boldsymbol{\Lambda}^T, \ \boldsymbol{\Gamma}^T]$ and $\tilde{\boldsymbol{C}}_{T\chi}$ is the right member in Eq. (4.13).

The inverse matrix calculation to solve Eq. (4.13) can be done by singular value decomposition (SVD) for small inverse problems or by preconditioned CGA for larger problems.

4.3.4 Depth weighting matrix in inversion

Gravity and magnetic data have no inherent depth resolution. As a result, structures tend to concentrate near the surface when a simple (e.g. smallest or flattest) model is produced, regardless of the true depth of the causative bodies. In terms of model construction, the kernel decreases with depth so that surface data are not sufficient to generate significant

structures at depth. To overcome this lack of sensitivity, depth weighting has been introduced by Li et Oldenburg (1996) to cancel the natural decay and give cells at different depths equal probability of entering the solution with a non-zero susceptibility. Their numerical experiments indicate that it is reasonable to approximate the decay with depth by a function of the form : $W(z) = \frac{1}{(z+z_0)^\beta}$ where β is close to 1.5 and z_0 depends on the observation level height. In accordance with the discretization used in the inversion, we use a depth weighting function of the form :

$$W = \begin{pmatrix} \frac{1}{z_{m1}^\beta} & 0 & \dots & 0 \\ 0 & \frac{1}{z_{m2}^\beta} & \ddots & \vdots \\ \vdots & \ddots & \ddots & 0 \\ 0 & \dots & 0 & \frac{1}{z_{mp}^\beta} \end{pmatrix} \tag{4.16}$$

To prevent singularity we can use a weighting matrix function of the form of $W_{m_i} = \frac{1}{(z_{m_i}+\epsilon)^\beta}$ Boulanger et Chouteau (2001). In our case, we found by trial and error $\beta = 0.7$ yielded the best fit of the recovered model to the synthetic model. Noted, the "best " value for β is really model dependent. Recall the cokriging estimates of susceptibility :

$$\chi^* = C_{\chi\chi} G^T (G C_{\chi\chi} G^T)^{-1} T, \tag{4.17}$$

the cokriging estimates with the depth weighting matrix are obtained by :

$$\chi^* = W^{-1} C_{\chi\chi} W^{-1} G^T (G W^{-1} C_{\chi\chi} W^{-1} G^T)^{-1} T. \tag{4.18}$$

As with cokriging, when there are no observation errors, the weighted cokriging susceptibility solution fits exactly the observed total magnetic field.

4.4 Conditional simulation

There is only one, smooth susceptibility model recovered by cokriging. It is useful to obtain various, less smooth, reasonable solutions to visualize the variability that can be expected from the inverted susceptibility model. This can be achieved using geostatistical conditional simulation algorithms rather than cokriging. In this paper we use the FFT-MA algorithm (Le Ravalec *et al.*, 2000) for generating non-conditional Gaussian stationary field on a regular grid. This algorithm is chosen because it is fast and easy to implement. The non-conditional realizations are post-conditioned by cokriging (Journel et Huijbregts, 1978; Myers, 1982). First, the cokriging of susceptibilities $\boldsymbol{\chi}^*$ with measured total magnetic field data $\boldsymbol{T}$ is performed. Then, for each realization $\boldsymbol{\chi}_s$, the total magnetic field data, $\boldsymbol{T}_s$ at sample points is computed. Keeping the same cokriging weights, cokriging of the susceptibilities $\boldsymbol{\chi}_s^*$ with $\boldsymbol{T}_s$ is performed. Finally, the conditional simulated susceptibilities $\boldsymbol{\chi_{cs}}$ are :

$$\boldsymbol{\chi}_{cs} = \boldsymbol{\chi}^* + (\boldsymbol{\chi}_s - \boldsymbol{\chi}_s^*) \tag{4.19}$$

As with cokriging, when there are no observation errors, each conditioned realization reproduces exactly the observed total field magnetic data.

4.5 Synthetic results

The proposed algorithms have been tested on two sets of synthetic data, a model consisting of two prisms buried in a nonsusceptible background and a stochastic susceptibility model.

4.5.1 Compact model

In this example, the model consists of two magnetic prisms $(400 \times 400 \times 160)$ m buried in a nonsusceptible background at different depths. Vertical and horizontal locations of prisms are shown in Figures 4.1 (a) and 4.1 (b). The 3D domain is divided into $20 \times 20 \times 18 = 7200$ cubic prisms with dimension $100 \times 100 \times 40$ m. Distances are given in meters but are arbitrary. The susceptibility of the two prisms is 0.05 SI. Under Earth's inducing field with a strength

of 50 000 nT, inclination angle $I = 75°$ and declination angle $D = 45°$, the model produces the surface total magnetic anomaly shown in Figure 4.1 (c). It consists of 400 data over a 20×20 grid of 100 m spacing. One vertical borehole is supposed to be at location ($x = 1150$ m, $y = 1050$ m) closer to the prism at the lower depth. Figure 4.1 (d) shows the magnetic field observed at the borehole.

Using the V-V plot method (Shamsipour *et al.*, 2010b) with $N_{lag} = 50$ (number of bins used in the fitting of theoretical covariances to data cross-products), we adjust the susceptibility covariance matrix $\boldsymbol{C}_{\chi\chi}$ such that experimental and theoretical covariances of the total magnetic field become similar. The adjusted susceptibility variogram model is spherical with $C = .000055$ and $a_x = 500$ m, $a_y = 500$ m, $a_z = 300$ m where C is the variogram sill and a_x, a_y and a_z are the ranges in x, y and z directions. Using this model, we calculate $\boldsymbol{C}_{\chi\chi}$, $\boldsymbol{C}_{T\chi}$ and $\boldsymbol{C}_{TT}$ covariance matrices needed for cokriging and estimate $\boldsymbol{\chi}^*$ as in Eq. (4.8). The estimated susceptibility distributions at section $y = 1050$ m are shown in Figure 4.2. The inverted model without any constraint is shown in Figure 4.2 (b). The inversion result using the depth weighting matrix ($\beta = 0.7$) is shown in Figure 4.2 (c). In Figures 4.2 (d), (e) and (f), we have used the suscebtibility of the borehole, the total field at the borehole and both the susceptibility and total field of the borehole respectively as constraints for inversion (without depth weighting). We see that these information from the borehole improves the inversion results especially for the depth resolution. The best result is obtained using both the susceptibility and the total field of the borehole as constraints shown in Figure 4.2 (f). We recall that all the illustrated solutions reproduce perfectly the observed data as indicated by Eq. (4.12). It should be mentioned even though we have used total field here, the algorithm can be easily adapted to use any magnetic component.

The inversion with the weighting matrix from surface data shows is not able to recover very well the synthetic model. The left zone appears a bit too deep and right zone too shallow.

Note that the borehole being intentionally located in the background, the measured susceptibilities are 0, but the total magnetic field in the borehole varies. Accordingly, when only the borehole susceptibilities are used (Figure 4.2 (d)), it cannot improve significantly the

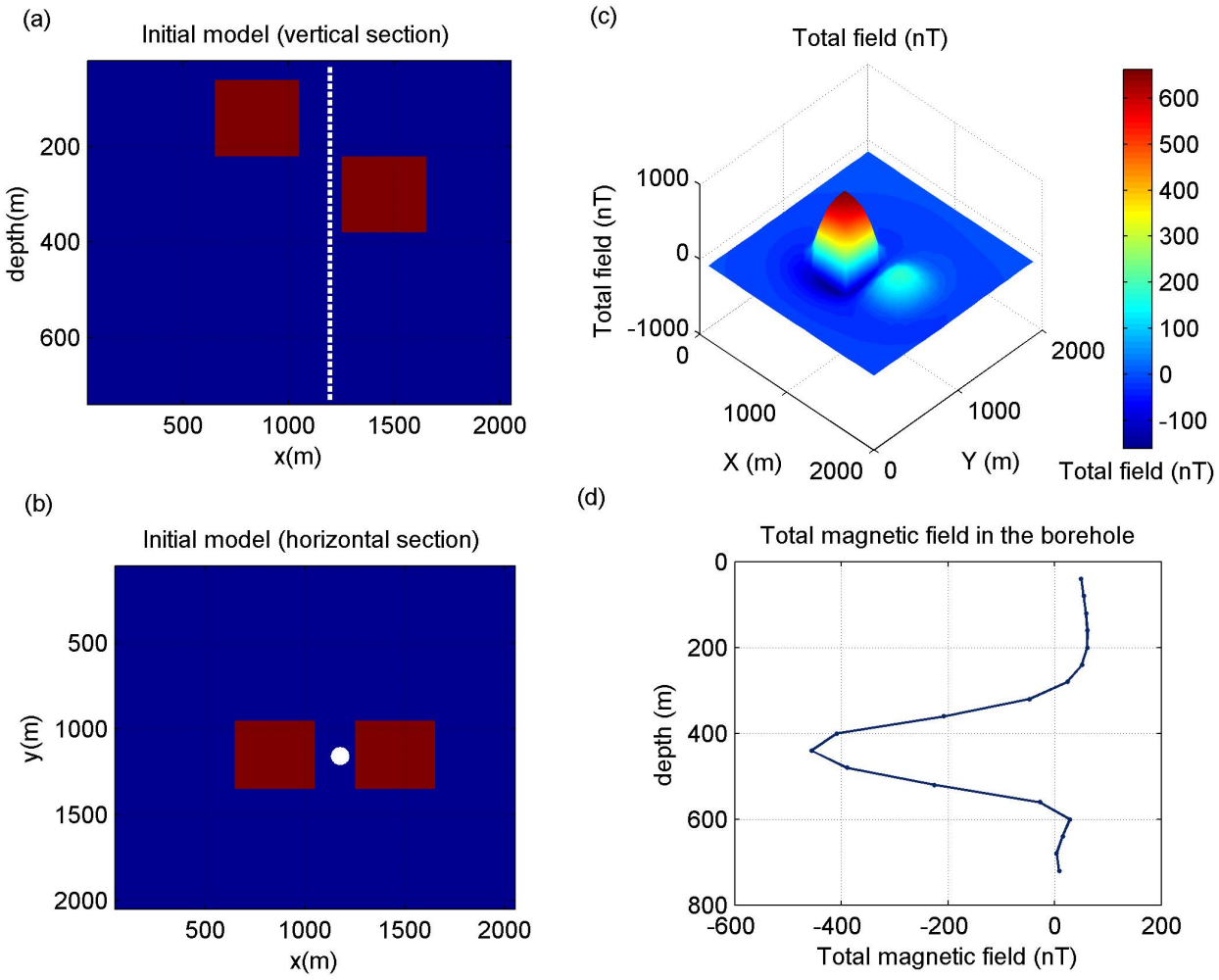

Figure 4.1 (a) Vertical locations of the prisms, (b) Horizontal locations of the prisms, (c) Total magnetic field, (d) The magnetic field produced by the model measured at the borehole.

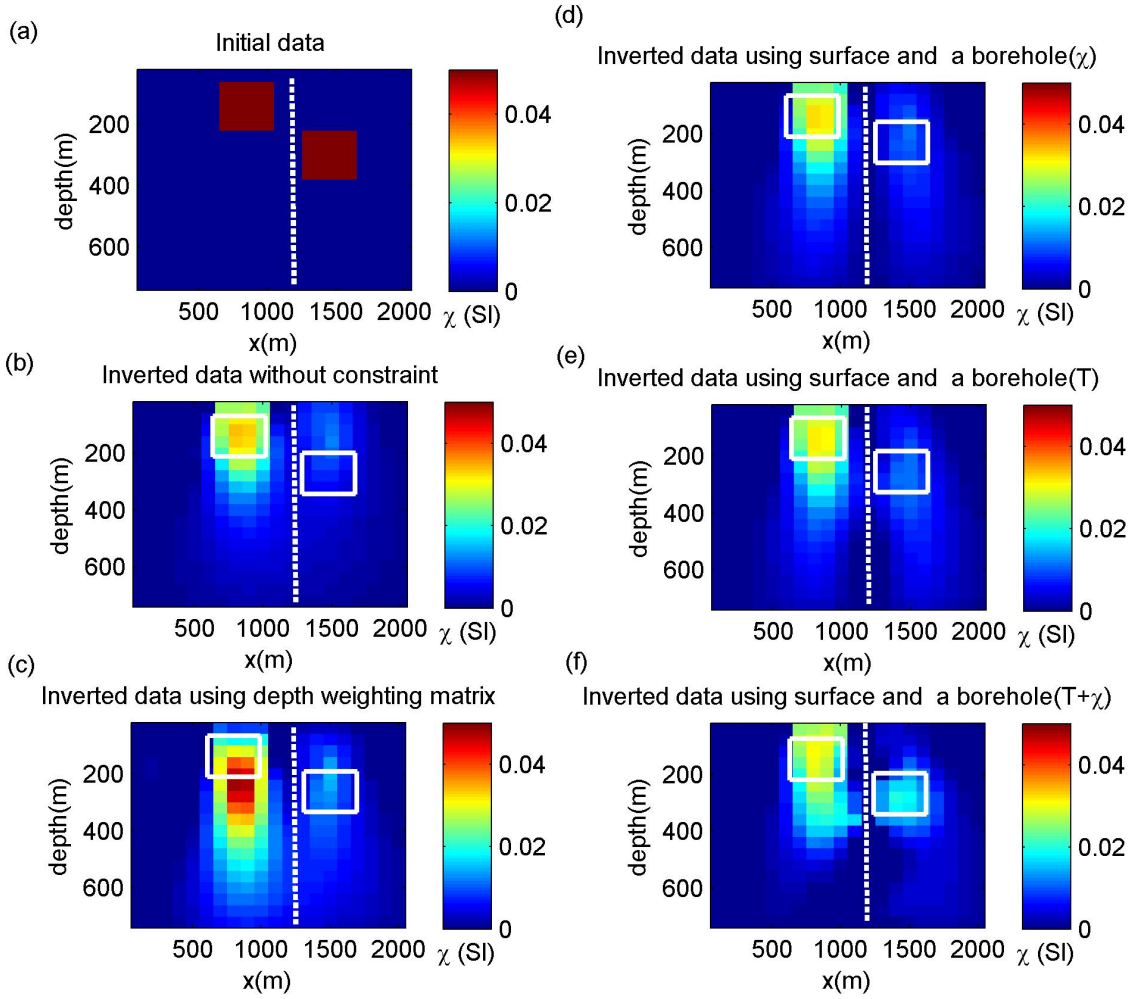

Figure 4.2 (a) Initial data, (b) Inverted data without constraints, (c) Inverted data using depth weighting matrix, (d) Inverted data using surface and a borehole (χ). (e) Inverted data using surface and a borehole (T), (f) Inverted data using surface and a borehole ($T + \chi$). All the results are shown in section $y = 1050$

inversion compared to surface data (Figure 4.2 (b)), the main difference being the zero susceptibilities in the borehole and the smaller susceptibilities in the immediate vicinity of the borehole. When borehole total magnetic field is used alone with surface data (Figure 4.2 (e)) we get slightly better results, but the susceptibilities along the borehole are not zero as they should be. When using both data, the susceptibilities along the borehole are now zero and this forces by compensation to "push" away from the borehole the non-zero susceptibilities and to increase their level. This provides the best inversion among the five tested.

4.5.2 Stochastic model

The 3D domain is divided into $20 \times 20 \times 20 = 8000$ cubic prisms. Susceptibilities on 100 m $\times$ 100 m $\times$ 40 m prisms were generated by non-conditional FFT-MA simulation using a spherical variogram model with $C = 0.0001$, $a_x = 1000$ m, $a_y = 800$ m, $a_z = 400$ m and a nugget effect of $C_0 = 0.000001$. The generated susceptibility distribution at section $y = 1050$ m is shown in Figure 4.3 (a). The Earth's inducing field has a strength of 50 000 nT and it has inclination angle $I = 45°$ and declination angle $D = 70°$. Using the susceptibility values, we calculate the synthetic total magnetic field data using equation $\boldsymbol{T} = \boldsymbol{G\chi}$ (Figure 4.4). Again, we suppose that the total magnetic field data without error are observed at the center of the top face of the surface prisms (n =400). From now on, we assume the generated magnetic total field are known and we invert them to estimate the susceptibility distribution. The adjusted susceptibility variogram model using the V-V plot method is spherical with $C = 0.00016$ and $a_x = 850$ m, $a_y = 850$ m, $a_z = 400$ m, values close to those of the parameters used to simulate the susceptibilities. The inverted data without any constraints is shown in Figure 3 (b). The inversion result using the depth weighting matrix with $\beta = 0.7$ is shown in Figure 4.3 (c). Inversions using the vertical borehole at $(x = 1050, y = 1050)$ m are shown in Figures 4.3 (d), (e) and (f) using respectively the susceptibility in the borehole, the total magnetic field and both information.

We have calculated the correlation (r) between the estimated model and the initial model. It is equal 0.5050, 0.5654, 0.5416 and 0.6211 for Figures 4.3 (b), (d), (e) and (f) respecti-

vely. As expected, cokriging provides smooth solutions and it gets more accurate as more constraints are added. The borehole information appears essential to identify the zone of low susceptibility at depth. Here, the weighting matrix approach is not useful as it pushes the central positive anomaly too deep and it does not reveal the central bottom negative anomaly. Also, depth resolution is improved using both the susceptibility and the total field of the borehole compared to using only either one of borehole information. With both data, even the highly magnetic area around $(x = 400, z = 600)$ m appears clearly in the inversion despite the measured data at surface and in borehole are quite remote from this location.

The Mean Absolute Errors (MAE) between the initial model and the estimated model without and with the constraint are 6.7×10^{-3} and 6.1×10^{-3} respectively. It confirms that adding constraints provides a better match between the estimated data and the initial data.

We simulated 60 conditional realizations of susceptibility using the susceptibilities and the total field along the borehole as constraints. Four realizations along section $y = 1050$ m are shown in Figure 4.5 (a)-(d). The four realizations were selected to show the kind of variations the solution can present given the data used for inversion. Also, cokriging variance and variance of conditional simulation realizations are shown in figure 4.6.

The results of conditional simulation can be used for calculating probability maps and non-linear functions of the model Shamsipour *et al.* (2010b). One example is the maximum susceptibility gradient norm which can be a good indicator of lithologic contact. The maximum susceptibility gradient obtained from conditional simulation is 0.0477 which is much closer to the maximum gradient of the initial model (0.0462) compared to the maximum gradient of cokriging (0.0333). As we can see, cokriging underestimates the maximum gradient norm and in such situations (nonlinear functions), conditional simulation is advantageous.

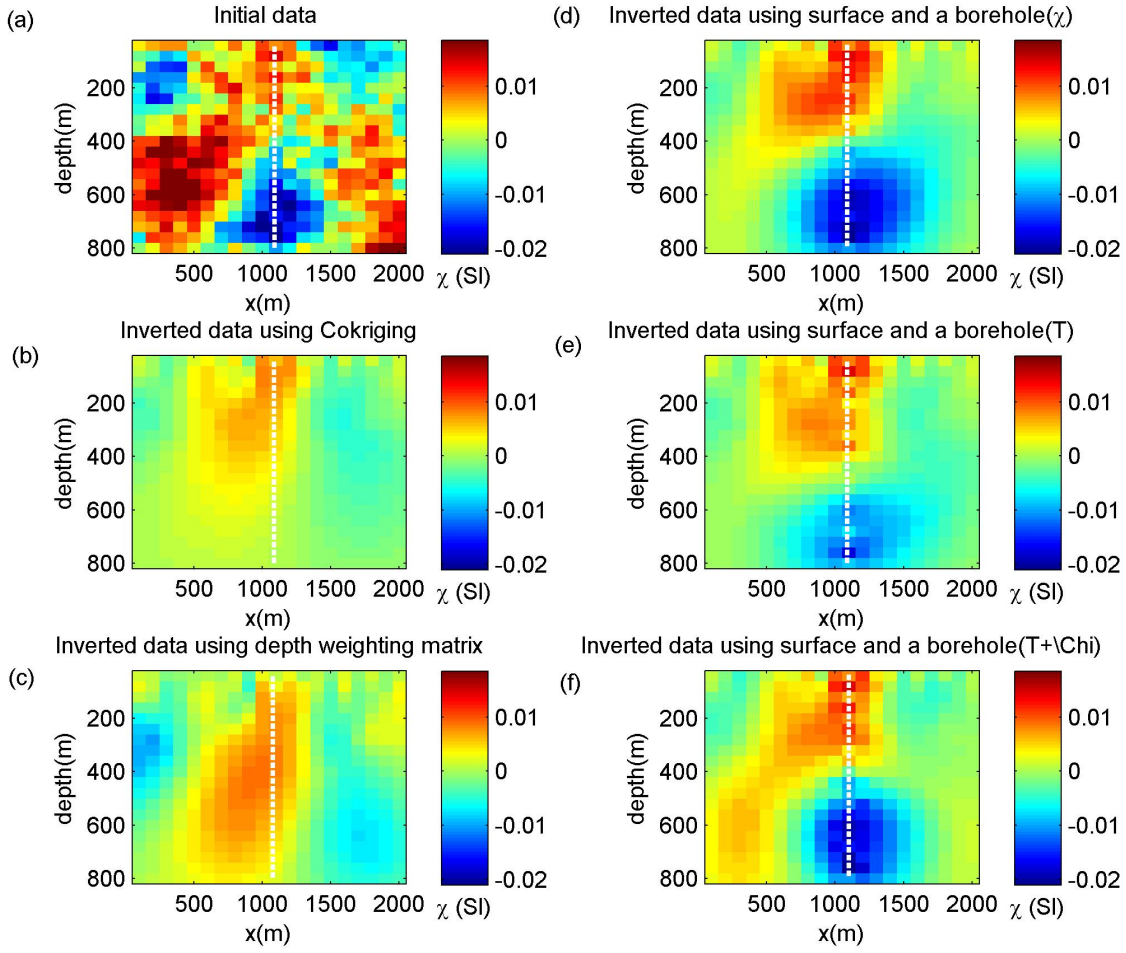

Figure 4.3 (a) Initial data, (b) Inverted data without constraints, (c) Inverted data using depth weighting matrix, (d) Inverted data using surface and a borehole (χ), (e) Inverted data using surface and a borehole (T), (f) Inverted data using surface and a borehole ($T + \chi$). All the results are shown in section $y = 1050$.

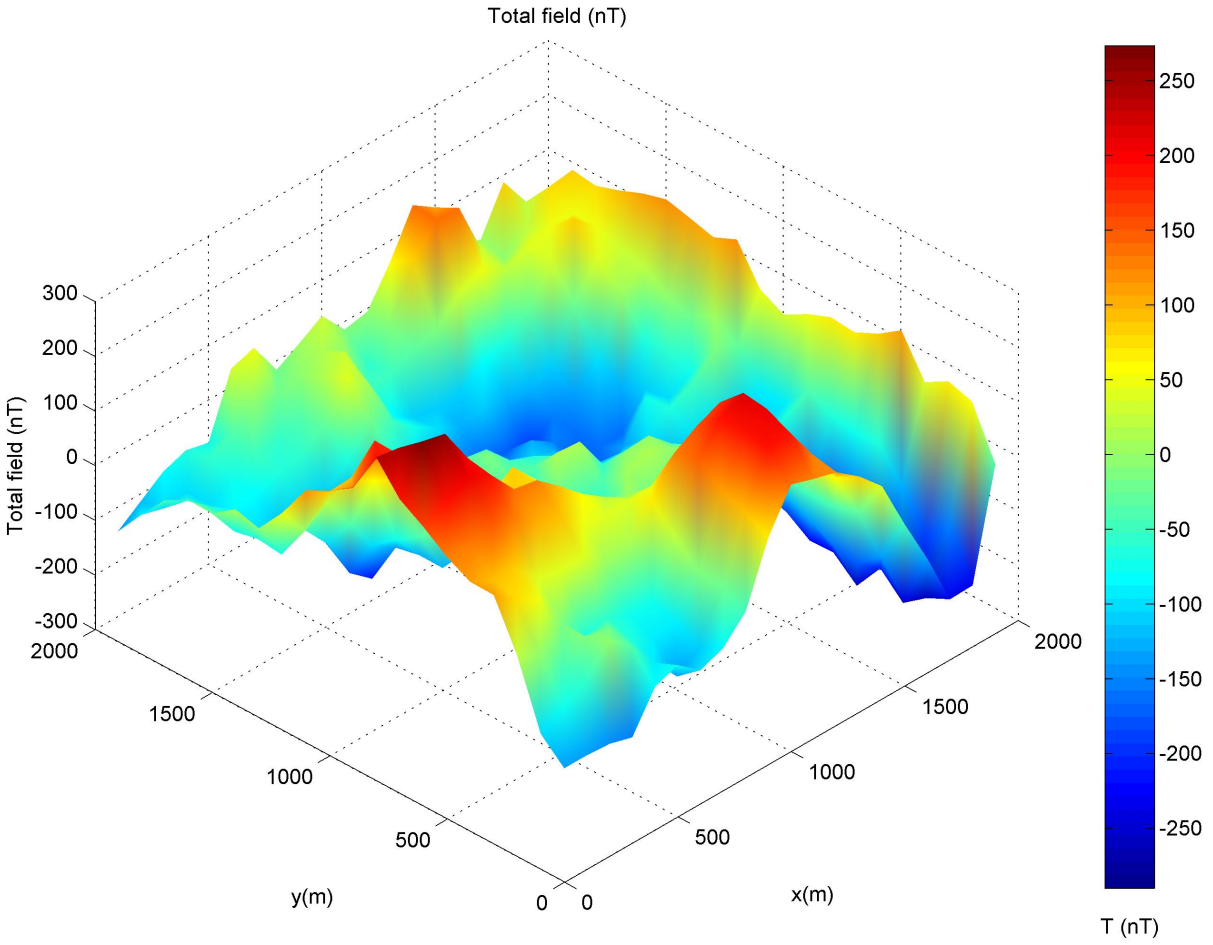

Figure 4.4 The synthetic total magnetic field data

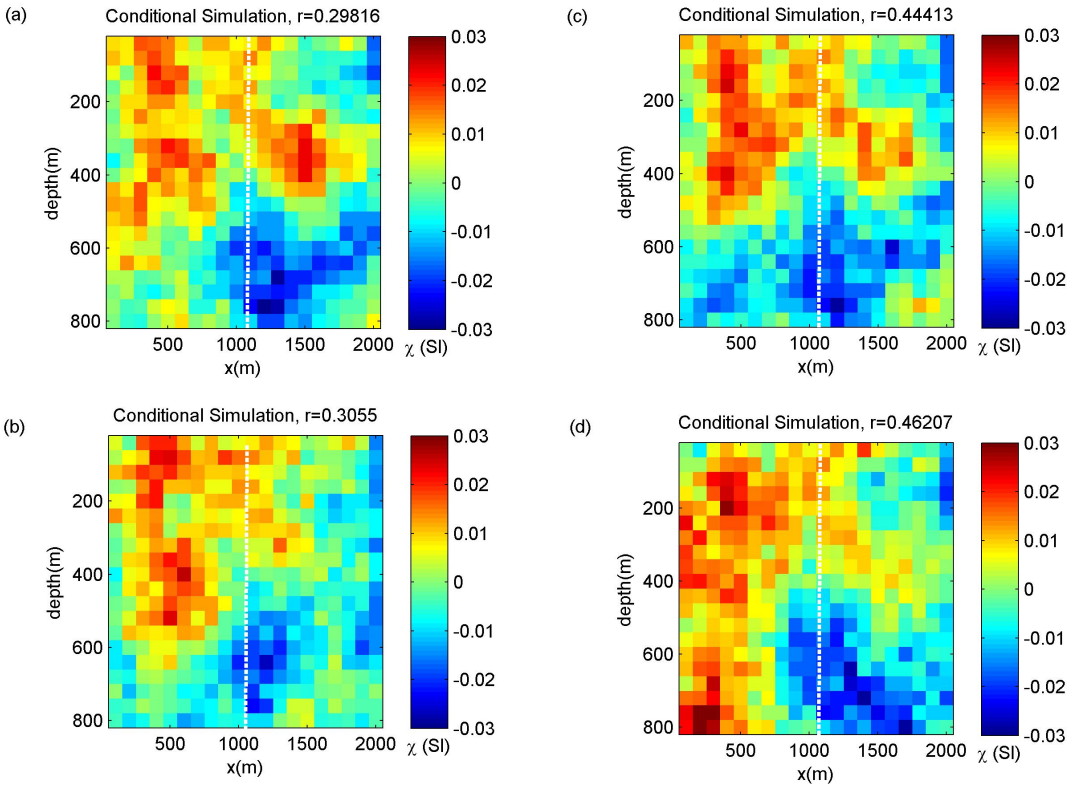

Figure 4.5 Four realizations of conditional simulated susceptibilities at section $y = 1050$ m with borehole susceptibilities and total field data as constraints.

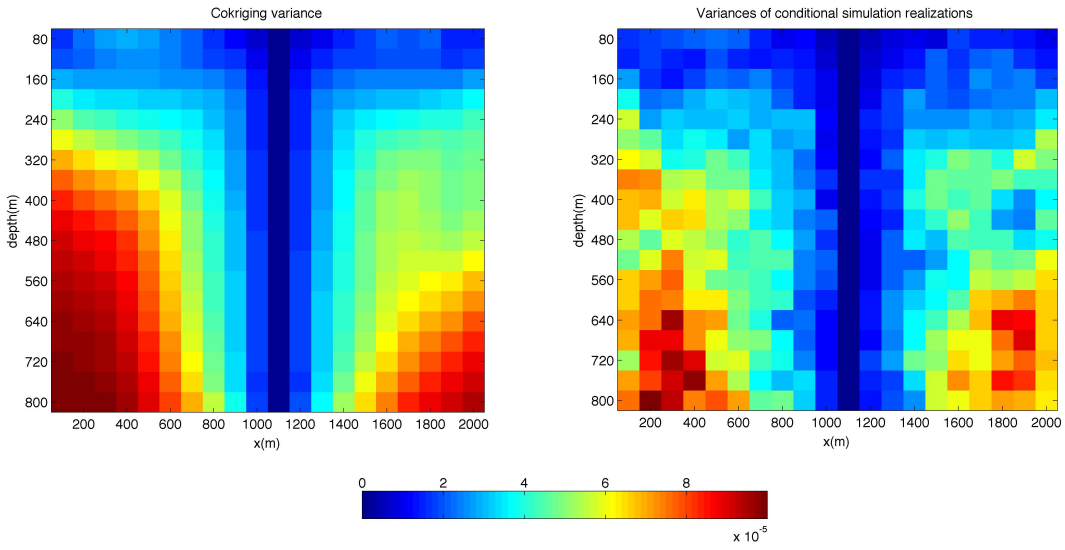

Figure 4.6 Cokriging variance and variance of conditional simulation realizations for synthetic stochastic model.

4.6 Case study

4.7 Application to Survey Data

The survey data was collected over the area of the Perseverance mine located in the Matagami region in Québec, Canada. The area of the 2001 total magnetic field survey extends from longitude 77° 47′ 46” W to 77° 46′ 59” W and from latitude 49° 45′ 13” N to 49° 45′ 59” N, where 2550 magnetic ground measurements with about a 20-m spacing were measured.

The study area is located in the northern part of the Abitibi Sub-province, one of the largest Archean greenstone belts in the world. Many volcanogenic massive sulfide (VMS) deposits have been identified in the Archean-age Abitibi greenstone belt, which is located on the border of the province of Ontario and Québec. The Matagami volcanic complex of northern Abitibi belt is formed by two major phases of volcanism (Piché *et al.*, 1993) :

– the initial phase was dominated by the extrusion of tholeiitic rhyolite and rhyodacite lavas (the Watson Lake Group)

– the second phase was distinguished primarily by calcalkaline basaltic to andesitic volcanism (the Wabassee Group)

A cherty, sulphidic chemical sediment known as the Key Tuffite marks the contact and discontinuity between the two groups. This thin horizon is the primary exploration target because it hosts most of the ore bodies discovered in the area (Calvert et Li, 1999). Exploration of the Key Tuffite by systematic drilling is very expensive especially with increasing depth, thus use of geophysical methods can be a very efficient solution. Exploration of VMS deposits lead to the opening of 11 mines. The largest mine was the Mattagami Lake mine with a total production of 25.64 Mt ore. A new discovery has been made by Xstrata Zinc Canada in 2007, the Bracemac-McLeod deposit, which is expected to be in production in 2013.

The Perseverance mine has been discovered in April 2000, a feasibility study was done in 2002 but did not enter production before 2008 due to the depressed zinc market. It is the only active mine in the study area. This mine consists of three major massive sulfide deposits, Perseverance, Perseverance west and Equinox shown in Figure 4.7 with A, C and B respectively. The Perseverance deposit has a total production of 1.2 MT (14.55% Zn and 1.20% Cu). Estimates for the Perseverance west deposit and the Equinox deposit are 1.1 MT (12.61% Zn and 1.38% Cu) and 2.5 MT (14.93% Zn and 0.98% Cu) respectively. Magnetite and pyrrhotite are often associated with the VMS deposits. For Perseverance lenses, the magnetic anomalies are mainly caused by the magnetite anomaly even if the pyrrhotite can have some local contribution.

4.7.1 Inversion

The residual anomaly was obtained by subtracting the IGRF from the measured total field. Knowing the total magnetic field residual anomalies (Figure 4.8), we use inversion by cokriging to estimate the susceptibility model. The inversion domain is divided into $n_x = 50$ by $n_y = 51$ by $n_z = 10$ cubes of dimension 20 m $\times$ 20 m $\times$ 25 m. Therefore, the whole domain is 1200 m $\times$ 1000 m $\times$ 250 m and the total number of prisms is $m = 25500$.

The adjusted susceptibility variogram model using the V-V plot method is anisotropic

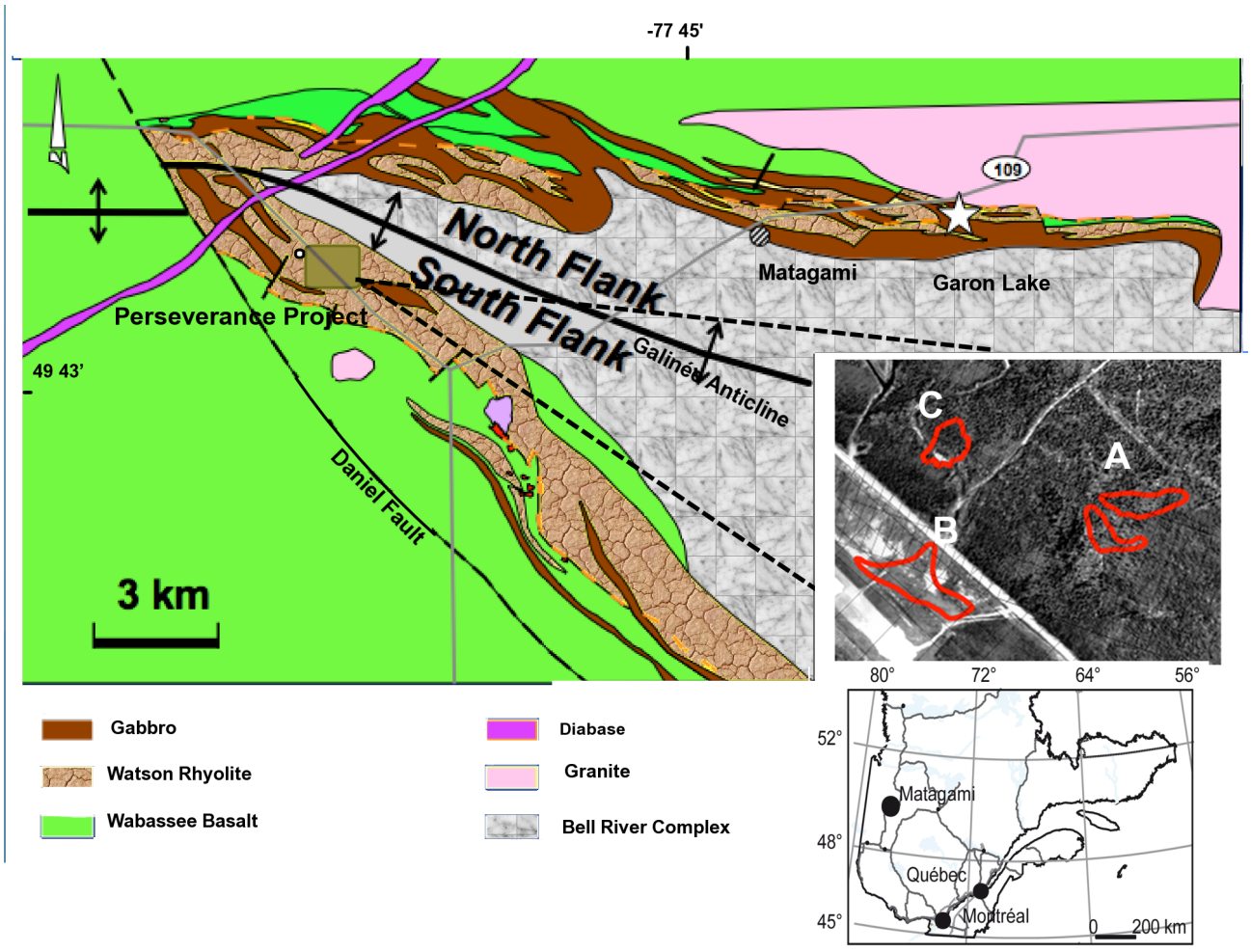

Figure 4.7 Geology map of Matagami camp with Perseverance mine highlighted.

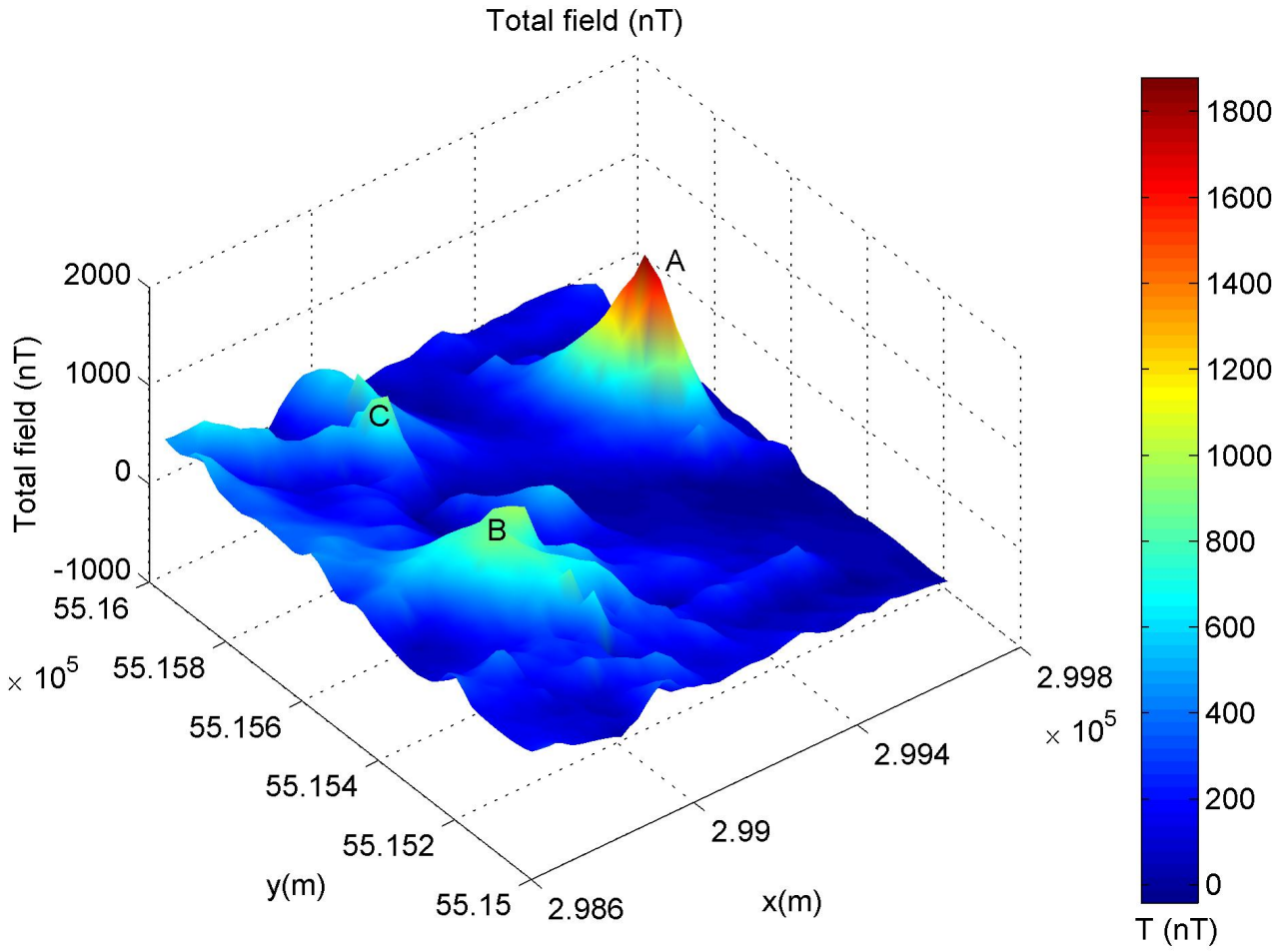

Figure 4.8 The total magnetic field residual anomalies from the studied area.

and spherical with $C_0 = 0.000001$, sill $C = 0.0003$ and ranges $a_x = 157$ m, $a_y = 294$ m and $a_z = 150$ m. The estimated susceptibilities by cokriging are actually susceptibility contrasts. A North-South section at $x = 298800$ m, an East-West section at $y = 5515600$ m and two horizontal sections at $z = 70$ m and $z = 100$ m are shown in Figure 4.9 (a)-(d). Three concentrated susceptibility highs are seen in the plane sections ($z = 70$ and $z = 40$). Comparing with the geology of the domain, they are correlated with three Perseverance deposits indicated in Figure 4.7. The largest susceptibility high is correlated with Perseverance deposit (A), the smallest susceptibility high is correlated with Perseverance west deposit (C) and the third susceptibility high is related to Equinox deposit (B). The cross section $y = 5515600$ m shows the extension of Perseverance deposit in the depth while the cross section $x = 298800$ m shows the extension of Perseverance West and Equinox deposits. In general, as expected in any inversion method, the structure near the surface is more detailed and it gets increasingly smooth at greater depths. In our case, all the three deposits tend to push upward in z direction because of the kernel decay. In order to compensate the tendency of the structure to lay near the surface, we have also performed cokriging with depth weighting. The inversion results are shown in Figure 4.10 (a)-(d). From cross sections $x = 298800$ m and $y = 5515600$ m shown in Figure 4.10 (a) and (b), we can see that the Perseverance deposit is approximately located at $z = 100$ m while the Perseverance West and the Equinox deposits are at depth $z = 125$ m. Comparing these results with the real location of the deposits (Persevrance : 30m-200m P-West : 100m-200m ; Equinoxe : 90m-275m) in perseverance mine (personal communications with Michel Allard, Xstrata Company) shows the positive effect of depth weighting in recovering the depth of deposits. However, the extension of deposits is a bit exaggerated. We should mention that depth weighting is an empirical method and the results can not always be trusted. For depth resolution, we strongly recommend using the borehole information.

In order to see the possible variabilities of the recovered model, different realizations of conditional simulation at $z = 70$ m are shown in Figure 4.11 and 4.12 (with depth weighting). All the three deposits (A, B and C) are recognizable in almost all the realizations. As indicated

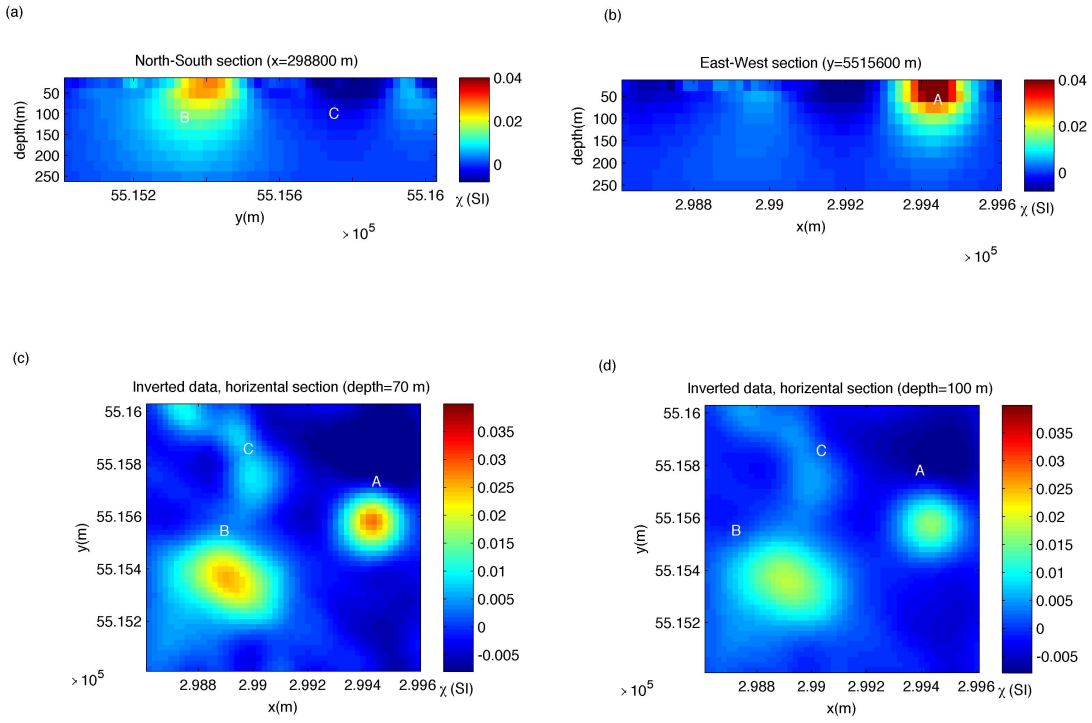

Figure 4.9 Estimated susceptibilities using cokriging : (a) North-South section at $x = 298800$ m, (b) East-West section at $y = 5515600$ m, (c) horizontal section at $z = 70$ m and (d) horizontal section at $z = 100$ m.

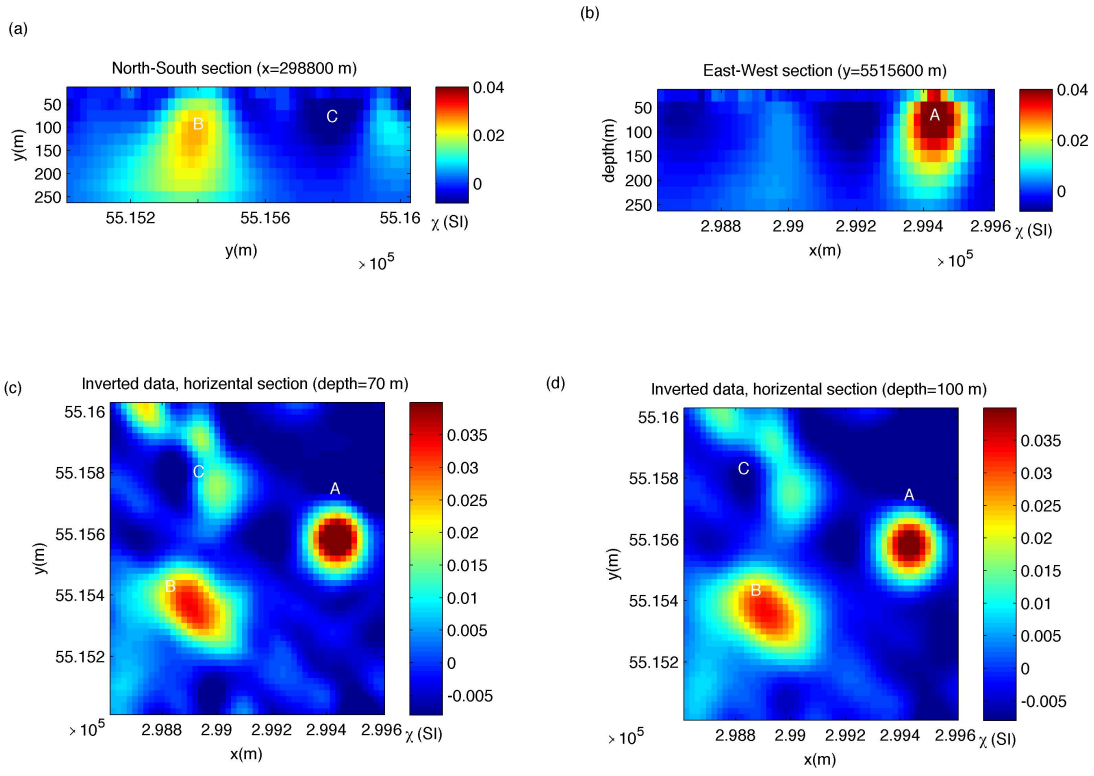

Figure 4.10 Estimated susceptibilities using cokriging with the depth weighting matrix : (a) North-South section at $x = 298800$ m, (b) East-West section at $y = 5515600$ m, (c) horizontal section at $z = 70$ m and (d) horizontal section at $z = 100$ m.

in Eq. (4.12), all these realizations recover the observed data precisely. Similarly to the synthetic case, we use the results of cosimulation to calculate the maximum gradient (1.99×10^{-3}). We expect that the maximum gradient of the actual model to be closer to this value than to the maximum gradient calculated from cokriging estimates (1.48×10^{-3}).

4.8 Discussion

The synthetic examples have shown that the weighting matrix approach can be useful essentially to push the anomalies deeper, but by no means can it be considered as a surrogate to real information found in the boreholes. The latter is essential to better "see" the geological structures at depth. One interesting finding is that the observation of the primary variable in the borehole (susceptibility) does not contain the same useful information as the observation of the total magnetic field. It is when using jointly both information in boreholes that best inversion results were obtained. The two informations are therefore complementary to one another rather than duplicating. Cokriging offers a rigorous approach to integrate both informations in a useful and simple way.

While cokriging produces one smooth solution to the underdetermined problem, we can make use of cosimulation to generate a set of equally possible solutions. The purpose is to recreate the spatial variability of the real susceptibility field. One important use of simulation is to generate scenarios as input for non-linear functions applied on the field. This ability of conditional simulation is further discussed in Shamsipour *et al.* (2010b).

The proposed non-iterative inversion method based on cokriging and cosimulation is computationally efficient. The algorithm can easily accommodate noise (observation error) in the form of nugget effect C_0 and is stable to the presence of data noise. As shown in synthetic example, the algorithm enables us to integrate easily any known constraints. Covariance matrix of parameters is the largest matrix ($m \times m$, m number of parameters) in solving cokriging system equations. Using the full matrix is expensive both in computing time and memory. When dealing with small compact ore body such as massive sulphides, the range of the variogram is likely to be small. Therefore, most covariances in $C_{\chi\chi}$ are 0 and sparse

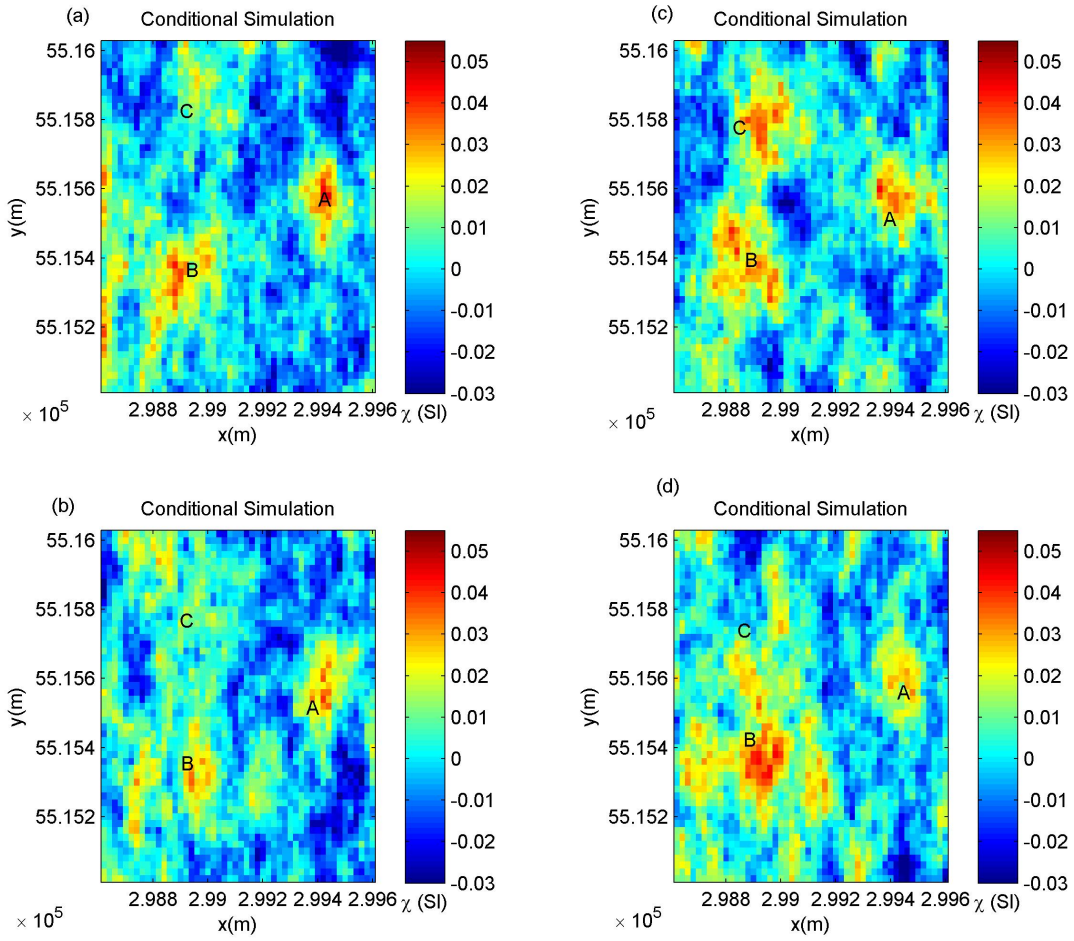

Figure 4.11 Four different realizations of conditional simulation in horizontal section at $z = 70$ m.

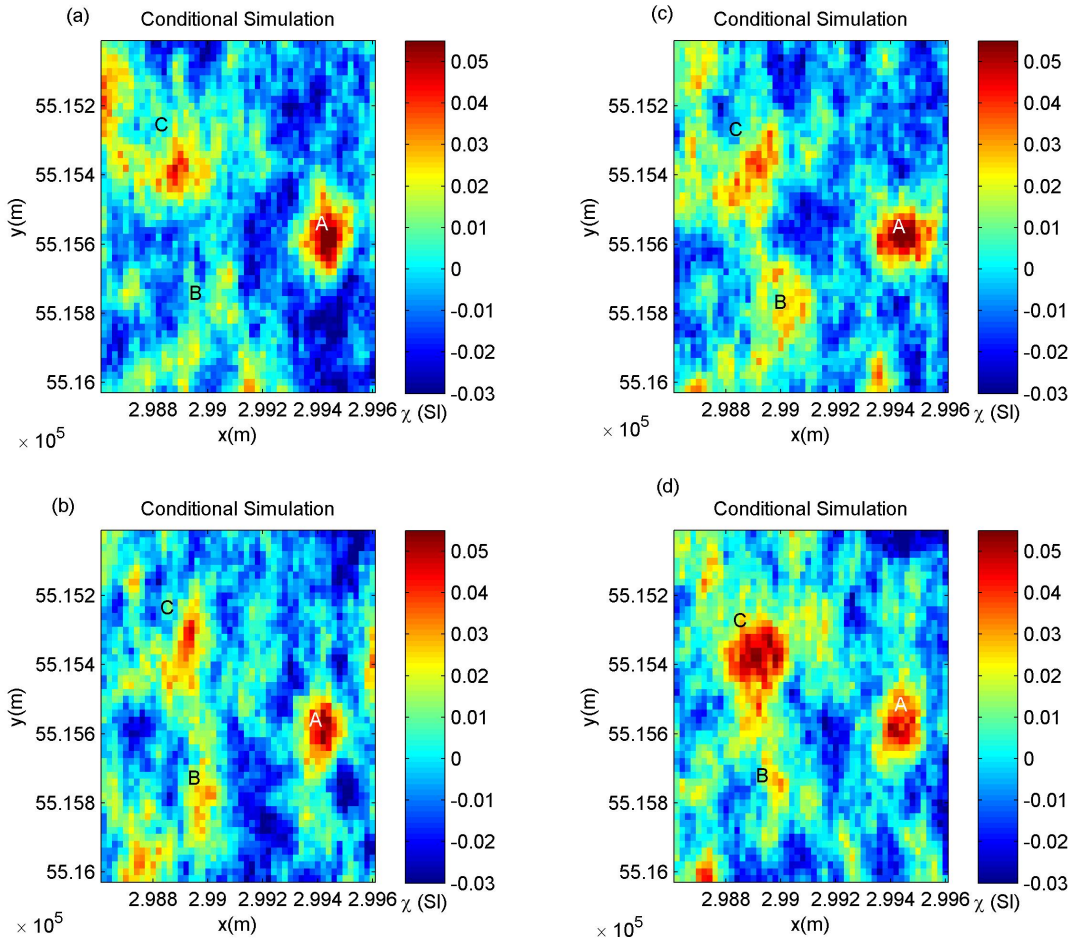

Figure 4.12 Four different realizations of conditional simulation with depth weighting matrix in horizontal section at $z = 70$ m.

matrix techniques can be used to solve efficiently the cokriging equations. Use of sparsity in cokriging system is shown in a simple example in appendix 4.11.

Cokriging inversion of real data has generated a susceptibility model that is consistent with the known geology and mineralization information. We assume there is no remanent magnetization. This assumption is valid, as a first approximation, for the Archean rocks in Québec. The method is adaptable for other geological contexts. Over all, despite the nonuniqueness of magnetic inversion in the presence of a large number of cells, by adjusting a proper variogram model the proposed method can generate susceptibility distributions with meaningful geologic information.

4.9 Conclusion

We introduce an inversion method based on a geostatistical approach (cokriging) for three dimensional inversion of total magnetic field data. The method was adapted to include the depth weighting matrix approach to reduce the lack of resolution in depth. However, it was shown that the weighting matrix approach does not compensate for valid data in borehole at depth. Moreover, both borehole susceptibility and total magnetic field data were shown to be complimentary information for the inversion. Therefore, they both need to be measured in boreholes to get the best inversion results. Finally, conditional simulation approach was applied to evaluate uncertainty of the solutions. The proposed method is tested on real data from Matagami mining camp (Perseverance mine) where the results of inversion prove in agreement with the known geology.

4.10 Acknowledgments

We would like to express sincere thanks to Michel Allard from Xstrata Zinc for providing the Matagami data, and for his guidance and support.

4.11 Appendix : A simple test on using sparse matrix

We assume a 3D domain divided into $20 \times 20 \times 20 = 8000$ cubic prisms. Susceptibilities on 1 m $\times$ 1 m $\times$ 0.2 m prisms were generated by non-conditional FFT-MA simulation using a spherical variogram model with $C = 0.0001$, $a = 4$ m and a nugget effect of $C_0 = 0.000001$. We suppose the domain is under an inducing field with a strength of 50 000 nT, inclination angle $I = 45^\circ$ and declination angle $D = 70^\circ$. We investigate the effect of sparsity of model covariance matrix when threshold is equal to the range and when it is 0.8 times the range. In fact, we can not apply a threshold directly to the covariance matrix because it is not guarantied to generate a positive definite matrix. Here, when we say threshold is equal to 0.8 range, it means generating a covariance matrix with range of $0.8 \times 4 = 3.2$ m.

The inversion results are shown in Figure 4.13. As we expected, when the threshold is equal to the range (Figure 4.13 (c) and (e)), there is no change in the inversion results. In the case that the threshold is 0.8 times the range (Figure 4.13 (d) and (f)), there is an acceptable correlation between the estimated susceptibilities with and without threshold (r=98.59%). Also Table 4.1 shows the required memory for model covariance matrix in each case and compare it with the case of non-sparse covariance matrix. It can be seen that sparsity saves considerable memory.

Table 4.1 The required memory for model covariance matrix

Covariance matrix	Size	Memory (mega bytes)	Class
Non-sparse	8000× 8000	512	double
Sparse (threshold=range)	8000× 8000	87.8	double
Sparse (threshold=0.8× range)	8000× 8000	43.41	double

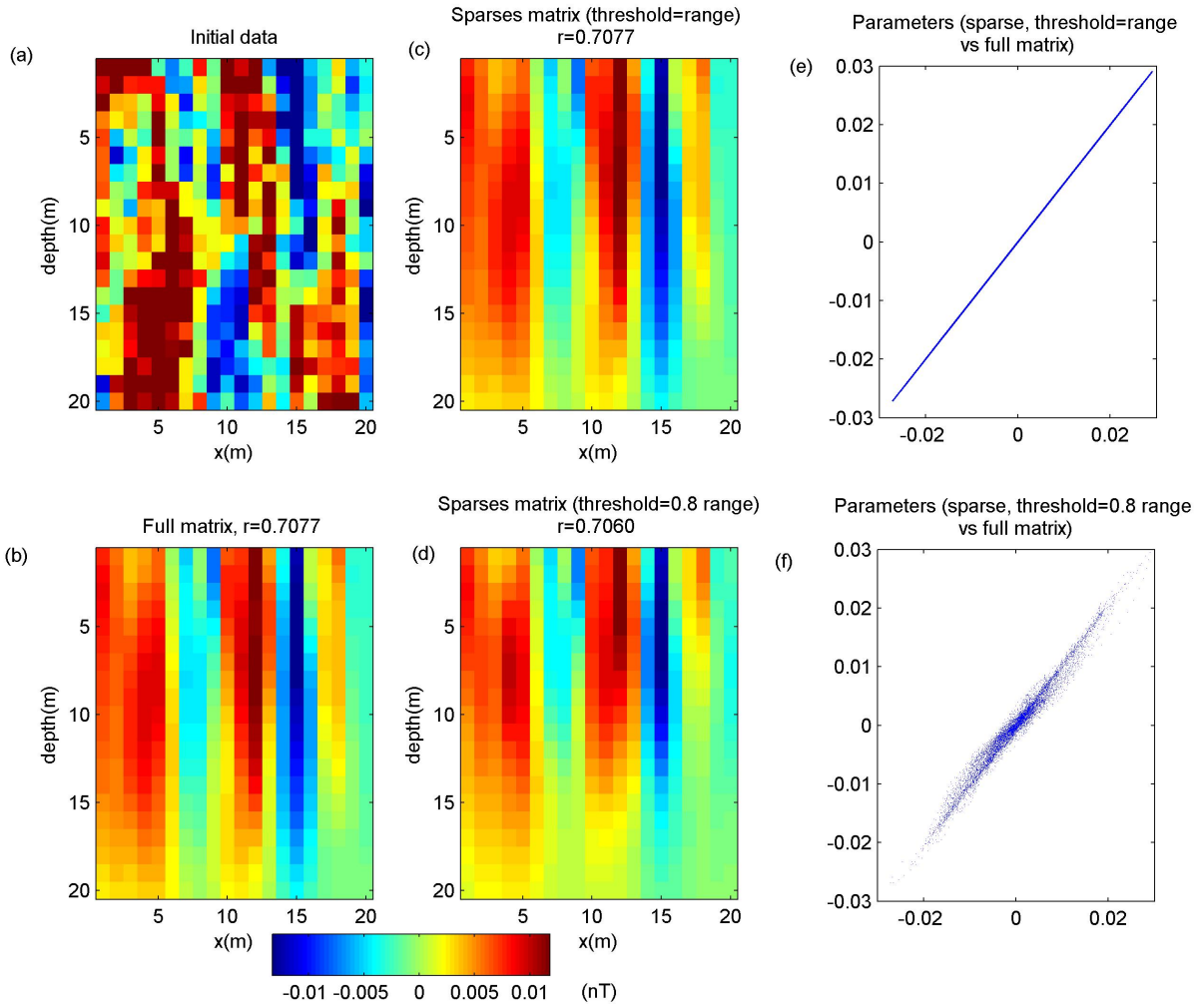

Figure 4.13 (a) Initial model, (b) Inversion using non-sparse matrix, (c) Inversion using sparse matrix, threshold=range, (d) Inversion using sparse matrix, threshold=0.8 range, (e) Inverted susceptibilities (sparse, threshold=range versus full matrix), (f) Inverted susceptibilities (sparse, threshold=0.8 range versus full matrix).

References

ASLI, M., MARCOTTE, D. et CHOUTEAU, M. (2000). Direct inversion of gravity data by cokriging. W. Kleingeld et D. Krige, éditeurs, *6th International Geostatistics Congress, Cape town, South Africa*, Cape Town, South Africa. 64–73.

BHATTACHARYYA, B. (1964). Magnetic anomalies due to prism-shaped bodies with arbitrary polarization. *Geophysics*, 29, 517.

BLAKELY, R. (1995). *Potential Theory in Gravity and Magnetic Applications*. Cambridge University Press.

BOSCH, M. et MCGAUGHEY, J. (2001). Joint inversion of gravity and magnetic data under lithologic constraints. *The Leading Edge*, 20, 877–881.

BOSCH, M., MEZA, R., JIMÉNEZ, R. et HÖNIG, A. (2006). Joint gravity and magnetic inversion in 3D using Monte Carlo methods. *Geophysics*, 71, G153.

BOULANGER, O. et CHOUTEAU, M. (2001). Constraints in 3D gravity inversion. *Geophysical Prospecting*, 49, 265 – 280.

CALVERT, A. et LI, Y. (1999). Seismic reflection imaging over a massive sulfide deposit at the Matagami mining camp, Québec. *Geophysics*, 64, 24–32.

CHASSERIAU, P. et CHOUTEAU, M. (2003). 3D gravity inversion using a model of parameter covariance. *Journal of Applied Geophysics*, 52, 59 – 74.

CHILÈS, J. et DELFINER, P. (1999). *Geostatistics : modeling spatial uncertainty*. Wiley.

FRANKLIN, J. (1970). Well posed stochastic extensions of Ill posed linear problems. *J. Math*, 31, 682–716.

FREGOSO, E. et GALLARDO, L. (2009). Cross-gradients joint 3D inversion with applications to gravity and magnetic data. *Geophysics*, 74, L31.

GIROUX, B., GLOAGUEN, E. et CHOUTEAU, M. (2007). bh_tomo–a Matlab borehole georadar 2D tomography package. *Computers and Geosciences*, 33, 126–137.

GLOAGUEN, E., MARCOTTE, D., CHOUTEAU, M. et PERROUD, H. (2005). Borehole radar velocity inversion using cokriging and cosimulation. *Journal of Applied Geophysics*, 57, 242 – 259.

GLOAGUEN, E., MARCOTTE, D., GIROUX, B., DUBREUIL-BOISCLAIR, C., CHOUTEAU, M. et AUBERTIN, M. (2007). Stochastic borehole radar velocity and attenuation tomographies using cokriging and cosimulation. *Journal of Applied Geophysics*, 62, 141 – 157.

GOMEZ-HERNANDEZ, J., FROIDEVAUX, R. et BIVER, P. (2004). Exact conditioning to linear constraints in kriging and simulation. O. Leuangthong et C. V. Deutsch, éditeurs, *Gestatistics Banff 2004*, Springer, Berlin.

HANSEN, T., JOURNEL, A., TARANTOLA, A. et MOSEGAARD, K. (2006). Linear inverse Gaussian theory and geostatistics. *Geophysics*, 71, R101.

JOURNEL, A. et HUIJBREGTS, C. (1978). *Mining Geostatistics* . Academic Press, London.

LE RAVALEC, M., NOETINGER, B. et HU, L. (2000). The FFT Moving Average (FFT-MA) Generator : An Efficient Numerical Method for Generating and Conditioning Gaussian Simulations. *Mathematical Geology*, 32, 701–723.

LI, Y. et OLDENBURG, D. (1996). 3-D inversion of magnetic data. *Geophysics*, 61, 394–408.

MYERS, D. (1982). Matrix formulation of co-kriging. *Mathematical Geology*, 14, 249–257.

PICHÉ, M., GUHA, J. et DAIGNEAULT, R. (1993). Stratigraphic and structural aspects of the volcanic rocks of the Matagami mining camp, Quebec ; implications for the Norita ore deposit. *Economic Geology*, 88, 1542–1558.

PILKINGTON, M. (1997). 3-D magnetic imaging using conjugate gradients. *Geophysics*, 62, 1132–1142.

RAO, D. et BABU, N. (1991). A rapid method for three-dimensional modeling of magnetic anomalies. *Geophysics*, 56, 1729.

SHAMSIPOUR, P., MARCOTTE, D. et CHOUTEAU, M. (2010a). 3D stochastic inversion of borehole and surface gravity data using Geostatistics. Capri, Italy.

SHAMSIPOUR, P., MARCOTTE, D., CHOUTEAU, M. et KEATING, P. (2010b). 3D stochastic inversion of gravity data using cokriging and cosimulation. *Geophysics*, 75, I1–I10.

TARANTOLA, A. et VALETTE, B. (1982). Generalized nonlinear inverse problems solved using the least squares criterion. *Rev. Geophys. Space Phys*, 20, 219–232.

CHAPITRE 5

Article 2 : STOCHASTIC INVERSION OF GRAVITY FIELD ON MULTIPLE SCALE PARAMETERS USING SURFACE AND BOREHOLE DATA

Article history : Submitted 30 November 2010, Accepted 18 April 2011, Published online 5 July 2011, Journal of geophysics prospecting.

Authors : Pejman Shamsipour, Denis Marcotte, Michel Chouteau and Michel Allard .

5.1 Abstract

A 3D stochastic inversion method based on a geostatistical approach is presented for three-dimensional inversion of gravity on multiple scale parameters using borehole density and gravity and surface gravity. The algorithm has the capability of inverting data on multiple supports. The method involves four main steps : i. upscaling of borehole densities to block densities, ii. selection of block densities to use as constraints, iii. inversion of gravity data with selected block densities as constraints, and iv. downscaling of inverted densities to small prisms. Two modes of application are presented : estimation and simulation. The method is first applied to a synthetic stochastic model. The results show the ability of the method to invert surface and borehole data simultaneously on multiple scale parameters. The results show the usefulness of borehole data to improve depth resolution. Finally, a case study using gravity measurements at the Perseverance mine (Quebec, Canada) is presented. The recovered 3D density model identifies well three known deposits and it provides beneficial information to analyze the geology of massive sulfide for the domain under study.

5.2 Introduction

Geophysical inversion of potential field is impeded because of the intrinsic non-uniqueness of the solution. Many strategies can be used to deal with the non-uniqueness problem in gravity inversion. They all involve some kind of constraints or regularization to limit the solutions. Smoothness and roughness of density distribution which control gradients of parameters in spatial directions are used in magnetic inversion by Pilkington (1997). Li et Oldenburg (1996) propose a generalized 3D inversion of gravity data. Their solutions are based on minimization of a global objective function composed of the model objective function and data misfit. Li et Oldenburg (1996) counteract the decreasing sensitivities of cells with depth by weighting with an inverse function of depth. Another 3D inversion technique proposed by Fedi et Rapolla (1999) allows the definition of depth resolution.

Linear stochastic inversion was originally introduced by Franklin (1970) and then simplified and popularized in geophysics by Tarantola et Valette (1982). Geostatistical methods in geophysical inversion were applied by Asli *et al.* (2000), Gloaguen *et al.* (2005, 2007), Giroux *et al.* (2007), Hansen *et al.* (2006), and Gomez-Hernandez *et al.* (2004). Bosch et McGaughey (2001) and Bosch *et al.* (2006) also used Monte Carlo techniques in gravity inversion for generating a posterior probability density function describing acceptable models. Chasseriau et Chouteau (2003) advocate 3D inversion of gravity data using an a priori model of covariance. Shamsipour *et al.* (2010b) proposed geostatistical techniques of cokriging and conditional simulation for the three-dimensional inversion of gravity data including geological constraints. They assumed all densities were known on a block support. However, in inversion of gravity data, one often needs to integrate a large diversity of data with different support volumes which convey information at different scales. In mineral exploration, it is crucial to use fine scale support data such as densities coming from drill cores to constrain the subsurface structures. Any mapping of densities should include all relevant information from different supports. Liu et journel (2009) proposed a method for integration of coarse and fine scale data built on a combination of kriging using both point and block data with

direct sequential simulation or error simulation.

In this paper, we extend the geostatistical algorithm proposed for gravity inversion by Shamsipour *et al.* (2010b) to multiscale inversion. Contrary to Shamsipour *et al.* (2010b), here the basic density covariance model is assumed to be known on the point scale rather than the block scale. All the required block-block and block-point covariances are computed by numerical integration. This ensures full coherency of the estimated or simulated densities at any scale. The same basic steps are followed for cokriging and cosimulation : i. upscaling of densities from borehole measurements to large blocks (block kriging or conditional cosimulation), ii. selection of block densities to use as constraints in the inversion, iii. joint inversion using block density constraints and gravity data (on surface and, if available, in boreholes), and iv. downscaling of the inverted large block densities to the small prisms. Step ii enables us to select as constraints only the blocks that are best informed by the boreholes. A threshold on the block density kriging variance is used for this selection. With a low threshold few blocks are selected as constraints so the joint inversion is mostly gravity-driven. A higher threshold selects more blocks as constraints and the resulting inversion becomes more borehole-density driven.

Inversions with and without large block density constraints are compared on a stochastic synthetic model. Inversions by both cokriging and cosimulation are applied. Inversions are done on a large scale (blocks) and then downscaled (prisms). The results show the ability of the method to integrate complex a priori information. Finally, the survey data collected over the Perseverance deposits of the Matagami mining camp (Quebec, Canada) are considered as a case study. To the authors' knowledge, this is the first time that cokriging and conditional simulations are applied for inversion of gravity data on multiscale parameters.

5.3 Methodology

5.3.1 Forward modeling

The purpose of forward modeling is to compute the gravimetric response $\boldsymbol{g}$ at the surface due to a subsurface density distribution $\boldsymbol{\rho}$. The most common method of evaluating the gravity response from the density based on Newton's law is to break down the 3D domain into geometrically simple bodies having constant density. In our case, and for the sake of simplicity, the domain studied is divided into a finite number of rectangular prisms of constant density. Considering that there are n gravity observations and m rectangular prisms, their relationship can be written in the following matrix form :

$$\boldsymbol{g}_{n\times 1} = \boldsymbol{G}_{n\times m}\boldsymbol{\rho}_{m\times 1} \tag{5.1}$$

with $\boldsymbol{G}$, the matrix of the geometric terms. The components of this matrix are obtained using the formula of Haáz (1953). Each row of this matrix shows the effect of all prisms on one observation point (Shamsipour *et al.*, 2010b). In the case when observation errors (e) are present, we have

$$\boldsymbol{g}_{obs} = \boldsymbol{g} + \boldsymbol{e}. \tag{5.2}$$

5.3.2 Cokriging

In geostatistics, cokriging (Myers (1982), Chilès et Delfiner (1999)) uses the spatial correlation between the secondary variables and a primary variable in order to interpolate or extrapolate primary variable at unsampled locations. The cokriging method gives weights to data so as to minimize the theoretical estimation variance (the cokriging variance).

In this paper, the primary variable is density ($\boldsymbol{\rho}$, estimated by $\boldsymbol{\rho}^*$) and the secondary variable is gravity ($\boldsymbol{g}$). $\boldsymbol{\rho}$ and $\boldsymbol{g}$ are multidimensional random variables. Assuming spatial homogeneity of the mean for the density and gravity field i.e., $E[\boldsymbol{\rho}] = E[\boldsymbol{g}] = 0$, the estimation variances can be calculated from Myers (1982). Minimization of the estimation variance yields

the simple cokriging solution :

$$\boldsymbol{C}_{gg}\boldsymbol{\Lambda} = \boldsymbol{C}_{g\rho} \tag{5.3}$$

where $\boldsymbol{C}_{gg}$ is the gravity covariance matrix, $\boldsymbol{C}_{\rho\rho}$ is the density covariance matrix, $\boldsymbol{C}_{g\rho}$ is the cross covariance between gravity and density and $\boldsymbol{\Lambda}$ is the vector of weighting coefficients. The estimate of densities are obtained from the gravity data using the optimal weights :

$$\boldsymbol{\rho}^* = \boldsymbol{\Lambda}^T\boldsymbol{g}. \tag{5.4}$$

The variance-covariance matrix of cokriging errors is obtained directly from equations (3) and (4) as : $Var(\rho - \rho^*) = C_{\rho\rho} - \Lambda^T C_{g\rho}$. Cokriging error variances are found on the diagonal of this matrix :

$$\boldsymbol{\sigma}_{ck} = diag(\boldsymbol{C}_{\rho\rho} - \boldsymbol{\Lambda}^T\boldsymbol{C}_{g\rho}). \tag{5.5}$$

The off-diagonal elements give the covariances between estimation errors.

5.3.3 Inversion by cokriging

From equations 5.1 and 5.2, density and gravity covariance matrices are linearly related :

$$\boldsymbol{C}_{gg} = \boldsymbol{G}\boldsymbol{C}_{\rho\rho}\boldsymbol{G}^T + \boldsymbol{C}_0 \tag{5.6}$$

where $\boldsymbol{C}_0$ is the gravity field observation error ($\boldsymbol{e}$) covariance matrix. This matrix is usually considered diagonal often with a constant value assuming an uncorrelated noise. We also have :

$$\boldsymbol{C}_{g\rho} = \boldsymbol{G}\boldsymbol{C}_{\rho\rho}. \tag{5.7}$$

When the data are observed without error, i.e. $C_0 = 0$, it has been proved by Shamsipour *et al.* (2010b) that the gravity anomaly of the cokriged density is equal to the observed gravity anomaly.

The model covariance matrix, $\boldsymbol{C}_{\rho\rho}$, can be obtained using the information from boreholes

in the domain under the study. In cases where there is not enough information available from the domain, the v-v plot method (Shamsipour *et al.*, 2010b) may be used.

Incorporating borehole gravity information

The information from boreholes may include not only some known density values (to be discussed in the next section) but also the gravity data along the boreholes. We can add these extra gravity measurements to the inversion system in order to get more accurate estimates of the density distribution for the whole domain. We denote the gravity measurements along boreholes by $\boldsymbol{g}_{bh}$. Assuming the number of prisms with known gravities to be n_{bh}, the total number of gravity measurements will be $n + n_{bh}$. The relationship between densities of the whole domain and all gravity measurements will be :

$$\begin{bmatrix} \boldsymbol{g} \\ \boldsymbol{g}_{bh} \end{bmatrix}_{(n+n_{bh})\times 1} = \begin{bmatrix} \boldsymbol{G} \\ \boldsymbol{G}_{bh} \end{bmatrix}_{(n+n_{bh})\times m} \boldsymbol{\rho}_{m\times 1} \tag{5.8}$$

where $\boldsymbol{G}_{bh}$ is the matrix of the geometric terms corresponding to the borehole gravities. Each of its rows contains the effect of all prisms on one of the measured borehole gravities.

Replacing $\boldsymbol{G}$ with $[\boldsymbol{G}, \boldsymbol{G}_{bh}]^T$ and $\boldsymbol{g}$ with $[\boldsymbol{g}, \boldsymbol{g}_{bh}]^T$ in the inversion equations, we can include the effect of gravity measurements along boreholes on our estimation of density distribution without any scaling problem (Shamsipour *et al.*, 2010a). This will result in an improved inversion.

Incorporating point density information

In addition to the gravity data, the point densities measured along boreholes need to be accounted for in the inversion process. Note that the inversion is done on large blocks whereas the measured densities are on point support. To incorporate the point density information, one idea is to krige block densities from point densities using standard block kriging (Journel et Huijbregts, 1978). Then, the most precise block estimates are considered as constraints in

the inversion.

Including constraints is straightforward in the cokriging system. These constraints are added to the cokriging system as secondary variables. Denoting the known block densities with ρ_{v_F} and all the block densities with ρ_v, the inversion system with cokriging will be as follows :

$$\begin{bmatrix} \boldsymbol{C}_{g,g} & \boldsymbol{C}_{g,\rho_{v_F}} \\ \boldsymbol{C}_{\rho_{v_F},g} & \boldsymbol{C}_{\rho_{v_F},\rho_{v_F}} \end{bmatrix} \begin{bmatrix} \boldsymbol{\Lambda} \\ \boldsymbol{\Gamma} \end{bmatrix} = \begin{bmatrix} \boldsymbol{C}_{g,\rho_v} \\ \boldsymbol{C}_{\rho_{v_F},\rho_v} \end{bmatrix}, \tag{5.9}$$

$$\boldsymbol{\rho}_v^* = \boldsymbol{\Lambda}^T \boldsymbol{g} + \boldsymbol{\Gamma}^T \boldsymbol{\rho}_{v_F}. \tag{5.10}$$

In the above equations, the index v indicates that the densities correspond to blocks, index F stands for fixed. All required block-block and point-block covariances are numerically computed by integration of the point-point density covariance model obtained from the borehole densities.

The vector of cokriging variances is

$$\boldsymbol{\sigma}_{ck} = diag(\boldsymbol{C}_{\rho\rho} - \tilde{\boldsymbol{\Lambda}}^T \tilde{\boldsymbol{C}}_{g\rho}) \tag{5.11}$$

where $\tilde{\boldsymbol{\Lambda}}^T = [\boldsymbol{\Lambda}^T, \ \boldsymbol{\Gamma}^T]$ and $\tilde{\boldsymbol{C}}_{g\rho}$ is the right member in equation 5.9.

To select the blocks considered as fixed, a threshold is applied on the kriging variance. The threshold is selected large enough to represent adequately the borehole information but sufficiently small to leave enough "free" blocks to ensure a solution matching perfectly the observed gravity (in the absence of measurement error). For example, fixing all the blocks to their kriged values leaves no degree of freedom in the inversion but then the gravity anomaly computed with this solution does not match the gravity observations. Fixing a very low threshold does not fix any block, so the inversion does not consider at all the borehole point densities. An intermediate threshold will fix the values of blocks with the most probable information and leave the other blocks free to adjust the gravity observations. A matching solution is obtained as soon as the number of free blocks is equal to or larger than the number

of gravity observations. The solution can however present unrealistic block densities (e.g. too variable from block to block, or too extreme values), an indication that the threshold needs to be reduced further to diminish the number of fixed blocks.

Alternatively, one can replace the block density cokriging by a series of block conditional cosimulations, conditioned by the borehole point densities, on the same fixed blocks. When combined with inversion obtained by conditional simulation (Shamsipour *et al.*, 2010b), rather than by cokriging, it allows to obtain multiple inversions representing the uncertainty of the inversions and accounting for both the gravity and the borehole density information.

5.3.4 Downscaling

After inversion, the densities of all large blocks are known. Then, we can use downscaling to find the density distribution for smaller prisms. Indeed, the downscaling must also incorporate the known borehole point density values. Here, three different supports are involved, the large blocks v, the small prisms p and the borehole point data bh. Knowing the point data covariance function, it is simple to compute by numerical integration all the required block, prisms and point simple and cross covariances. Then, the downscaling is obtained by the following cokriging system :

$$\begin{bmatrix} \boldsymbol{C}_{\rho_v,\rho_v} & \boldsymbol{C}_{\rho_v,\rho_{bh}} \\ \boldsymbol{C}_{\rho_{bh},\rho_v} & \boldsymbol{C}_{\rho_{bh},\rho_{bh}} \end{bmatrix} \begin{bmatrix} \boldsymbol{\Lambda_1} \\ \boldsymbol{\Gamma_1} \end{bmatrix} = \begin{bmatrix} \boldsymbol{C}_{\rho_v,\rho_p} \\ \boldsymbol{C}_{\rho_{bh},\rho_p} \end{bmatrix}, \tag{5.12}$$

where subscripts v, p and bh stands respectively for large blocks, small prisms and borehole densities. Then,

$$\boldsymbol{\rho_p^*} = \boldsymbol{\Lambda_1}^T \boldsymbol{\rho}_v^* + \boldsymbol{\Gamma_1}^T \boldsymbol{\rho}_{bh}. \tag{5.13}$$

Algorithm 1 presents the method for inversion with constraints including upscaling and downscaling.

As for the upscaling and the inversion, conditional simulations can be used in the downscaling if one wants to reflect the variability that can be expected from the inverted density

Algorithm 1: Inversion with constraints and downscaling

Data: Observed gravity g, variogram model of the point densities, borehole densities $\boldsymbol{\rho}_{bh}$.
Result: Estimated densities on large blocks $\boldsymbol{\rho}_v^*$ and small prisms $\boldsymbol{\rho}_{\boldsymbol{p}}^*$.
begin
a) Upscaling :
1 Use block kriging to estimate the densities of large blocks from the borehole densities $\boldsymbol{\rho}_{bh}$.
2 Select the most precise block estimates as constraints, $\boldsymbol{\rho}_{v_F}$ by applying a threshold on kriging variances.
3 Inversion with constraints on large blocks, $\boldsymbol{\rho}_v^* = \boldsymbol{\Lambda}^T \boldsymbol{g} + \boldsymbol{\Gamma}^T \boldsymbol{\rho}_{v_F}$. Weights are obtained from Eq. 5.9.
b) Downscaling :
4 $\boldsymbol{\rho}_{\boldsymbol{p}}^* = \boldsymbol{\Lambda}_{\mathbf{1}}^T \boldsymbol{\rho}_v^* + \boldsymbol{\Gamma}_{\mathbf{1}}^T \boldsymbol{\rho}_{bh}$. Weights are obtained from Eq. 5.12.
end

model. In this paper, we use the FFT-MA algorithm (Le Ravalec *et al.*, 2000) for generating unconditional Gaussian stationary field on a regular grid. This algorithm is chosen because it is fast and easy to implement. For non-regular grids, we use the turning band method. A comprehensive description of this algorithm can be found in Chilès et Delfiner (1999).

First N_s different realizations of unconditional simulated densities $\boldsymbol{\rho}_s$ are generated at the point level (including points in boreholes where density is known). The simulated densities are averaged over prisms and blocks and then post-conditioned by cokriging (Journel et Huijbregts, 1978; Myers, 1982) using :

$$\boldsymbol{\rho}_{p,cs} = \boldsymbol{\rho}_{\boldsymbol{p}}^* + (\boldsymbol{\rho}_{p,s} - \boldsymbol{\rho}_{p,s}^*) \tag{5.14}$$

where $\boldsymbol{\rho}_{p,cs}$ stands for prism density, conditionally simulated, $\boldsymbol{\rho}_{\boldsymbol{p}}^*$ is the prisms density estimate obtained using cokriging (see Eq. 5.12,5.13) with inverted block densities and measured borehole density, $\boldsymbol{\rho}_{p,s}$ is the unconditionally simulated prism density and $\boldsymbol{\rho}_{p,s}^*$ is the cokriging estimate obtained using the large block and borehole unconditionally simulated densities. Algorithm 2 presents the method for conditional simulation of densities and downscaling.

Algorithm 2: Conditional simulation of densities and downscaling

Data: Cokriging weights $\mathbf{\Lambda}$ and $\mathbf{\Gamma}$, downscaling weights $\mathbf{\Lambda}_1$ and $\mathbf{\Gamma}_1$, variogram model of the point densities, Number of realizations of unconditional simulated densities N_s. Estimated densities on small prisms $\boldsymbol{\rho}_{\boldsymbol{p}}^*$.

Result: A set of conditionally simulated prisms densities $\boldsymbol{\rho}_{p,cs}$.

begin

Initialization : $k = 1$.

while $k \leq N_s$ **do**

Generate one realization of unconditionally simulated point densities $\boldsymbol{\rho}_s$. Denote the simulated densities at boreholes by $\boldsymbol{\rho}_{bh,s}$.

a) Upscaling :

Average $\boldsymbol{\rho}_s$ to find prism densities $\boldsymbol{\rho}_{p,s}$ and block densities $\boldsymbol{\rho}_{v,s}$. Denote the averaged densities at certain blocks of constraints (from Algorithm 1) with $\boldsymbol{\rho}_{v_F,s}$.

Calculate the gravity data $\boldsymbol{g}_s = G \times \boldsymbol{\rho}_{v,s}$.

Inversion of $\boldsymbol{g}_s$: $\boldsymbol{\rho}_{v,s}^* = \mathbf{\Lambda}^T \boldsymbol{g_s} + \mathbf{\Gamma}^T \boldsymbol{\rho}_{v_F,s}$.

b) Downscaling : $\boldsymbol{\rho}_{p,s}^* = \mathbf{\Lambda_1}^T \boldsymbol{\rho}_{v,s}^* + \mathbf{\Gamma_1}^T \boldsymbol{\rho}_{bh,s}$.

Conditional simulation of point densities : $\boldsymbol{\rho}_{p,cs} = \boldsymbol{\rho}_{\boldsymbol{p}}^* + (\boldsymbol{\rho}_{p,s} - \boldsymbol{\rho}_{p,s}^*)$.

k=k+1.

end

5.4 Synthetic results

The proposed algorithms are tested on a stochastic density model. The 3D domain is divided into $35 \times 35 \times 20 = 24500$ small cubic prisms with dimentions $1 \times 1 \times 0.5$ m. Densities of these prisms are generated by unconditional FFT-MA simulation using a spherical variogram model with $C = 50000$ $(Kg/m^3)^2$, $a_x = 13$ m, $a_y = 15$ m, $a_z = 5$ m and a nugget effect of $C_0 = 100$ $(Kg/m^3)^2$.

We convert this domain into $7 \times 7 \times 5 = 245$ large blocks with dimensions $5 \times 5 \times 2$ m. The densities of these large blocks are calculated using the densities in small prisms. The generated density distributions at section $y = 17.5$ m for both small scale and large scale are shown in Figure 5.1 (a) and (b). Using the density values of large blocks, we calculate the synthetic gravity data using equation $\boldsymbol{g} = \boldsymbol{G\rho}$ (Figure 5.2). The gravity data with error $C_0 = 10^{-7}$ mGal^2 are observed at the center of the top face of the surface prisms ($n = 7 \times 7 = 49$).

We assume there are five boreholes in the domain at $(x = 7.5, y = 7.5)$, $(x = 7.5, y = 27.5)$

, $(x = 27.5, y = 7.5)$, $(x = 27.5, y = 27.5)$ and $(x = 17.5, y = 17.5)$. Knowing the density values at the boreholes and the point density covariance model, the borehole density is upscaled to large blocks using block kriging. The estimated densities of large blocks along the boreholes (i.e. the blocks most precisely estimated) are considered as constraints.

Figure 5.1 (c) to (f) presents inversion results on the large scale using different information. In (c) the inversion is done using only the surface gravity data ; in (d) the surface gravity data and the gravity data computed along the central borehole are used ; in (e), surface gravity data and densities in all 5 boreholes are used ; finally, (f) inversion uses the same data as for (e) with also the central borehole gravity data. The mean absolute errors (MAE) obtained by comparing (c-f) to (b) steadily declines as more information is incorporated in the inversion (94.8, 88.0, 84.5, 83.9). Visually, the best improvement over (c) appears at depth in the central portion. The correlation (r) coefficients between (c-f) and (b) are 0.66, 0.70, 0.72 and 0.74 respectively. As expected, MAE diminishes and correlation increases as more information is used in the inversion. Despite a small observation error was added to the synthetic gravity data, all inverted models reproduce almost perfectly the gravity data as shown in Figure 5.3.

After finding the densities of all large blocks, downscaling using Eq. 5.12 and 5.13 is applied to simulate the density distribution for small prisms $\boldsymbol{\rho}^*$. Using Algorithm 2, $N_s = 100$ conditional realizations of point densities were obtained using the densities along the boreholes and the inverted (simulated) densities on large blocks. Six realizations along section $y = 17.5$ m are shown in Figure 5.5 (a)-(f). The same realizations are also presented on the large blocks (Figure 5.4 (a)-(f)).

Figure 5.6 (a) and (c) show the average of 100 realizations on large blocks and small prisms respectively ; (b) and (d) show the corresponding gravity computed at observation points compared to observed gravity (initially determined from the large block densities). For comparison, the inverted small prisms densities obtained by cokriging (algorithm 1) and the computed gravities are shown in (e) and (f). As expected, because the physical link between density and gravity is linear, the average of the simulated densities corresponds to the cokriging estimates of the densities. Note that the gravity computed from the downscaled

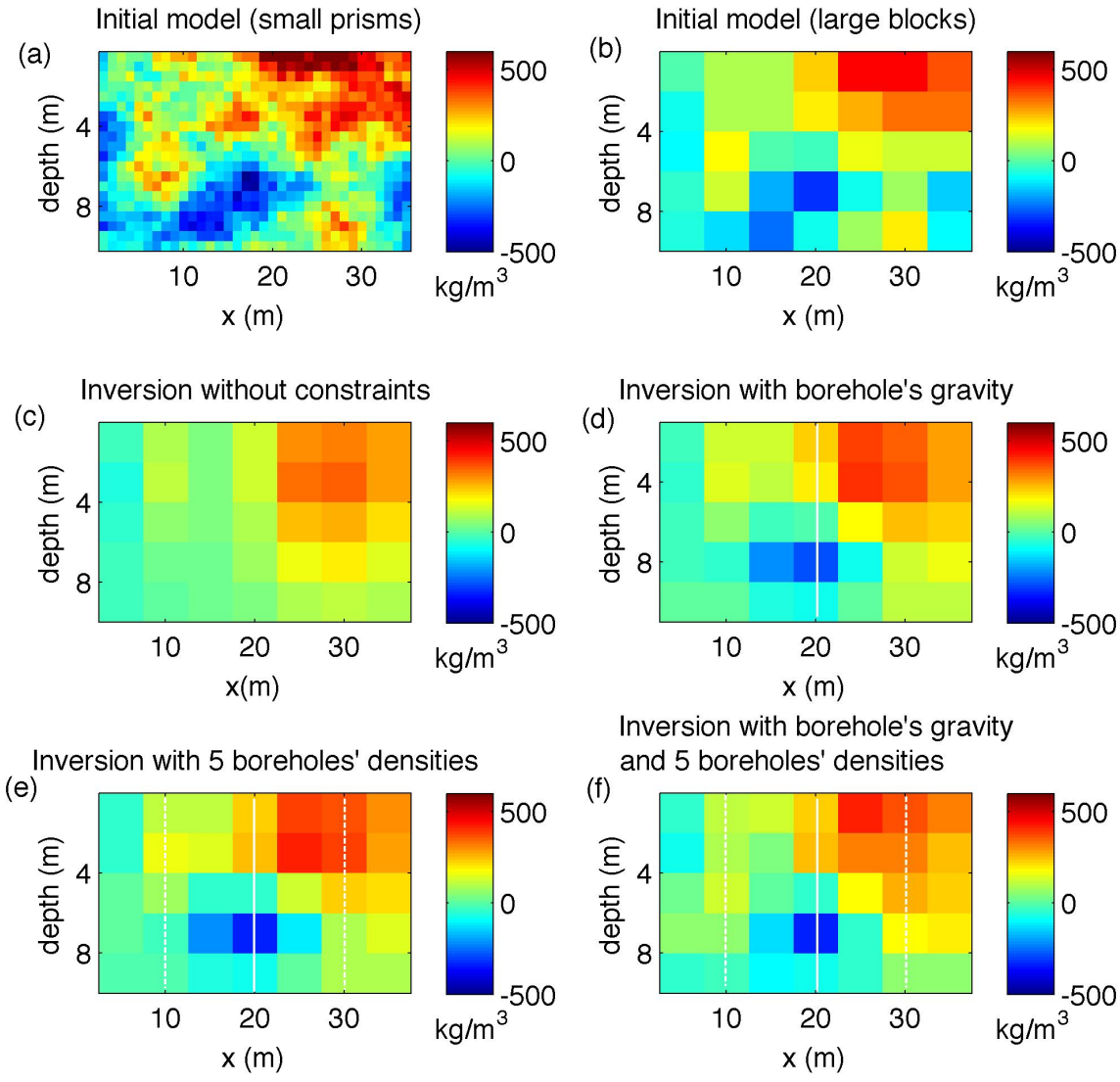

Figure 5.1 (a) Initial data, small prisms, (b) Initial data, large blocks, (c) Inverted data without constraints, (d) Inverted data using surface gravities and gravities of the central borehole, (e) Inverted data using surface gravities and density constraints of all 5 boreholes, (f) Inverted data using surface gravities, gravities of the central borehole and density constrants of all 5 boreholes. All the results are shown in section $y = 17.5$ m.

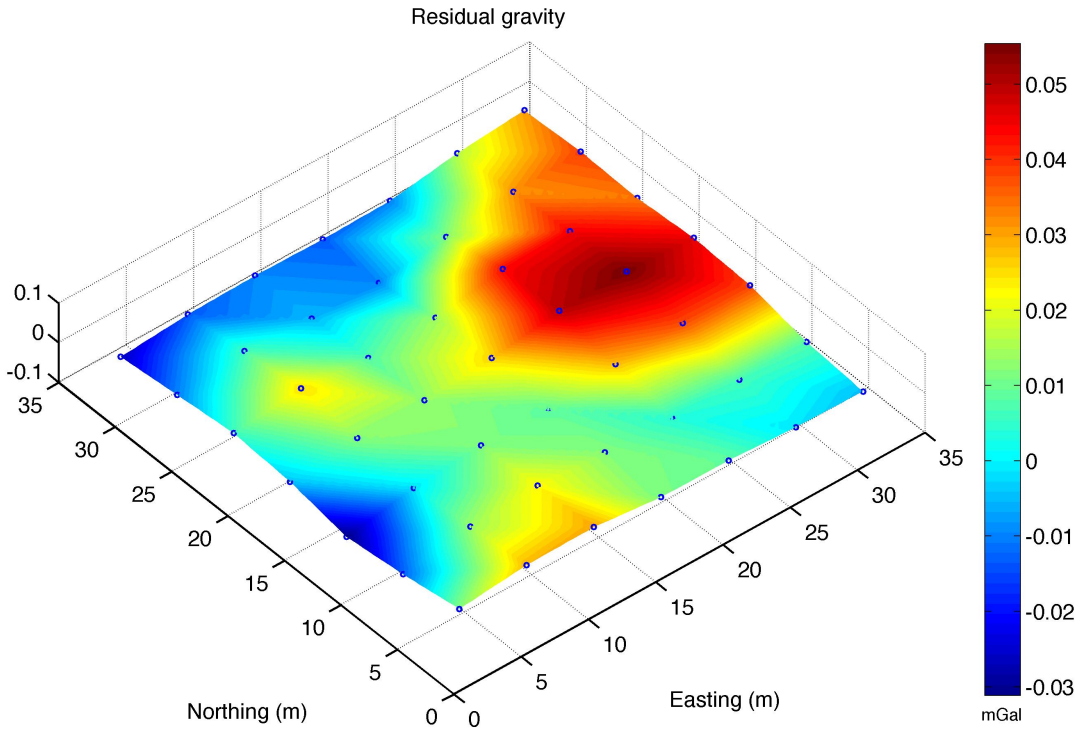

Figure 5.2 The synthetic gravity data from the large blocks.

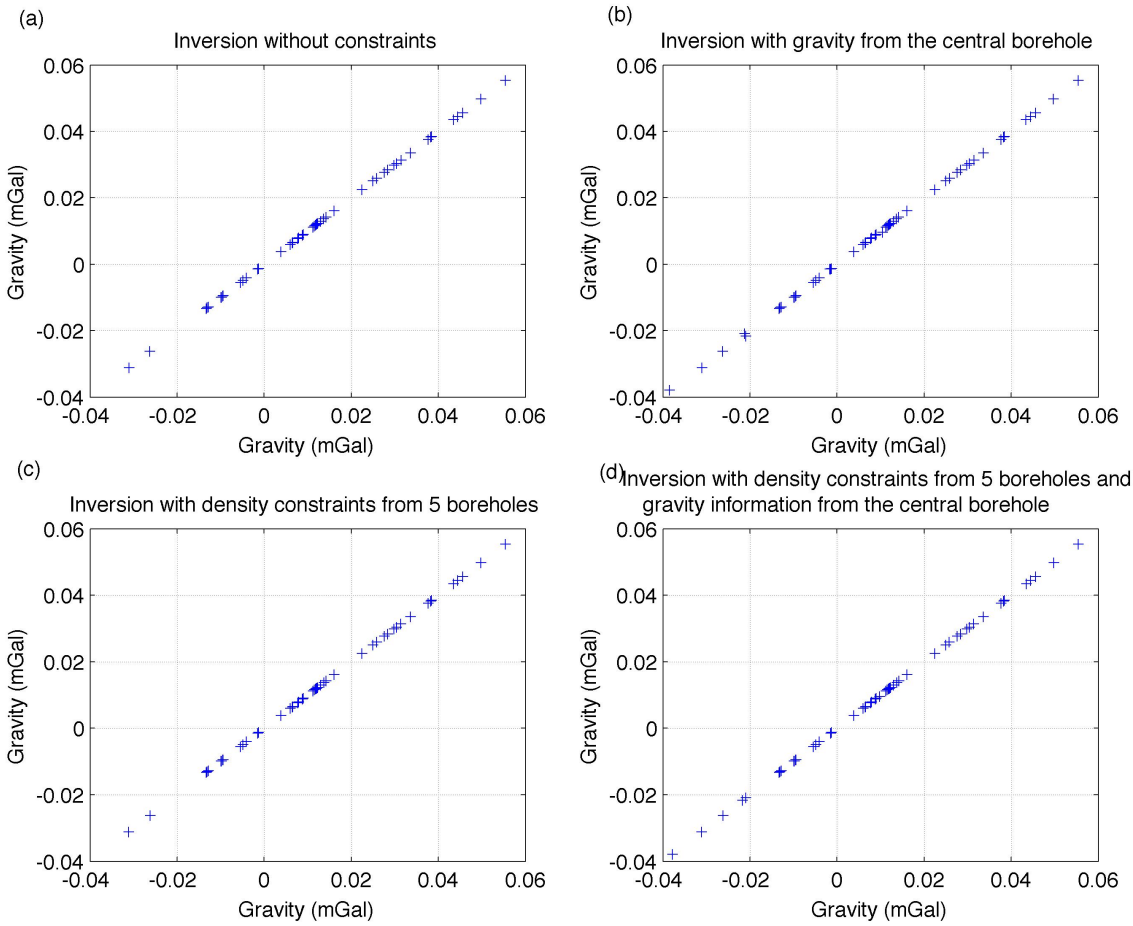

Figure 5.3 Observed versus calculated gravity data : (a) correlation r=1, (b) correlation r=0.999, (c) correlation r=1, (d) correlation r=1.

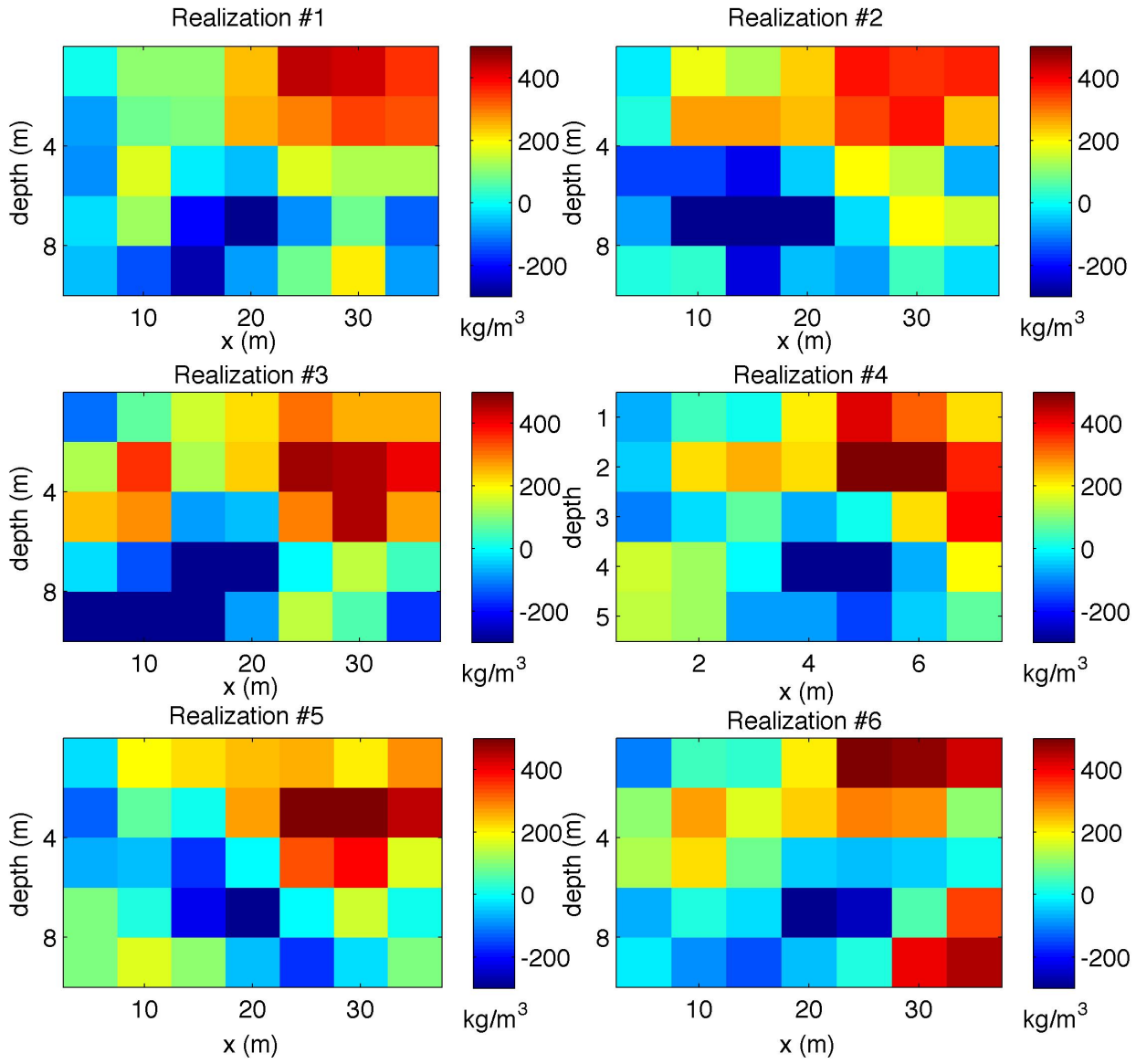

Figure 5.4 Six realizations of conditional simulated densities at section $y = 17.5$ m (large blocks) with borehole densities as constraints.

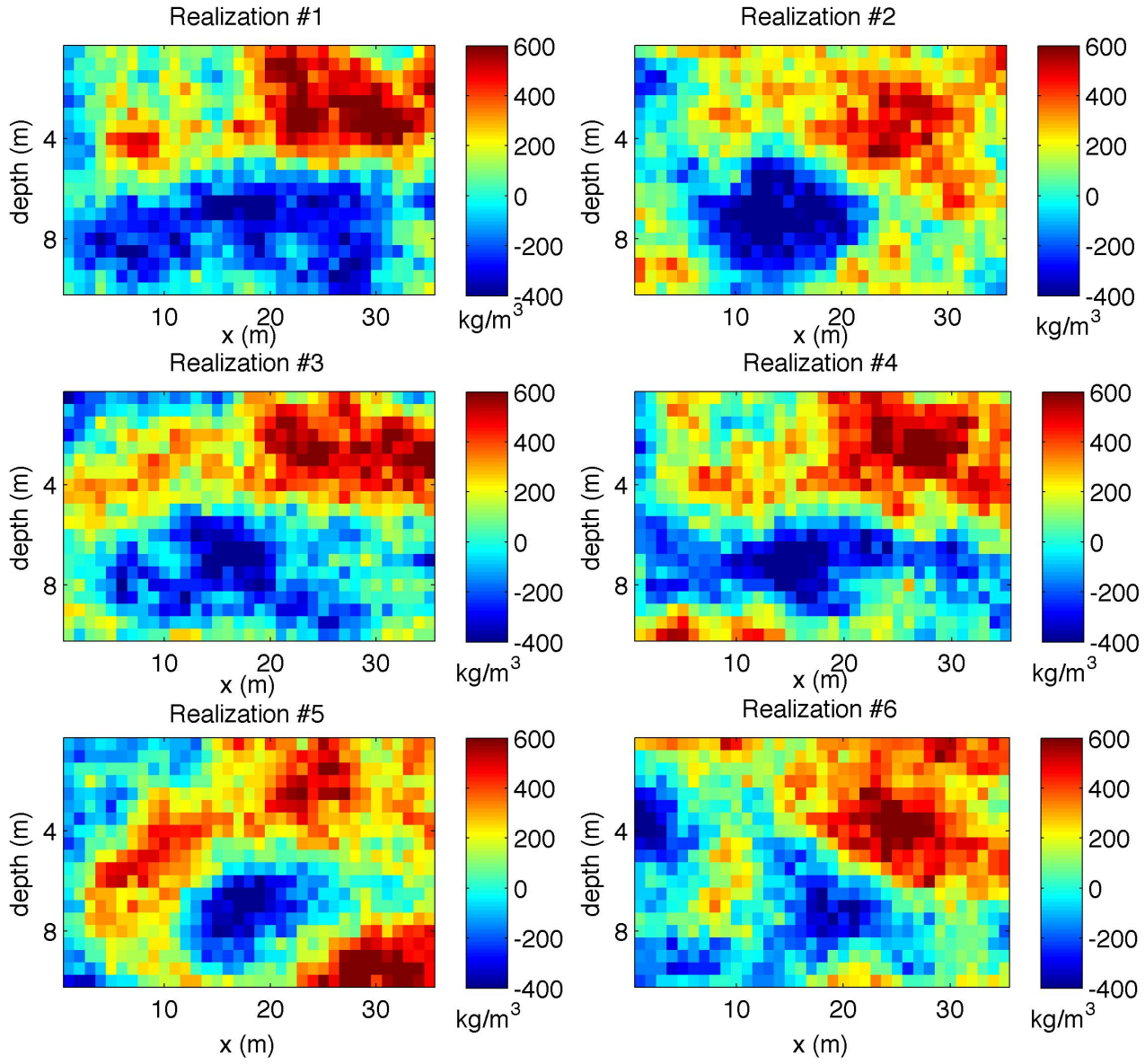

Figure 5.5 Six realizations of conditional simulated densities at section $y = 17.5$ m (small prisms) with borehole densities as constraints.

estimates still matches quite well the observed gravity, despite the gravity data were not directly included in the downscaling process.

The different realizations can be used to calculate quantile estimators, or probability maps of exceeding a target density threshold for example, but they are most useful as input for non-linear transfer functions (Shamsipour *et al.*, 2010b) such as flow simulation and production history matching, in petroleum applications, or to assess uncertainty on recovery functions in mining applications.

5.5 Case study : application to survey data

The survey data was collected over the area of the Perseverance mine located in the Matagami region in Quebec, Canada. The area of the 2001 gravity survey extends from longitude 77° 48′ 3" W to 77° 46′ 45" W and from latitude 49° 45′ 47" N to 49° 45′ 58" N, where 620 gravity ground measurements are available.

Gravity data were collected using a Scintrex CG5 gravity meter (accuracy .005 mGal) every 25 m along northeast-southwest lines separated by 100 m except in a restricted area around the Perseverance mine (anomaly A in Figure 7) were the line separation was halved. The data were graciously provided by Xstrata Zinc inc. The sites of gravity measurements are shown in Figure 5.7.

The gravity data have been corrected for drift, elevation and latitude to yield the Bouguer anomaly. The maximum error and the standard deviation of the errors were estimated to be 0.17mGal and 0.1 mGal respectively (Dr Pierre Keating, personal communication, 2011). No terrain correction was included in the reduction of the Bouguer anomaly because the topography is flat in the survey area (maximum elevation differences are 2.7 m with a standard deviation of less than 1.1 m. We checked (not shown) that the gravity variogram has negligible nugget effect and a nice parabolic behaviour at the origin, features supporting data with little error. A valid regional gravity field was obtained by calculating a first order trend from the Bouguer anomaly data. Subtracting the regional from the Bouguer anomaly results in the residual anomaly (Figure 5.7) ranging between-0.5 and 0.5 mGal.

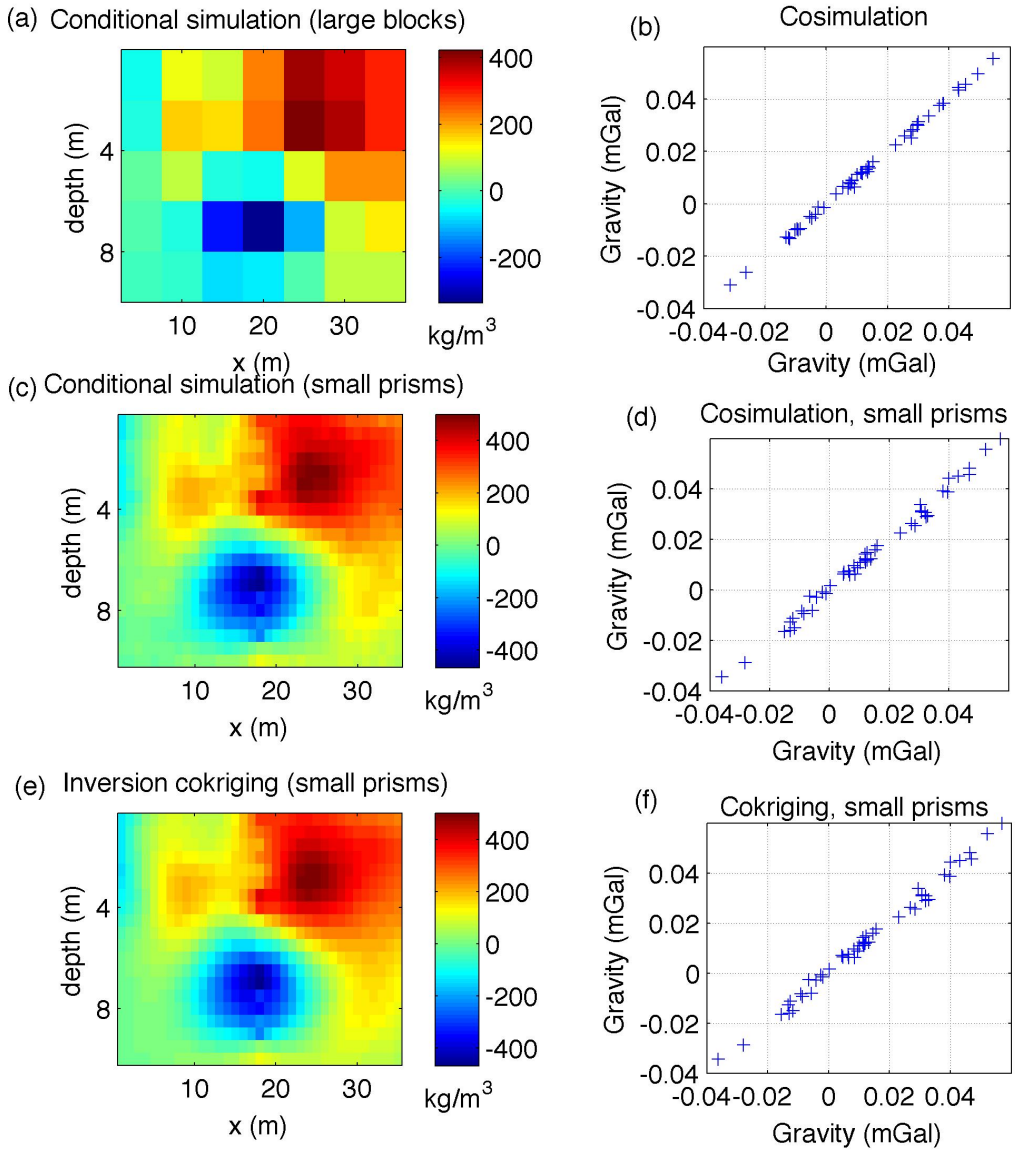

Figure 5.6 (a) Average of conditional simulations, large blocks, (b) Calculated versus observed gravities, conditional simulation, large blocks, correlation r=0.999, (c) Average of conditional simulations, small prisms, (d) Calculated versus observed gravities, conditional simulation, small prisms, correlation r=0.996, (e) Inversion by cokriging, small prisms, (f) Calculated versus observed gravities, Cokriging, small prisms, correlation r=0.995. All the density pictures are from section $y = 17.5$ m.

The study area is located in the northern part of the Abitibi region, one of the largest Archean greenstone belts in the world. It hosts many volcanogenic massive sulfides (Cu, Zn, Ni, Au, Ag) deposits. The Matagami volcanic complex of the northern Abitibi belt is formed by two major phases of volcanism (Piché *et al.*, 1993) . The end of the initial volcanic phase produced rhyolites of the Watson Lake Group. The beginning of the late volcanic phase formed the basaltic Wabassee Group.

A cherty, sulphidic chemical sediment known as the Key Tuffite marks the contact and discontinuity between the two groups. This thin horizon is the primary exploration target because it hosts most of the zinc rich orebodies discovered in the area (Calvert et Li (1999), Adam *et al.* (1998)). As the search for new reserves expands to greater depths, exploration costs increase geometrically providing a strong impetus to develop alternate methods of prospecting favourable horizons. Exploration of VMS deposits in the area lead to the opening of 11 mines. The largest mine was the Mattagami Lake mine with a total production of 25.64 Mt ore. A new discovery has been made by Xstrata Zinc Canada in 2007, the Bracemac-McLeod deposit, which is expected to start production in 2013 [1].

The Perseverance mine is the only active mine in the study area. It consists of three small massive sulfide deposits, Perseverance, Perseverance west and Equinox shown in Figure 6.7 with A, C and B respectively. The Perseverance deposit has a total production of 1.2 MT (14.55% Zn and 1.20% Cu). Estimates for the Perseverance west deposit and the Equinox deposit are 1.1 MT (12.61% Zn and 1.38% Cu) and 2.5 MT (14.93% Zn and 0.98% Cu) respectively [2].

5.5.1 Inversion

A total of 950 borehole density samples are found close to areas marked A, B and C in Figure 5.7. The borehole density samples are used for the inversion. The density samples were also used to compute the (point) density variogram. The fitted variogram model is

1. Donner Metals Ltd, http ://www.donnermetals.com/projects.asp, accessed March 2011
2. Noranda Inc, 2001 Annual Report, p.63

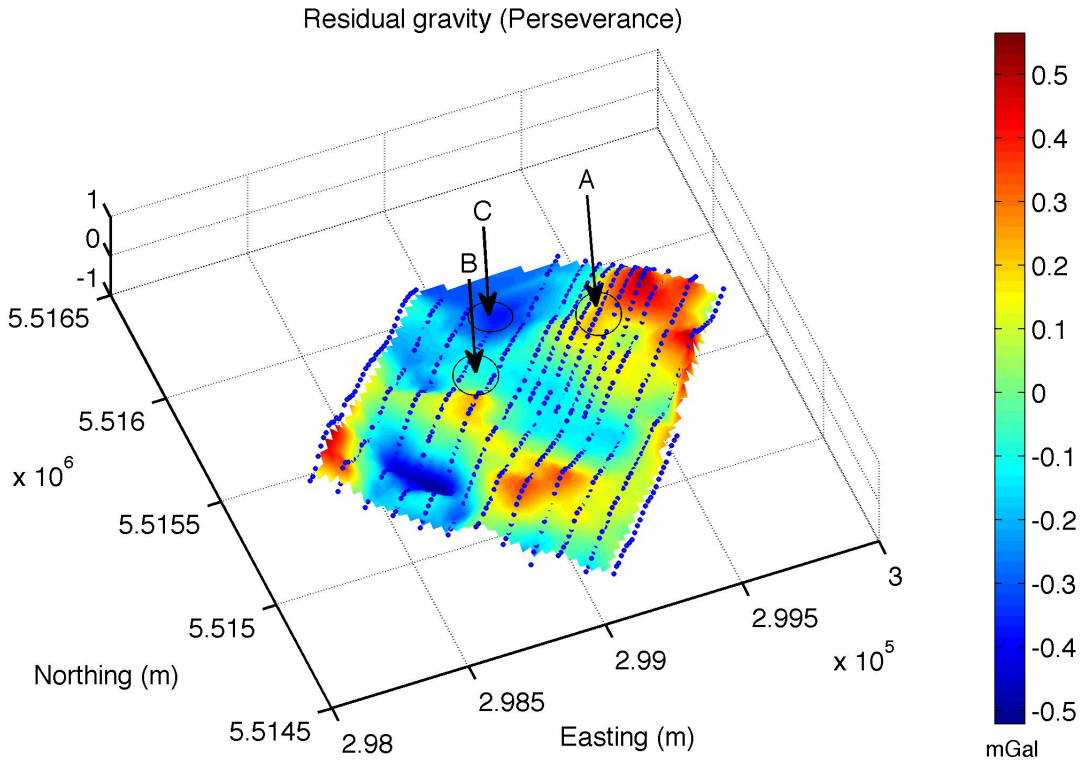

Figure 5.7 The residual anomalies from the studied area. Dots on the map indicate the points of observation

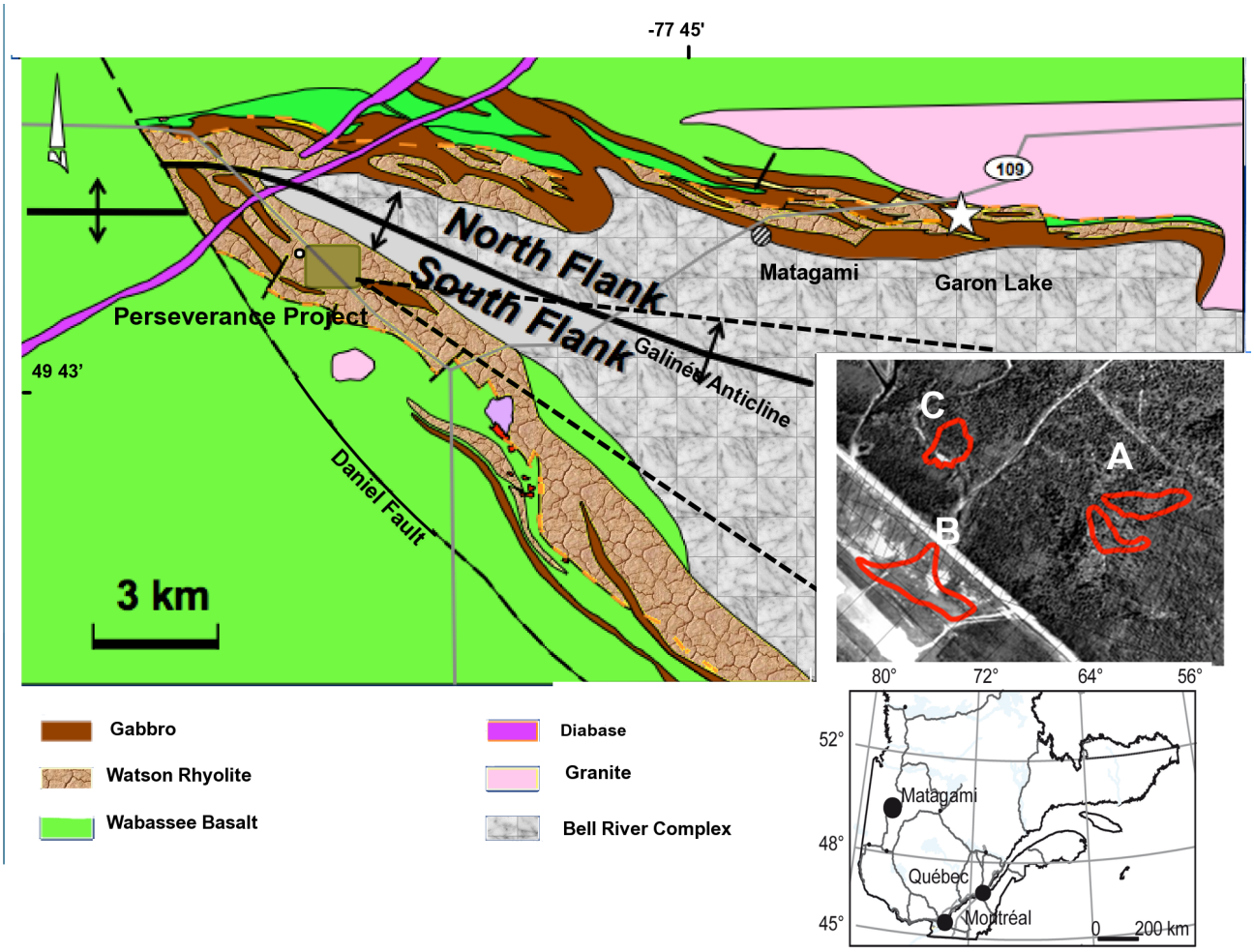

Figure 5.8 Geology map of Matagami camp with Perseverance mine highlighted Adapted from Xstrata Zinc company.

exponential, isotropic, with nugget $C_0 = 1000$ $(kg/m^3)^2$, sill $C = 6000$ $(kg/m^3)^2$ and range $a = 90$ m. The block-block and block-point covariances required for the inversion are then computed by numerical integration using this model.

The inversion domain is divided into $n_x = 29$ by $n_y = 26$ by $n_z = 7$ cubes of dimension $60 \times 60 \times 60$ m (large blocks). Therefore, the whole domain is $1740 \times 1560 \times 420$ m and the total number of blocks is $m = 5278$. Small prisms of size $10 \times 10 \times 20$ m are used for the downscaling. The inversion results on 3 sections at $x = 298900$ m, $y = 5515600$ m and $z = 170$ m (sections pass through the deposits) are shown in Figures 5.9, 5.10 and 5.11 respectively. In Figures 5.9, 5.10 and 5.11, six different results are shown : (a) inversion by cokriging using only surface gravity, (b) inversion by cokriging using surface gravity and block constraints, The fixed block densities are from 58 blocks with kriging variance less than 250 $(kg/m^3)^2$, This variance represents only 15% of the block variance, so the fixed blocks are well estimated ; (c) the inversion downscaled on the small prisms of size $10 \times 10 \times 20 \times$ m ; (d), (e) and (f) present three different realizations of a conditional simulation (algorithm 2) obtained using surface gravity with constraints and then downscaled on the small prisms.

The inversions obtained without constraints, (a) in Figures 5.9, 5.10 and 5.11, are very smooth and put all the density anomalies close to the surface. They miss almost completely the known deposits A, B, and C. On the contrary, inversions obtained using constraints, (b), clearly recognize the presence of the denser mineralized bodies (A, B, C). Better contrasts and resolution are achieved in the downscaled version (c). For example, note how the density varies sharply close to A. Such quick variations are impossible to detect from surface gravity measurements only. It must come directly from the density observed in the boreholes. Finally, the 3 realizations (d) to (f) add realism to the smooth (c) inversion.

Figures 5.12 shows the calculated versus observed gravities, for inversions (a), (b) and (c) of Figures 5.9, 5.10 and 5.11. As mentioned, the inversion on the large blocks reconstruct exactly gravity observations when there is no measurement error in the gravity data. On the other hand, the downscaled densities are not any more exact as they are obtained by cokriging using only the inverted densities, not the observed gravity. To be exact, inversion

must be done by cokriging (or cosimulation) directly on the small prisms using the gravity data. This is not practical as it requires to store the prism-prism covariance matrix, here of size (570024×570024). Nevertheless, the reconstructed gravity remains highly correlated (r=0.98) to the observed surface gravity.

5.6 Discussion and Conclusion

We introduced an inversion method based on a geostatistical approach for multiple scale parameter. The method can include both density and gravity data measured in boreholes to increase the resolution at depth. Both borehole gravity and density data were shown to be complimentary information for the inversion. The algorithm is flexible as it allows all combinations of conditioning point and block density support data simultaneously. The algorithms proposed are fast and non-iterative.

The method relies on the fact that density data can be linearly averaged to compute the required block-block and point-block covariances by numerical integration. This ensures full consistency of the cokriging and cosimulation inversions. Indeed, because the physical link between point density, block density and gravity is fully accounted for, the inverted densities perfectly reconstruct the observed gravity data when the latter is considered error free (i.e. no nugget effect in the C_{gg} covariance matrix) and when a sufficient number of free blocks is left for the inversion. When gravity data is considered with error, inverted densities then reconstruct with high correlation the observed gravity. Therefore, the block averaging provides a statistically coherent method for moving between points and blocks of different sizes.

The method merges numerous borehole density measurements by an initial upscaling step : block kriging of density. We proposed the use of a threshold on the block kriging variance to identify the block densities that will be used as constraints in the inversion on large blocks. By selecting a low threshold, the inversion is essentially driven by the gravity anomaly. By selecting a higher threshold, the inversion is more controlled by the borehole densities. The threshold should be low enough to ensure exact reproduction of gravity observations. It

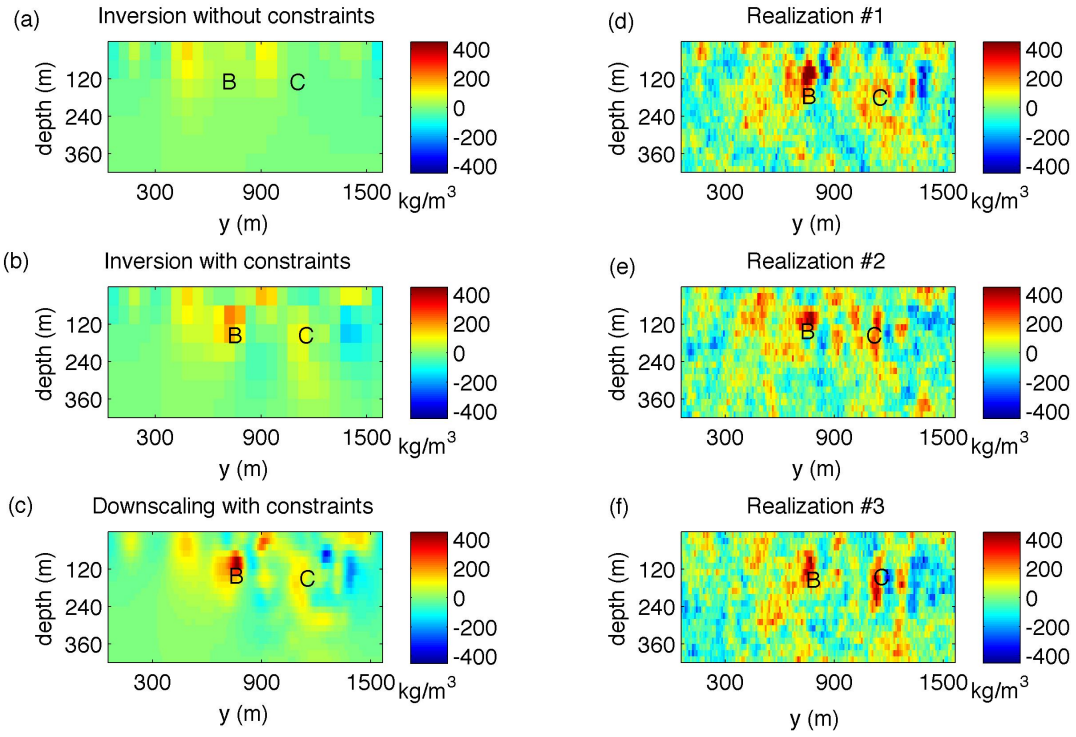

Figure 5.9 Estimated densities along vertical North-South section at $x = 298900$ m : (a) Inversion without constraints, (b) Inversion with density constraints estimated from boreholes, (c) Downscaling using the block densities from inversion with constraints and the point densities from boreholes, (d)-(f) Downscaling realizations.

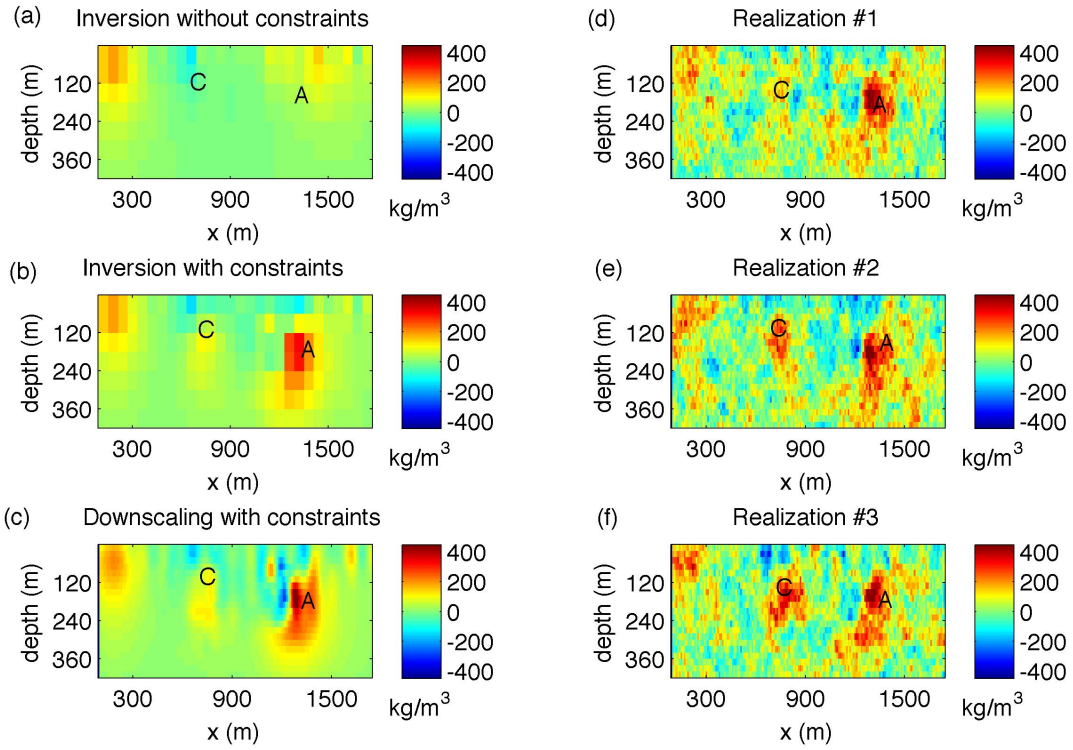

Figure 5.10 Estimated densities along vertical East-West section at $y = 5515600$ m : (a) Inversion without constraints, (b) Inversion with density constraints estimated from boreholes, (c) Downscaling using the block densities from inversion with constraints and the point densities from boreholes, (d)-(f) Downscaling realizations.

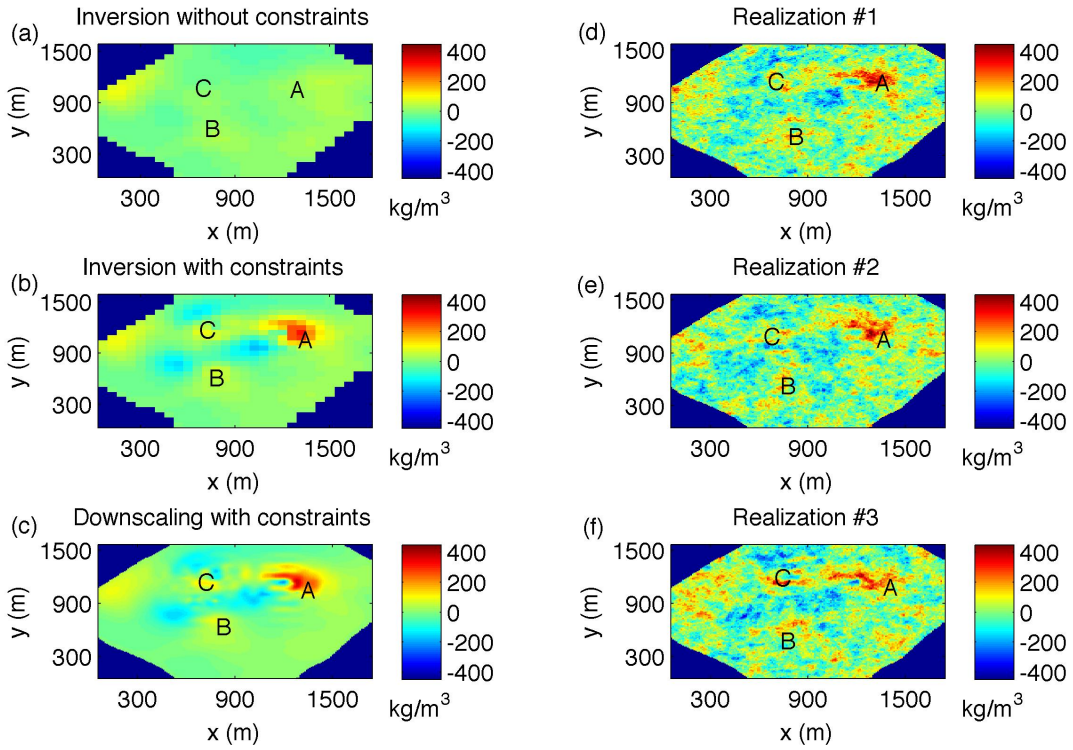

Figure 5.11 Estimated densities on the horizontal section $z = 170$ m : (a) Inversion without constraints, (b) Inversion with density constraints estimated from boreholes, (c) Downscaling using the block densities from inversion with constraints and the point densities from boreholes, (d)-(f) Downscaling realizations.

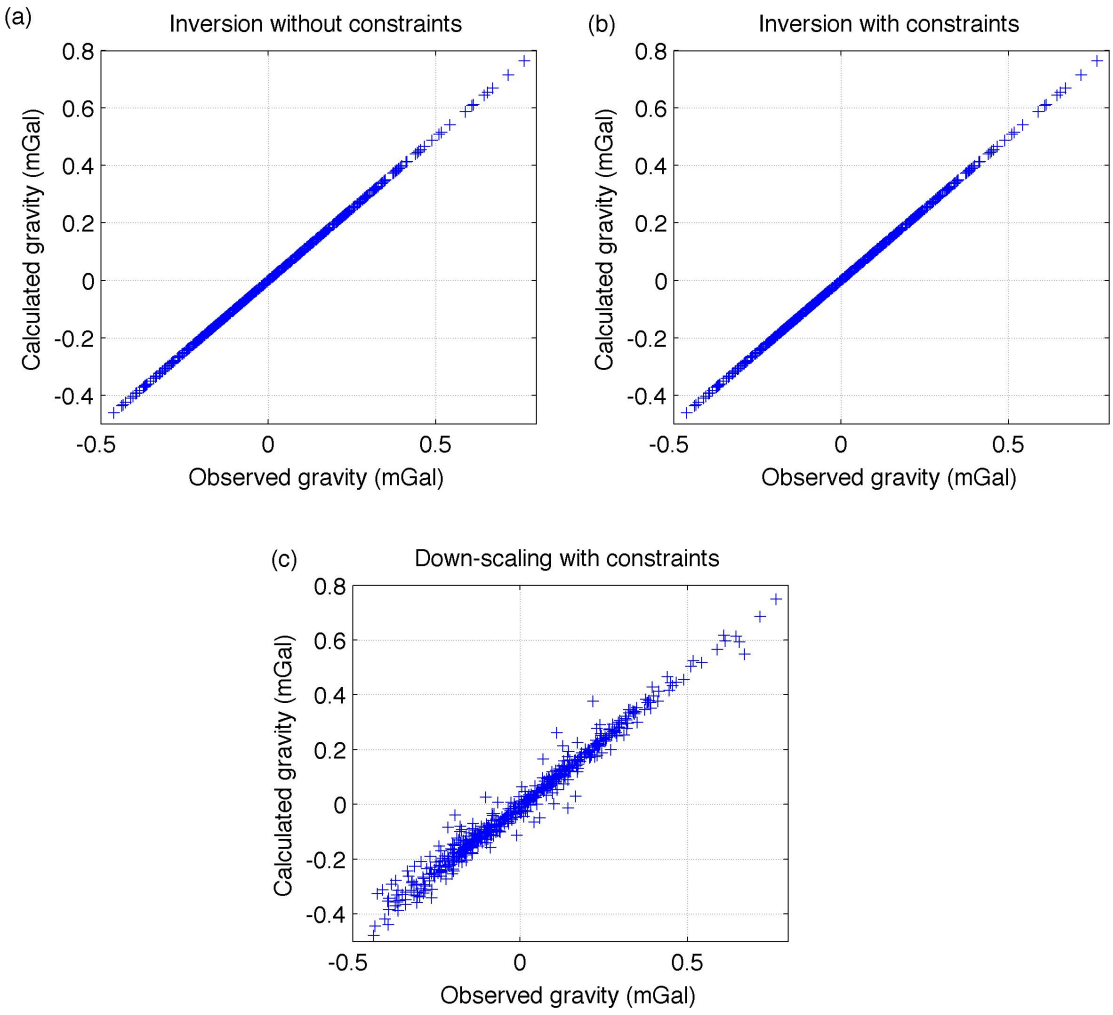

Figure 5.12 (a) Calculated versus observed gravity data, Inversion without constraints, correlation r=1, (b) Calculated versus observed gravity data, Inversion with constraints, correlation r=1, (c) Calculated versus observed gravity data, Downscaling, small prisms, correlation r=0.98.

should leave as many, and preferably more, free blocks as there are gravity observations. The threshold enables to control nicely the contribution of each data source.

Finally, we note that the approach can be easily extended to account for blocks of various sizes. For example one can consider smaller blocks close to the informed boreholes in a central area and larger blocks on the periphery of the model and at larger depths. The only additional difficulty lies in the management of the various block-block covariances.

Direct inversion by cokriging (or cosimulation) on small blocks (prisms) is, in many cases, hardly feasible due to the huge size of the prism-prism covariance matrix that needs to be computed to obtain the gravity-gravity and the gravity-prism density covariance matrices (Eq. 5.3, 5.6). We propose instead to first perform the inversion on large blocks and then downscale this inversion by kriging to the small prisms. The downscaling step is fast. In particular, there is no need to compute and store the huge prism-prism covariance matrix. There is a price to pay however, the reconstructed gravity obtained from the prisms does not any more reconstruct perfectly the observed gravity. However, the correlations obtained between reconstructed-observed gravity are strong. Note also that, thanks to the cokriging (and cosimulation) properties, the average of the prisms (estimated or simulated) inside a large block reproduces exactly the large block density. Therefore, the gravity anomaly also is still perfectly reconstructed on the larger scale.

The downscaling approach is studied on both synthetic and real data. In the resulting fine scale numerical representations, main elements and heterogeneities of the initial model are well recovered. All inverted models respect the block support data, the point support data as well as gravity data. The spatial correlation is well reproduced in terms of variogram reproduction (not shown).

While cokriging produces one smooth solution to the underdetermined problem, cosimulations enable to generate a set of equally possible solutions. The purpose is to recreate the spatial variability of the real density field. One important use of simulation is to generate scenarios as input for non-linear transfer function applied on the field (e.g. flow simulation, recovery functions, etc.).

The proposed method is tested on real data from Matagami mining camp (Perseverance mine) where the results of inversion are proved to be in agreement with the known geology. In particular, the three known deposits, missed by the inversion using only gravity surface data, are well recognized by the inversion using gravity data and borehole densities.

5.7 Acknowledgments

We would like to express sincere thanks to Xstrata Zinc Canada for providing the geological information and for the permission to use and release the gravity data that covers the Perseverance Mine. We also would like to extend our thanks to Dr. Pierre Keating from the Geological Survey of Canada for providing us with detailed information about the gravity survey.

References

ADAM, E., MILKEREIT, B. et MARESCHAL, M. (1998). Seismic reflection and borehole geophysical investigations in the matagami mining camp. *Canadian Journal of Earth Sciences*, 35, 686–695.

ASLI, M., MARCOTTE, D. et CHOUTEAU, M. (2000). Direct inversion of gravity data by cokriging. W. Kleingeld et D. Krige, éditeurs, *6th International Geostatistics Congress, Cape town, South Africa*, Cape Town, South Africa. 64–73.

BOSCH, M. et MCGAUGHEY, J. (2001). Joint inversion of gravity and magnetic data under lithologic constraints. *The Leading Edge*, 20, 877–881.

BOSCH, M., MEZA, R., JIMÉNEZ, R. et HÖNIG, A. (2006). Joint gravity and magnetic inversion in 3D using Monte Carlo methods. *Geophysics*, 71, G153.

CALVERT, A. et LI, Y. (1999). Seismic reflection imaging over a massive sulfide deposit at the Matagami mining camp, Québec. *Geophysics*, 64, 24–32.

CHASSERIAU, P. et CHOUTEAU, M. (2003). 3D gravity inversion using a model of parameter covariance. *Journal of Applied Geophysics*, 52, 59 – 74.

CHILÈS, J. et DELFINER, P. (1999). *Geostatistics : modeling spatial uncertainty*. Wiley.

FEDI, M. et RAPOLLA, A. (1999). 3-D inversion of gravity and magnetic data with depth resolution. *Geophysics*, 64, 452–460.

FRANKLIN, J. (1970). Well posed stochastic extensions of Ill posed linear problems. *J. Math*, 31, 682–716.

GIROUX, B., GLOAGUEN, E. et CHOUTEAU, M. (2007). bh_tomo–a Matlab borehole georadar 2D tomography package. *Computers and Geosciences*, 33, 126–137.

GLOAGUEN, E., MARCOTTE, D., CHOUTEAU, M. et PERROUD, H. (2005). Borehole radar velocity inversion using cokriging and cosimulation. *Journal of Applied Geophysics*, 57, 242 – 259.

GLOAGUEN, E., MARCOTTE, D., GIROUX, B., DUBREUIL-BOISCLAIR, C., CHOUTEAU, M. et AUBERTIN, M. (2007). Stochastic borehole radar velocity and attenuation tomographies using cokriging and cosimulation. *Journal of Applied Geophysics*, 62, 141 – 157.

GOMEZ-HERNANDEZ, J., FROIDEVAUX, R. et BIVER, P. (2004). Exact conditioning to linear constraints in kriging and simulation. O. Leuangthong et C. V. Deutsch, éditeurs, *Gestatistics Banff 2004*, Springer, Berlin.

HAÁZ, I. (1953). Relations between the potential of the attraction of the mass contained in a finite rectangular prism and its first and second derivatives. *Geophysical Transactions II*, 7, 57–66.

HANSEN, T., JOURNEL, A., TARANTOLA, A. et MOSEGAARD, K. (2006). Linear inverse Gaussian theory and geostatistics. *Geophysics*, 71, R101.

JOURNEL, A. et HUIJBREGTS, C. (1978). *Mining Geostatistics* . Academic Press, London.

LE RAVALEC, M., NOETINGER, B. et HU, L. (2000). The FFT Moving Average (FFT-MA) Generator : An Efficient Numerical Method for Generating and Conditioning Gaussian Simulations. *Mathematical Geology*, 32, 701–723.

LI, Y. et OLDENBURG, D. (1996). 3-D inversion of magnetic data. *Geophysics*, 61, 394–408.

LIU, Y. et JOURNEL, A. J. (2009). A package for geostatistical integration of coarse and fine scale data. *Computer and Geosciences*, 35, 527–547.

MYERS, D. (1982). Matrix formulation of co-kriging. *Mathematical Geology*, 14, 249–257.

PICHÉ, M., GUHA, J. et DAIGNEAULT, R. (1993). Stratigraphic and structural aspects of the volcanic rocks of the Matagami mining camp, Quebec ; implications for the Norita ore deposit. *Economic Geology*, 88, 1542–1558.

PILKINGTON, M. (1997). 3-D magnetic imaging using conjugate gradients. *Geophysics*, 62, 1132–1142.

SHAMSIPOUR, P., MARCOTTE, D. et CHOUTEAU, M. (2010a). 3D stochastic inversion of borehole and surface gravity data using Geostatistics. Capri, Italy.

SHAMSIPOUR, P., MARCOTTE, D., CHOUTEAU, M. et KEATING, P. (2010b). 3D stochastic inversion of gravity data using cokriging and cosimulation. *Geophysics*, 75, I1–I10.

TARANTOLA, A. et VALETTE, B. (1982). Generalized nonlinear inverse problems solved using the least squares criterion. *Rev. Geophys. Space Phys*, 20, 219–232.

CHAPITRE 6

Article 3 : 3D STOCHASTIC JOINT INVERSION OF GRAVITY AND MAGNETIC DATA

Article history : Submitted 15 July 2011, Currently under review, Journal of applied geophysics.

Authors : Pejman Shamsipour, Denis Marcotte, Michel Chouteau.

6.1 Abstract

A novel stochastic joint inversion method based on cokriging is applied to estimate density and magnetic susceptibility distributions from gravity and total magnetic field data. The method fully integrates the physical relations between the properties (density and magnetic susceptibility) and the indirect observations (gravity and total magnetic field). As a consequence, when the data are considered noise-free, the inverted fields exactly reproduce the observed data. The required density and magnetic susceptibility auto- and cross covariance are assumed to follow a linear model of coregionalization (LCM). The parameters of the LCM are estimated from v-v plot fitting of the gravity and total magnetic experimental covariances. The model is tested on two synthetic cases and one real data set, the Perseverance mine (Quebec, Canada). Joint inversions are compared to separate inversions. The joint inversions better recover the known models in the synthetic cases. With the real data set, better definition and location of the mineralized lenses is achieved by joint inversion. The benefit of joint inversion is especially noticeable when the two data sources are not co-located, therefore providing information from different parts of the study area.

6.2 Introduction

Interpretation of geophysical data needs to bring together different types of information to make the proposed model geologically more realistic. Multiple data sets can reduce ambiguity and non uniqueness present in separate geophysical data inversions. Potential fields surveys (gravity and magnetic) are suitable candidates for the joint inversion as they are among the most economical methods in geophysics. Moreover, the gravity and magnetic fields are closely related fields, yet complementary. Most often, the magnetic minerals are dense minerals so they cause also gravimetric anomalies. However, many dense rocks are not magnetic. Also, magnetic field display higher frequency variations than gravity data, so they are often more effective than gravity at resolving shallow or complex structures. The method presented exploits the complementary nature of the two potential fields to provide joint inversions better than with separate inversion of each field. For this purpose, a 3D stochastic inversion approach based on cokriging is used.

3D joint inversion of magnetic and gravity data was first described in the work by Zeyen et Pous (1993). They applied a priori information to reduce ambiguity of potential field inversion and interpolation. Gallardo-Delgado *et al.* (2003) proposed the method based on optimization to minimize the joint data misfit. The stochastic formulation for joint inversion is presented by Bosch *et al.* (2006). The approach is based on lithology discrimination and classification. This methods allows for joint inversion of gravity, magnetic and other a priori information to provide a model for major layers and properties inside layers. Gravity and magnetic data were inverted also jointly by Pilkington (2006) where the model consists of an interface separating two layers with different, but constant, densities and magnetization. In Fregoso et Gallardo (2009), the authors propose using cross gradient for 3D inversion of gravity and magnetic data. Most of methods directly, or indirectly, adapt the Tarantola et Valette (1982) techniques to generalize minimization problem in the Bayesian framework. Their approach builds on the earlier works of Franklin (1970) who was the first in geophysics to introduce the concept of stochastic inversion. Geostatistical methods in geophysical inversion were

applied by Asli *et al.* (2000), Gloaguen *et al.* (2005, 2007), Giroux *et al.* (2007) and Hansen *et al.* (2006) among the most cited. Bosch *et al.* (2006) also used Monte Carlo techniques in gravity inversion for generating a posterior probability density function describing acceptable models. Chasseriau et Chouteau (2003) advocate 3D inversion of gravity data using an a priori model of covariance. Shamsipour *et al.* (2010b, 2011) proposed geostatistical techniques of cokriging and conditional simulation for the separate three-dimensional inversion of gravity and magnetic data respectively, including geological constraints.

We propose a new method, based on cokriging, for the joint inversion of gravity and magnetic data. The method is a useful extension of Shamsipour *et al.* (2010b, 2011). After a brief description of the method, it is tested on two synthetic models : a model consisting of two prisms buried in a homogeneous background and a model with stochastic distribution of parameters. The results illustrate the capacity of the method to improve the inverted model compared to the separate inverted models with either gravity or magnetic data. In addition, the survey data collected over the Perseverance and Equinox deposits in the Matagami mining camp (Quebec, Canada) are studied. The recovered 3D joint-models better identify the known deposits within the survey area than do the separate inverted models. It provides also useful information to analyze and re-interpret the geology of the area under study.

6.3 Methodology

6.3.1 Forward modeling

The purpose of forward modeling is to compute the magnetic field T and the gravimetric response g at the surface due to a susceptibility distribution in the sub-surface χ and a density distribution ρ respectively. The magnetization vector $\vec{m}$ can be obtained as a vector sum :

$$\vec{m} = \chi\vec{H} + \vec{m}_r \tag{6.1}$$

where $\vec{H}$ is earth's magnetic field and $\vec{m}_r$ is the remanent component. If we assume no remanent magnetisation, $\vec{m}$ is in the direction of the earth's field and can be obtained simply

as : $\overrightarrow{m} = \chi \vec{H}$. We assume there is no remanent magnetization in this paper. This assumption is valid for the Archean rocks in Quebec, (If known, existing remanent magnetisation would have to be filtered out prior to applying the cokriging method described in the next section.)

The most common method used to evaluate the potential responses is to break down the 3D domain into geometrically simple bodies having constant susceptibilities or densities. In our case, and for the sake of simplicity, the domain studied is divided into a finite number of rectangular prisms of uniform parameters. It should be noted this classic method can consume memory space for a fine domain discretization. Note however that the method can easily be generalized to accommodate for prisms of different sizes or for other shapes than prisms.

Closed form solutions for magnetic forward modeling were first presented by Bhattacharyya (1964), later simplified in Rao et Babu (1991) into a form more suitable for fast computer implementation. For closed form of gravity modeling also several equivalent analytical forms were proposed (see Li et Chouteau (1998) for a critical review of different formulas). Using Eq. (1) in Shamsipour *et al.* (2010b) and Eq. (3) in Shamsipour *et al.* (2011), the response at the observation point (x_0, y_0, z_0) of all the prisms included within the subsurface model is the sum of the contribution of each prism :

$$T_0 = \sum_{i=1}^{m} T_i(x, y, z) \tag{6.2}$$

$$g_0 = \sum_{i=1}^{m} g_i(x, y, z) \tag{6.3}$$

Considering that there are n total magnetic field or gravity observations and m rectangular prisms, the preceding relationship can also be written in the matrix form :

$$T_{n\times 1} = G_{T(n\times m)}\chi_{m\times 1}, \tag{6.4}$$

$$g_{n\times 1} = G_{g(n\times m)}\rho_{m\times 1} \tag{6.5}$$

with G_T and G_g, matrices of geometric terms (or kernel matrices).

6.3.2 Cokriging

Cokriging (Myers, 1982; Chilès et Delfiner, 1999) is a geostatistical tool that utilizes the spatial correlation between the secondary variables and a primary variable to interpolate or extrapolate primary variable at unsampled locations. The cokriging method provides weights to data so as to minimize the theoretical estimation variance (the cokriging variance). The primary variable could be susceptibility $\boldsymbol{\chi}$, estimated by $\boldsymbol{\chi}^*$ using the secondary variable, here the of total magnetic field $\boldsymbol{T}$. Also, the primary variable could be density $\boldsymbol{\rho}$, estimated by $\boldsymbol{\rho}^*$, using the secondary variable, the gravity data $\boldsymbol{g}$. To allow the use of simple cokriging, and without loss of generality, it is assumed that the inverted densities and magnetic susceptibilities are zero mean variations around a fixed arbitrary mean value.

Assuming spatial homogeneity of the mean for the parameter and observation fields i.e., $E[\boldsymbol{\chi}] = E[\boldsymbol{T}] = 0$ and $E[\boldsymbol{\rho}] = E[\boldsymbol{g}] = 0$, the simple cokriging solution (Myers, 1982) can be obtained by

$$\boldsymbol{C}_{TT}\boldsymbol{\Lambda}_{\boldsymbol{T}} = \boldsymbol{C}_{T\chi}, \tag{6.6}$$

$$\boldsymbol{C}_{gg}\boldsymbol{\Lambda}_{\boldsymbol{g}} = \boldsymbol{C}_{g\rho} \tag{6.7}$$

where all variable here are zero mean random variables and the estimated parameters are defined on the rectangular prism support. C stands for covariance and the indexes indicate auto or cross correlation between random variables. $\boldsymbol{\Lambda_t}$ and $\boldsymbol{\Lambda_g}$ are vectors of weighting coefficients. From above equations, the estimates of susceptibilities and densities are obtained from the observation data using the optimal weights :

$$\boldsymbol{\chi}^* = \boldsymbol{\Lambda}_{\boldsymbol{T}}^T\boldsymbol{T}, \tag{6.8}$$

$$\boldsymbol{\rho}^* = \boldsymbol{\Lambda}_{\boldsymbol{g}}^T\boldsymbol{g}. \tag{6.9}$$

The vectors of cokriging variances are obtained from :

$$\boldsymbol{\sigma}_{ck_\chi} = diag(\boldsymbol{C}_{\chi\chi} - \boldsymbol{\Lambda}_{\boldsymbol{T}}^T \boldsymbol{C}_{T\chi}), \tag{6.10}$$

$$\boldsymbol{\sigma}_{ck_\rho} = diag(\boldsymbol{C}_{\rho\rho} - \boldsymbol{\Lambda}_{\boldsymbol{g}}^T \boldsymbol{C}_{g\rho}). \tag{6.11}$$

The off-diagonal elements give the covariances between estimation errors.

6.3.3 Joint inversion using cokriging

From Eqs. (6.4) and (6.5), parameters and observation fields covariance matrices are linearly related :

$$\boldsymbol{C}_{TT} = \boldsymbol{G_T} \boldsymbol{C}_{\chi\chi} \boldsymbol{G}_{\boldsymbol{T}}^T + \boldsymbol{C}_0, \tag{6.12}$$

$$\boldsymbol{C}_{gg} = \boldsymbol{G_g} \boldsymbol{C}_{\rho\rho} \boldsymbol{G}_{\boldsymbol{g}}^T + \boldsymbol{C}_0, \tag{6.13}$$

$$\boldsymbol{C}_{gT} = \boldsymbol{G_g} \boldsymbol{C}_{\rho\chi} \boldsymbol{G}_{\boldsymbol{T}}^T. \tag{6.14}$$

where $\boldsymbol{C_0}$ in Eqs. 6.12 and 6.13 are diagonal matrices called nugget effect in geostatistics. They represent the data noise variances which can be constant for each observation or vary for different observation subsets (e.g. if different data acquisitions are used). Note that in Eq. 6.14 $\boldsymbol{C_0} = 0$ as noises on gravity and total magnetic field observations can be considered uncorrelated. We also know :

$$\boldsymbol{C}_{T\chi} = \boldsymbol{G_T} \boldsymbol{C}_{\chi\chi}, \tag{6.15}$$

$$\boldsymbol{C}_{g\rho} = \boldsymbol{G_g} \boldsymbol{C}_{\rho\rho}, \tag{6.16}$$

$$\boldsymbol{C}_{T\rho} = \boldsymbol{G_T} \boldsymbol{C}_{\chi\rho}, \tag{6.17}$$

$$\boldsymbol{C}_{g\chi} = \boldsymbol{G_g} \boldsymbol{C}_{\chi\rho}^T. \tag{6.18}$$

The model covariance matrices $\boldsymbol{C}_{\chi\chi}$, $\boldsymbol{C}_{\rho\rho}$ and $\boldsymbol{C}_{\chi\rho}$ and nugget effect matrices $\boldsymbol{C_0}$ are estimated using the multivariate v-v plot method (see next section). Once the covariance models are obtained, the density and magnetic susceptibility parameters are cokriged using

the gravity and magnetic fields data together with any known or fixed parameter value. The cokriging systems are :

$$\begin{bmatrix} \boldsymbol{C}_{T,T} & \boldsymbol{C}_{T,g} \\ \boldsymbol{C}_{g,T} & \boldsymbol{C}_{g,g} \end{bmatrix} \begin{bmatrix} \boldsymbol{\Lambda_1} \\ \boldsymbol{\Gamma_1} \end{bmatrix} = \begin{bmatrix} \boldsymbol{C}_{T,\chi} \\ \boldsymbol{C}_{g,\chi} \end{bmatrix}, \tag{6.19}$$

$$\boldsymbol{\chi}^* = \boldsymbol{\Lambda}_\mathbf{1}^T \boldsymbol{T} + \boldsymbol{\Gamma}_\mathbf{1}^T \boldsymbol{g}, \tag{6.20}$$

$$\begin{bmatrix} \boldsymbol{C}_{g,g} & \boldsymbol{C}_{g,T} \\ \boldsymbol{C}_{T,g} & \boldsymbol{C}_{T,T} \end{bmatrix} \begin{bmatrix} \boldsymbol{\Lambda_2} \\ \boldsymbol{\Gamma_2} \end{bmatrix} = \begin{bmatrix} \boldsymbol{C}_{g,\rho} \\ \boldsymbol{C}_{T,\rho} \end{bmatrix}, \tag{6.21}$$

$$\boldsymbol{\rho}^* = \boldsymbol{\Lambda}_\mathbf{2}^T \boldsymbol{g} + \boldsymbol{\Gamma}_\mathbf{2}^T \boldsymbol{T}. \tag{6.22}$$

Note that the two cokriging systems are solved simultaneously as the left elements of the member in the cokriging equations is identical. For each cokriging system, the vector of cokriging variances is obtained from :

$$\boldsymbol{\sigma}_{ck} = diag(\boldsymbol{C}_L - \tilde{\boldsymbol{\Lambda}}^T \tilde{\boldsymbol{C}}_R) \tag{6.23}$$

where $\tilde{\boldsymbol{\Lambda}}^T = [\boldsymbol{\Lambda}^T, \ \boldsymbol{\Gamma}^T]$ is the coefficient vector, $\tilde{\boldsymbol{C}}_R$ is the right member matrix and $\boldsymbol{C_L}$ is the left member matrix in either Eq. (6.19) or Eq. (6.21).

The inverse matrix calculation to solve Eqs. (6.19) and (6.21) can be done by singular value decomposition (SVD) for small inverse problems or by preconditioned CGA for larger problems.

6.3.4 Linear model of coregionalization (LCM)

Matheron (1965) introduced the proportional covariance model (which he named 'intrinsic model'). This model assumes all cross-covariances and simple-covariances are proportional to an elementary covariance function. The LCM is the sum of proportional covariance models.

For joint inversion of gravity and magnetic data, the LCM can be written as Chilès et Delfiner (1999)

$$\begin{bmatrix} \boldsymbol{C}_{\rho,\rho} & \boldsymbol{C}_{\rho,\chi} \\ \boldsymbol{C}_{\chi,\rho} & \boldsymbol{C}_{\chi,\chi} \end{bmatrix} = \sum_{k=1}^{s} B_k C_k(h) \tag{6.24}$$

with

$$B_k = \begin{bmatrix} b_{\rho,\rho;k} & b_{\rho,\chi;k} \\ b_{\chi,\rho;k} & b_{\chi,\chi;k} \end{bmatrix} \tag{6.25}$$

In this model, all covariances are linear combinations of the same basic structures indexed by k and $k = 1, ..., s$. A sufficient condition for the model to be valid is that for each k, matrix B_k is positive semidefinite. The extension of the LCM to more than 2 variables is immediate. Note that the theoretical simple correlation coefficient between density and susceptibility can be computed from the LCM coefficients :

$$Corr(\chi, \rho) = \frac{\sum_{k=1}^{s} b_{\chi,\rho;k}}{\sqrt{(\sum_{k=1}^{s} b_{\chi,\chi;k})(\sum_{k=1}^{s} b_{\rho,\rho;k})}} \tag{6.26}$$

6.3.5 Multivariate v-v plot

The multivariate v-v plot is the extended version of the v-v plot method Asli *et al.* (2000), Gloaguen *et al.* (2005) and Shamsipour *et al.* (2010b, 2011). In this method the B_k matrices of coefficients and elementary structures parameters $C_k(h)$ are optimized such that the theoretical covariances $C_{g,g}$, $C_{T,T}$ and $C_{g,T}$ computed from the LCM (Eqs. 6.24, 6.12-6.14) show good correlations with their experimental counterparts. In essence, the multivariate v-v plot approach follows exactly the steps for variogram computation except that the binning is done directly on the theoretical direct and cross-covariances instead of the euclidean distance.

6.4 Synthetic cases

The proposed method is tested on two sets of synthetic data : i) a compact model and ii) a stochastic model. In the first synthetic example $Corr(\chi, \rho)$=1, in the second, $Corr(\chi, \rho)$=0.7.

6.4.1 Compact model

The model consists of two cubes of $3 \times 3 \times 2$ m buried in a homogeneous background. The center of the cubes are at locations (x=5.5, y=7.5, z=4) and (x=9.5, y=7.5, z=2) . The 3D domain is divided into $15 \times 15 \times 10 = 2250$ cubic prisms with dimensions $1 \times 1 \times 1$ m. Therefore, each cube consists of 18 prisms. Distances are given in meters but are arbitrary. The susceptibility anomaly of all the prisms inside the cubes is 0.005 SI and their density anomaly is 1000 kg/m^3. The initial density and susceptibility distributions at section $y = 7.5$ m are shown in Figure 6.2 (a) and (b). Because of the constant densities and susceptibilities, $Corr(\chi, \rho)$=1. The surface gravity anomaly is shown in Figure 6.1 (a). We assume that the total magnetic field is only available in a borehole at (x=5.5, y=7.5). With an Earth's inducing field with a strength of 50 000 nT, inclination angle $I = 75°$ and declination angle $D = 45°$, the susceptibility model produces the borehole total magnetic anomaly shown in Figure 6.1 (b).

Using inversion by cokriging (Shamsipour *et al.*, 2010b), we invert gravity data at the surface to estimate the density distribution. The densities at section $y = 7.5$ m are shown in Figure 6.2 (c). Then, we invert the total magnetic field at the borehole to estimate the susceptibility distribution. The results at section $y = 7.5$ m are shown in Figure 6.2 (d). Shamsipour *et al.* (2010b, 2011) have proved that the calculated gravity and total magnetic field from the inverted models match perfectly the observed values when C_0=0 in Eqs 6.12 and 6.13. Note that independent inversion of gravity data does not recover the depth of the cubes. Also, as the total magnetic field data is measured in a single borehole, the inverted susceptibility field shows radially symmetric variations.

The joint inversion of gravity and magnetic data are shown in Figure 6.2 (e-f) for the density and the susceptibility respectively. Both density and susceptibility distributions better reproduce the synthetic model compared to the separate inversions. In particular, the depths of the cubes are close to the initial model.

As mentioned, the observed gravity and total magnetic field are perfectly reproduced by both the separate and joint inversion models Figure 6.3 (a).

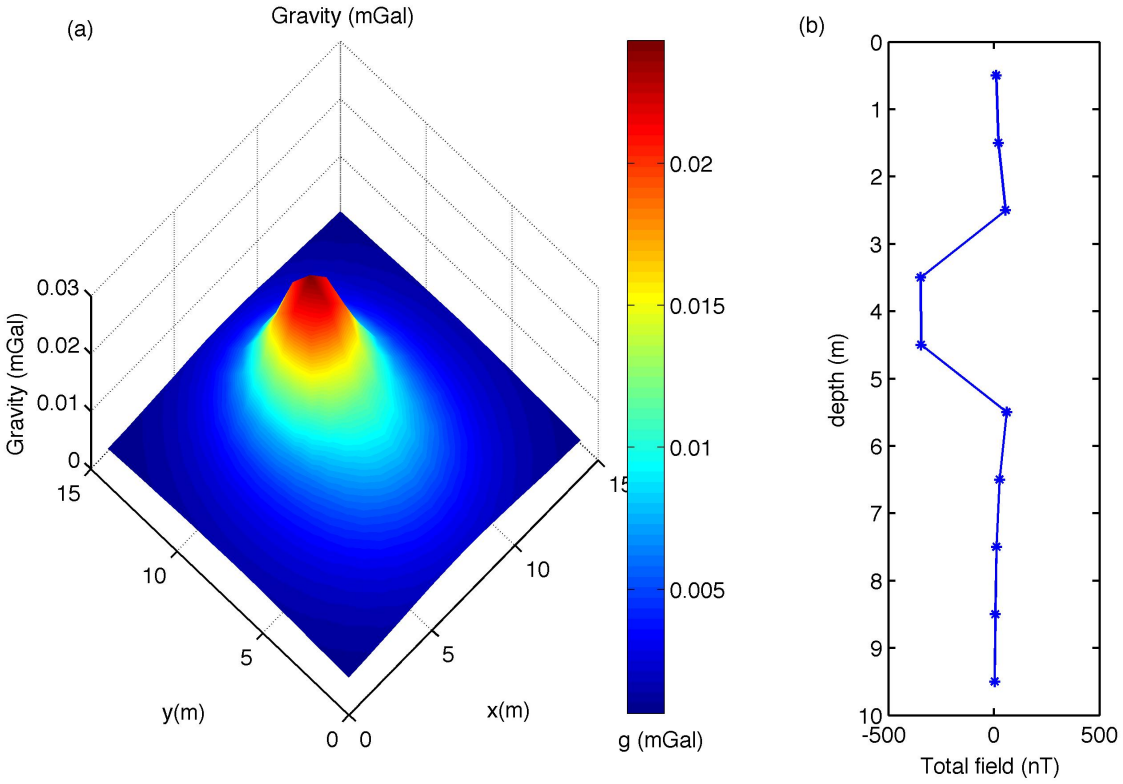

Figure 6.1 (a) Gravity data at the surface, (b) Total magnetic field in the borehole.

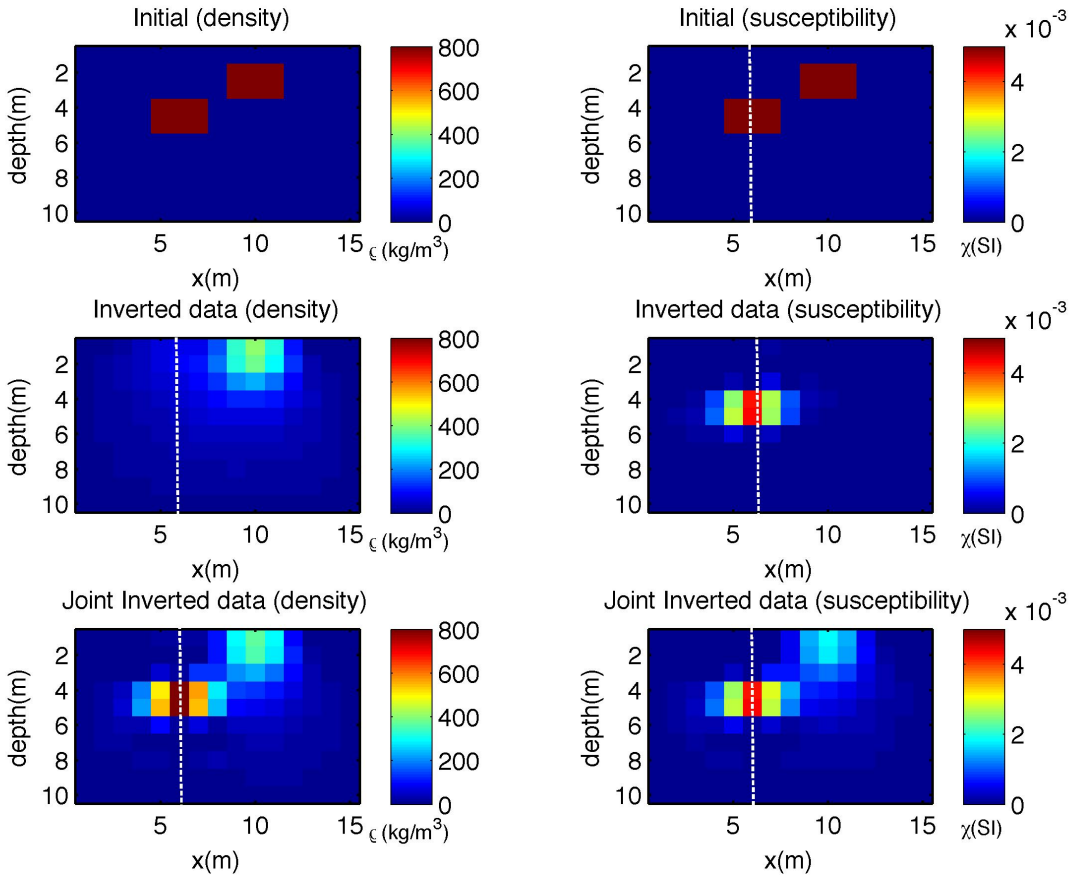

Figure 6.2 (a) Initial density distribution, (b) Initial susceptibility distribution, (c) Inverted density values using the surface gravity data, (d) Inverted susceptibility values using the surface total magnetic field, (e) Inverted density values using both the surface total magnetic field and gravity data, (f) Inverted susceptibility values using both the surface total magnetic field and gravity data. All the results are shown in section $y = 7.5$ m

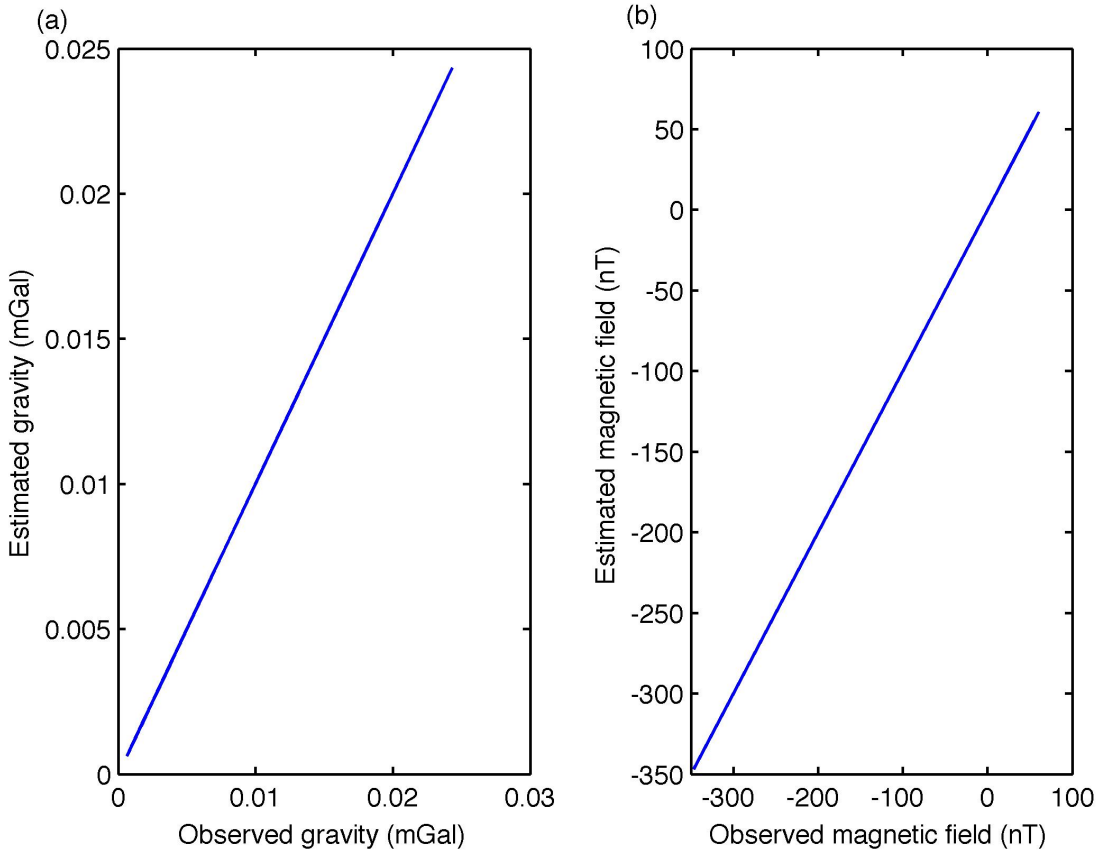

Figure 6.3 (a) Observed gravity versus calculated gravity using the estimated densities by joint inversion, (b) observed total magnetic field versus calculated total magnetic field using the estimated susceptibilities by joint inversion.

6.4.2 Stochastic model

The 3D domain is divided into $15 \times 15 \times 10 = 2250$ cubic prisms. Susceptibilities and densities are generated on 1 m $\times$ 1 m $\times$ 1 m prisms using LU simulation (Chilès et Delfiner, 1999). The LCM has a single spherical structure with range $a = 5$ m, density variance of 50000 $(kg/m^3)^2$ and susceptibility variance of 0.0001 SI. The correlation $Corr(\chi, \rho)$ is 0.7, thus, the magnetic field and gravity field are not caused by the exact same source.

The generated density and susceptibility distributions at section $y = 7.5$ m are shown in Figure 6.5 (a) and (b) respectively. The Earth's inducing field has a strength of 50 000 nT and inclination and declination are $I = 45°$ and $D = 70°$ respectively. Using the susceptibility values, we calculate the synthetic total magnetic field data at the surface from susceptibility values (Figure 6.4 (a)). Using the density values, we calculate the synthetic gravity data along a borehole, at x=7.5 m and y=7.5 m, shown in Figure 6.4 (b). We suppose that the total magnetic field data and gravity data are observed without error. From now on, we assume the gravity and total magnetic field data are known and we invert them to estimate the density and susceptibility distributions.

Figure 6.5 shows the results of the separate (c)-(d) and joint density and susceptibility inversions (e)-(f). Using the multivariate v-v plot method, the adjusted LCM is spherical with $a = 4.8$ m and variances $C = 0.00012$ SI and $C = 50000$ $(kg/m^3)^2$ and correlation coefficient 0.75, values close to those of the parameters used to simulate the data.

In the separate density inversion (c), the model shows circular symmetry around the borehole as this was the only available data. Density and susceptibility distributions in the joint inversions (e)-(f) are closer to the initial models (a)-(b) than the separate inversions (c)-(d). The estimated densities have especially been improved close to the surface because of the extra information provided by the total magnetic filed data. On the other hand, the susceptibilities have been improved at depths because of the extra information from gravity data along the borehole. The joint density and susceptibility inversions are significantly more correlated with the true model compared to separate inversions (0.29 and 0.46 vs 0.12 and 0.41). Also, we note that the correlation between the separate density and susceptibility

inverted fields is close to zero while the jointly inverted fields have a correlation of 0.77, a value close to the initial model correlation (0.7).

Figure 6.6 (a), confirms that gravity and magnetic data are perfectly reproduced by calculated fields from both the separate and joint inversions.

6.5 Case study

6.6 Application to Survey Data

The survey data was collected over the area of the Perseverance mine located in the Matagami region in Quebec, Canada. The area of the 2001 total magnetic field survey extends from longitude 77° 47′ 46” W to 77° 46′ 59” W and from latitude 49° 45′ 13” N to 49° 45′ 59” N, where 441 magnetic ground measurements with about 50-m spacing are available. 44 ground gravity data were collected using a Scintrex CG5 gravity meter (accuracy .005 mGal) in a restricted area of the Perseverance mine (anomaly A in Figure 6.7). The data were provided by Xstrata Zinc inc., owner and operator of the Perseverance zinc mine. The maximum error and the standard deviation of the errors were estimated to be 0.17 mGal and 0.1 mGal respectively (Dr Pierre Keating, personal communication, 2011). No terrain correction was included in the reduction of the Bouguer anomaly because the topography is flat in the survey area (maximum elevation differences are 2.7 m with a standard deviation of less than 1.1 m).

The study area is located in the northern part of the Abitibi Subprovince, one of the largest Archean greenstone belts in the world. Many volcanogenic massive sulfide (VMS) deposits have been identified in the Archean-age Abitibi greenstone belt, which straddles across the provincial border of Ontario and Quebec. The Matagami volcanic complex of northern Abitibi belt was formed by two major phases of volcanism (Piché *et al.*, 1993) :

- the initial phase was dominated by the extrusion of tholeiitic rhyolite and rhyodacite lavas (the Watson Lake Group)
- the second phase was distinguished primarily by calcalkaline basaltic to andesitic vol-

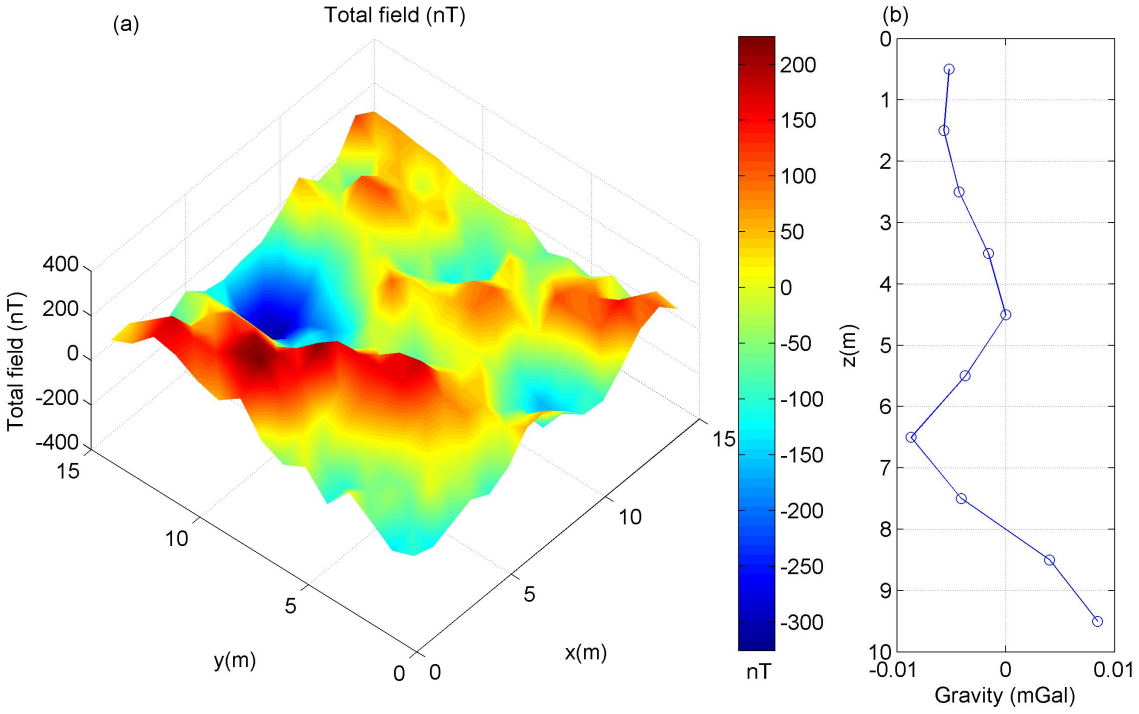

Figure 6.4 (a) Synthetic total magnetic field data at surface, (b) Synthetic gravity data collected in the borehole.

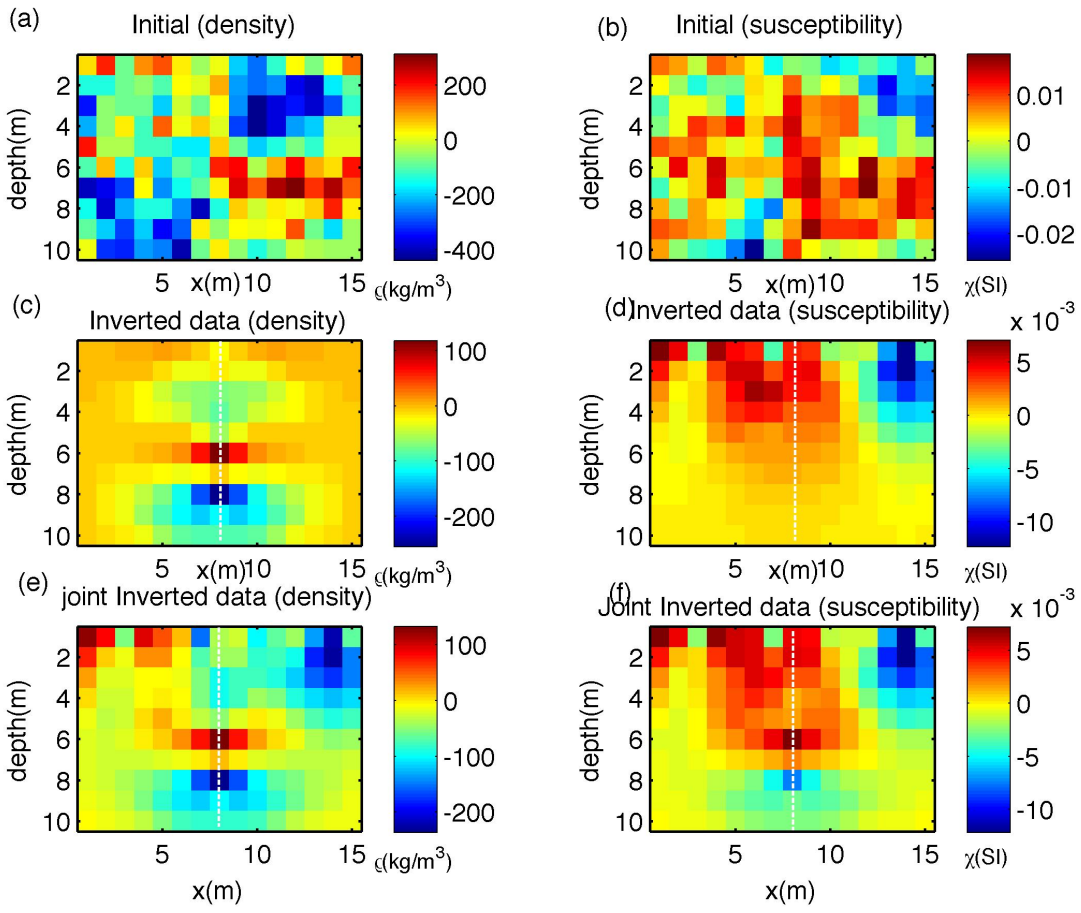

Figure 6.5 (a) Initial density distribution, (b) Initial susceptibility distribution, (c) Inverted density distribution using borehole gravity data, (d) Inverted susceptibility distribution using surface total magnetic field data, (e) Inverted density distribution using joint inversion of borehole gravity data and surface total magnetic field data, (f) Inverted susceptibility distribution using joint inversion of borehole gravity and surface total magnetic field data. All the results are shown for section $y = 7.5$ m.

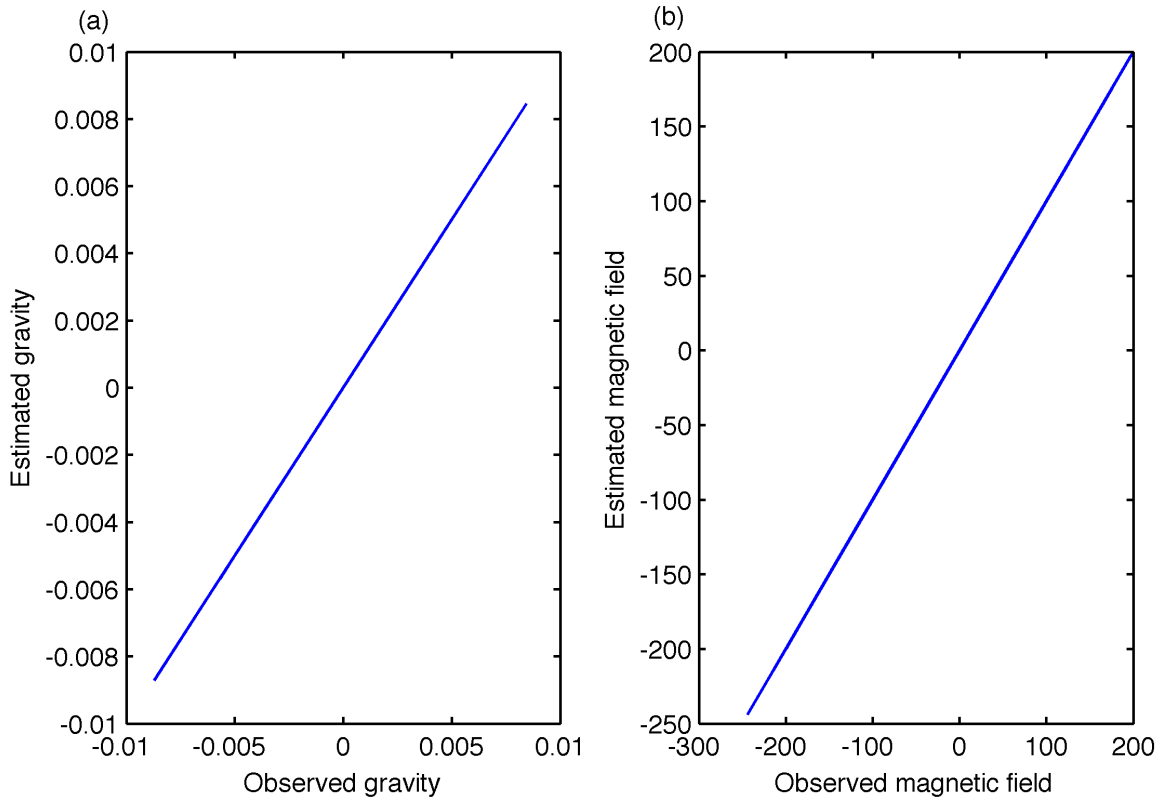

Figure 6.6 (a) Observed gravity versus the calculated gravity using the estimated densities by joint inversion, (b) observed total magnetic field versus the calculated total magnetic field using the estimated susceptibilities by joint inversion.

canism (the Wabassee Group)

A cherty, sulphidic chemical sediment known as the Key Tuffite marks the contact and discontinuity between the two groups. This 1-6 m thin horizon is the primary exploration target because it hosts most of the ore bodies discovered in the area (Calvert et Li, 1999). Exploration of the Key Tuffite by systematic drilling is very expensive especially with increasing depth, thus geophysical methods can provide a valuable alternative. Exploration of VMS deposits in the whole Matagami area lead to the opening of 11 mines in the past 50 years. The largest mine was the Mattagami Lake mine with a total production of 25.64 Mt ore. A new discovery has been made by Xstrata Zinc Canada in 2007, the Bracemac-McLeod deposit, which is expected to be in production in 2013.

The Perseverance mine was discovered in April 2000, a feasibility study was done in 2002 but did not enter production before 2008 due to the depressed zinc market. It is the only active mine in the study area. This mine consists of three major massive sulfide deposits, Perseverance, Perseverance west and Equinox indicated in Figure 6.7 as A, C and B respectively. The Perseverance deposit has a total production of 1.2 MT (14.55% Zn and 1.20% Cu). Estimates for the Perseverance west deposit and the Equinox deposit are 1.1 MT (12.61% Zn and 1.38% Cu) and 2.5 MT (14.93% Zn and 0.98% Cu) respectively. Magnetite and pyrrhotite are often associated with the VMS deposits. For Perseverance lenses, the magnetic anomalies are mainly caused by the presence of magnetite although the pyrrhotite can have some local contributions.

6.6.1 Inversion

The residual magnetic field anomaly was obtained by subtracting the IGRF (International Geomagnetic Reference Field) from the measured total field (Figure 6.8 (a)). The regional gravity field was obtained by calculating the first order trend from the Bouguer anomaly data. Subtracting the regional from the Bouguer anomaly produced the residual anomaly (Figure 6.8 (b)) ranging between 0.04 and 0.4 mGal.

The inversion domain is divided into $n_x = 26$ by $n_y = 26$ by $n_z = 10$ cubes of dimension

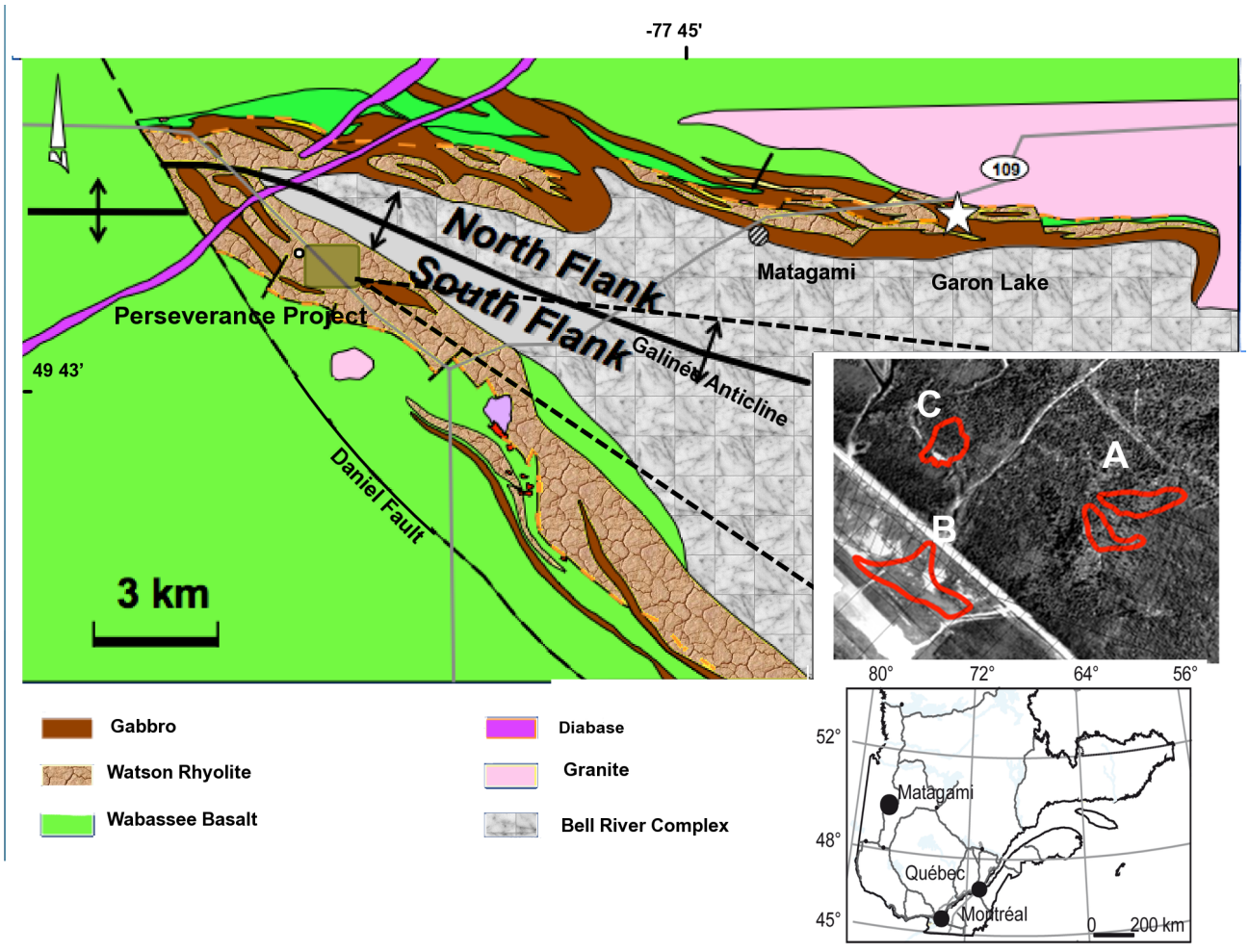

Figure 6.7 Geology map of Matagami camp with Perseverance mine highlighted.

40 m $\times$ 40 m $\times$ 30 m. Therefore, the whole domain is 1040 m $\times$ 1040 m $\times$ 300 m and the total number of prisms is $m = 6760$.

Sections from separate and joint inversions for densities and susceptibilities are shown in Figure 6.9(a)-(d)for an East-West vertical section at $y = 5515450$ m, and in Figures 6.10 and 6.11(a)-(d) for horizontal sections at $z = 150$ m and $z = 200$ m respectively. The LCM was adjusted using the v-v plot method. The basic structure is spherical with $a = 130$ m and sills $C = .0003$ SI and $C = 17000$ $(kg/m^3)^2$ respectively. Fitted correlation obtained using multivariate v-v plot is 0.89.

Two strongs and one weak susceptibility highs are seen in the plane sections ($z = 150$ and $z = 200$ m) for both separate and joint inversions. The highs are well correlated with the three Perseverance deposits indicated by letters A, B and C. The largest susceptibility high is correlated with Perseverance deposit (A), the smallest susceptibility high is correlated with Perseverance west deposit (C) and the third susceptibility high is related to Equinox deposit (B). The susceptibilities at cross section $y = 5515450$ m (Figure 6.9 (b) show the extension of Perseverance deposit (A) and Equinox deposit (B) at depth. For the inversion of densities however, only the Perseverance deposit (A) can be recognized in plans and cross-sections. The reason is that the gravity data used only cover the area of the Perseverance mine (anomaly A). Therefore, separate inversion of gravities can not recover Perseverance west deposit (C) or Equinox deposit (B).

With joint inversion, the main improvement compared to separate inversion is for the densities, due to the extra information from the total magnetic field data at the surface. In plane sections, one now clearly recognize in the densities inversion three deposits (A, B and C), a noticeable improvement. Even deposit A has now better depth resolution compared to the separate densities inversion. The susceptibilities have also been improved at depths (especially at deposit A) because of the extra information from gravity data (compare Figure 6.9 (b) and (d)).

Depths of the deposits are the following : Perseverance (30 m-200 m), Perseverance-West (100 m-200 m) and Equinoxe (90 m-275 m) (Allard, 2011, personal communication). Clearly,

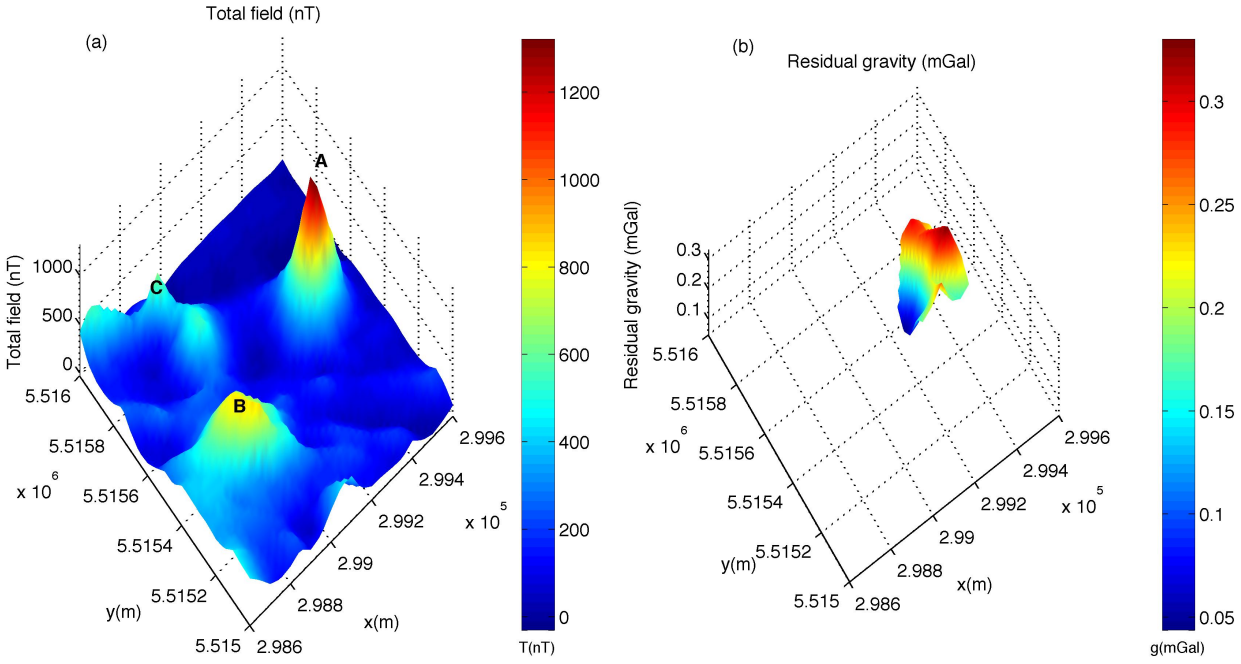

Figure 6.8 (a) Total magnetic field residual anomaly in the study area. (b) residual gravity anomaly above Perseverance mine (anomaly A).

the joint inversion better recovers than separate inversions the top and bottom location of Perseverance A deposit in the susceptibility inverted fields, and of all three deposits in the density inverted fields.

As before, the calculated gravity and total magnetic field computed from the inverted fields are identical to the observed data.

6.7 Discussion

One advantage of the inversion by cokriging is that the magnetic field and gravity field do not need to be caused by the exact same source. In one of our synthetic case study, a correlation of 0.7 only exists between the density-susceptibility fields. Similarly, in the real case study, the correlation was found to be 0.89 between the density-susceptibility fields. This correlation is obtained by adjusting experimentally the gravity and total magnetic field data available, using the v-v plot approach. Therefore, the joint inversion will use the auxiliary information only when this correlation is significant. For example, $Corr_{\chi,\rho} = 0$ would result in joint inversions identical to the separate inversions.

The proportional covariance model has the following general screening property : when all the variables are measured at the same points the cokriging estimator boils down to the kriging estimator based on that variable alone. Translated in the present context, this means that the joint inversion is identical to the separate inversions when data are located at the same points, whatever the value for $Corr_{\chi,\rho}$. This property does not hold strictly when a LCM model different from the proportional model is used (e.g. a spherical component plus a a nugget effect). However, the gain expected from joint inversion in this case is not expected to be important.

Obtaining a good fit between the theoretical and experimental covariances by the v-v plot method is sometimes challenging. Nevertheless, it is possible to obtain from geological knowledge, at least crude estimates of the variances of each variable and of the ranges along the principal geologic directions. This could dictate good starting parameter values for the LCM model. As for any optimization, it can be useful to consider various starting values

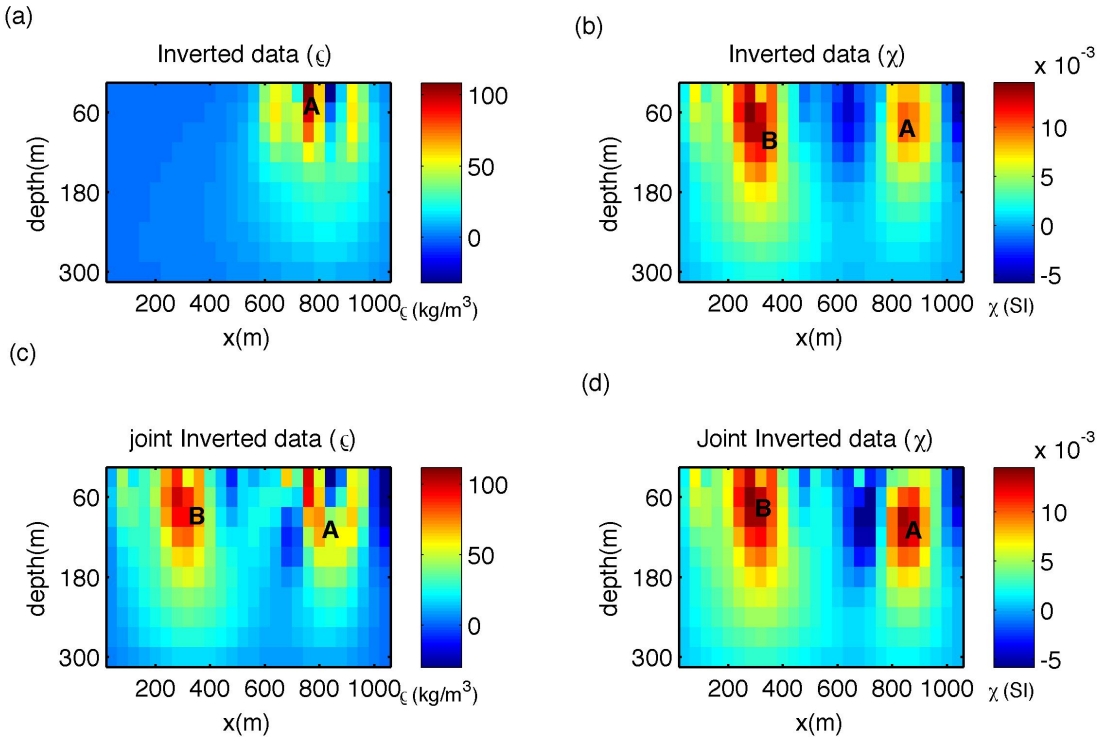

Figure 6.9 (a) Inverted density distribution using gravity data, (b) Inverted susceptibility distribution using surface total magnetic field data, (c) Inverted density distribution using joint inversion of gravity data and total magnetic field data, (d) Inverted susceptibility distribution using joint inversion of gravity data and total magnetic field data. All the results are shown for an East-West cross-section at $y = 5515450$ m from the 3D inverted models.

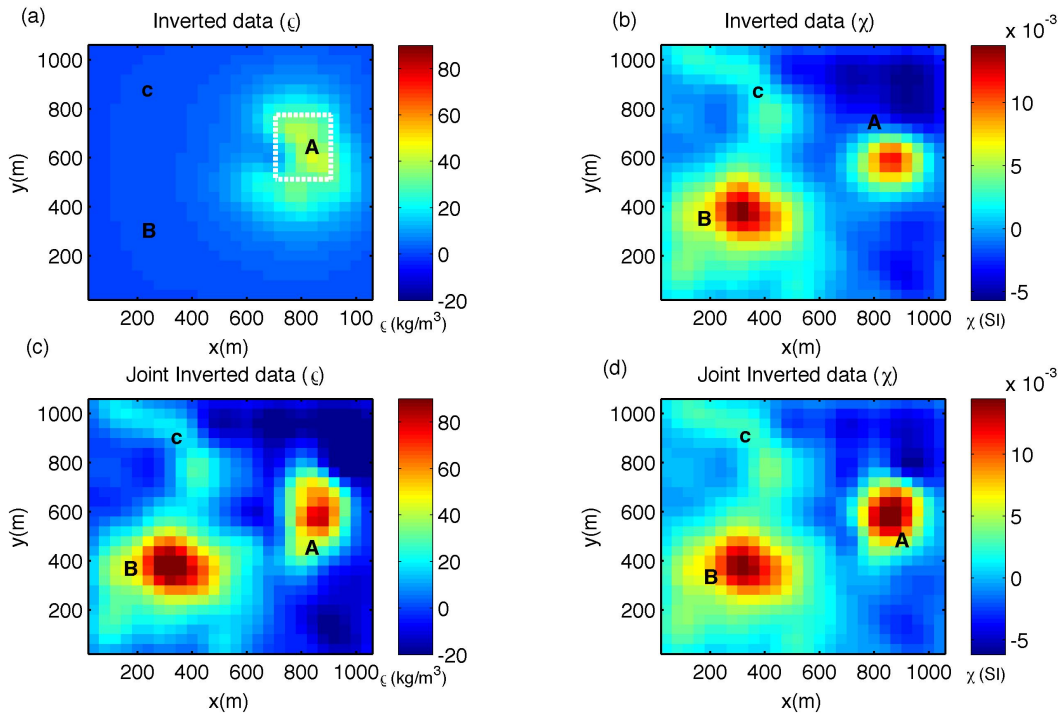

Figure 6.10 (a) Inverted density distribution using gravity data (The gravity survey area over Perseverance deposit is delimited with a white dashed square) , (b) Inverted susceptibility distribution using surface total magnetic field data, (c) Inverted density distribution using joint inversion of gravity data and total magnetic field data, (f) Inverted susceptibility distribution using joint inversion of gravity and total magnetic field data. All the results are shown for horizontal section $z = 150$ m.

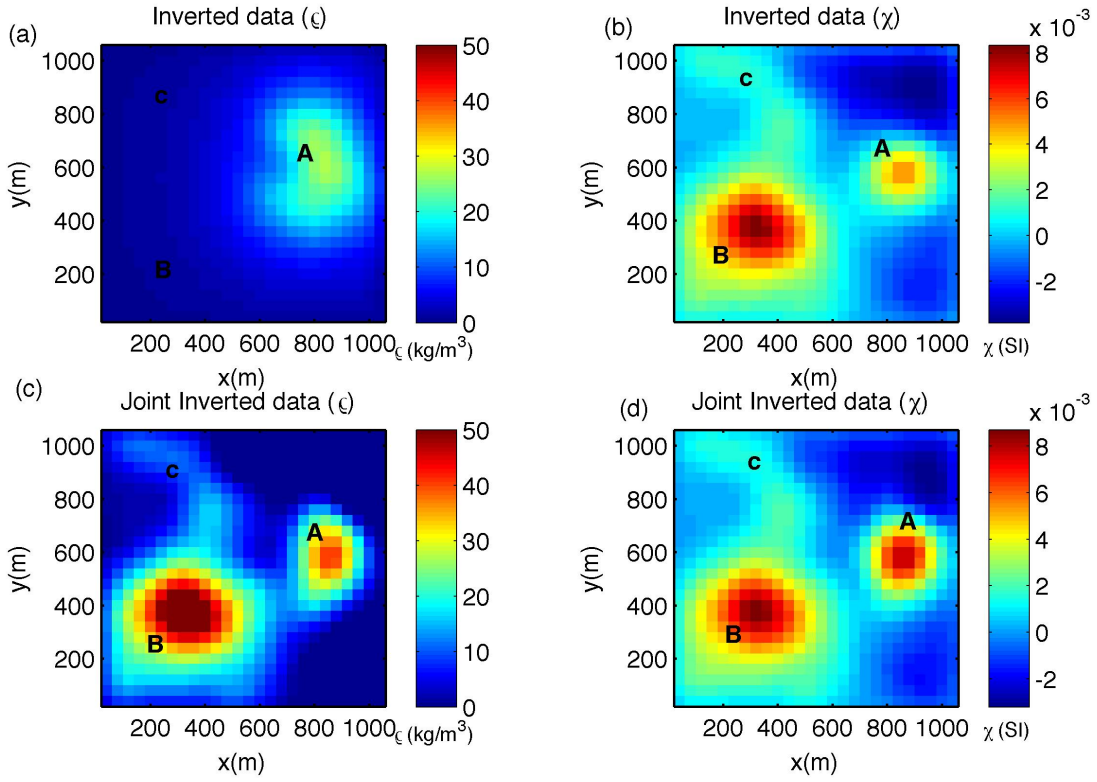

Figure 6.11 (a) Inverted density distribution using gravity data, (b) Inverted susceptibility distribution using surface total magnetic field data, (c) Inverted density distribution using joint inversion of gravity data and total magnetic field data, (f) Inverted susceptibility distribution using joint inversion of gravity and total magnetic field data. All the results are shown for horizontal section $z = 200$ m.

to help identify the presence of local minimums. The adjustment is usually best done semi-automatically. The structure of LCM model (number and type of elementary structures) is selected first manually after a few trials with different elementary structures. Then, the LCM parameters are adjusted automatically and modified at the end, when judged necessary (e.g. unrealistic parameter values upon stopping criteria). The method accommodates white noise (observation errors) in the form of a nugget effect $\boldsymbol{C_0}$ matrix (see Eqs. 6.12 and 6.13). Results are stable (as for any kriging or cokriging) in the presence of noise. When $\boldsymbol{C_0}$ is present in Eqs. 6.12 and 6.13, the computed gravity and magnetic field anomalies do not match perfectly the observed data, however the observed discrepancies are compatible with the noise level described by $\boldsymbol{C_0}$. Note that when $\boldsymbol{C_0}$ is set to 0, the computed gravity and magnetic field match perfectly the observed data (as long as there are more parameters in the model than observations), irrespective of the data being really noise-free or not. Conversely, when $\boldsymbol{C_0} \neq 0$, the computed gravity and magnetic field match the observed data more or less depending of the noise variance level. The v-v plot helps determinate the values of $\boldsymbol{C_0}$, but other knowledge like the expected level of noise for a given data acquisition could also be used to estimate this matrix.

The proposed non-iterative joint inversion method based on cokriging is computationally efficient. For mid-size problem like the case study, the inversion is done on standard laptop in less than 10 minutes. For larger problems, the bottleneck is the available memory to store the required covariance matrices. However, practical solutions exist. A simple one is to adopt isotropic covariance function with a finite range (e.g. spherical model) with the sparse matrix coding. Moreover, for an isotropic model, the parameter covariance matrices are all circulant matrices. Hence only the covariances of the first row need really be computed and stored (see Nowak *et al.* (2003)).

6.8 Conclusion

We present a joint inversion method based on the cokriging geostatistical approach for the joint 3D inversion of total magnetic field and gravity data. Tests on synthetic data show

the potential advantages of this method. The proposed joint inversion applied on data from Matagami mining camp (Perseverance mine) prove better agreement with the known geology. The method can be easily applied to other geophysical variables and it can accommodate more than two variables. Greater gains from the joint inversion with respect to the separate inversions are expected when the data are not collocated and when the correlation between the physical properties is strong.

6.9 Acknowledgments

We would like to express sincere thanks to Michel Allard from Xstrata Zinc for providing the Matagami data, and for his guidance and support.

References

ASLI, M., MARCOTTE, D. et CHOUTEAU, M. (2000). Direct inversion of gravity data by cokriging. W. Kleingeld et D. Krige, éditeurs, *6th International Geostatistics Congress, Cape town, South Africa*, Cape Town, South Africa. 64–73.

BHATTACHARYYA, B. (1964). Magnetic anomalies due to prism-shaped bodies with arbitrary polarization. *Geophysics*, 29, 517.

BOSCH, M., MEZA, R., JIMÉNEZ, R. et HÖNIG, A. (2006). Joint gravity and magnetic inversion in 3D using Monte Carlo methods. *Geophysics*, 71, G153.

CALVERT, A. et LI, Y. (1999). Seismic reflection imaging over a massive sulfide deposit at the Matagami mining camp, Québec. *Geophysics*, 64, 24–32.

CHASSERIAU, P. et CHOUTEAU, M. (2003). 3D gravity inversion using a model of parameter covariance. *Journal of Applied Geophysics*, 52, 59 – 74.

CHILÈS, J. et DELFINER, P. (1999). *Geostatistics : modeling spatial uncertainty*. Wiley.

FRANKLIN, J. (1970). Well posed stochastic extensions of Ill posed linear problems. *J. Math*, 31, 682–716.

FREGOSO, E. et GALLARDO, L. (2009). Cross-gradients joint 3D inversion with applications to gravity and magnetic data. *Geophysics*, 74, L31.

GALLARDO-DELGADO, L., PEREZ-FLORES, M. et GÓMEZ-TREVIÑO, E. (2003). A versatile algorithm for joint 3D inversion of gravity and magnetic data. *Geophysics*, 68, 949–959.

GIROUX, B., GLOAGUEN, E. et CHOUTEAU, M. (2007). bh_tomo–a Matlab borehole georadar 2D tomography package. *Computers and Geosciences*, 33, 126–137.

GLOAGUEN, E., MARCOTTE, D., CHOUTEAU, M. et PERROUD, H. (2005). Borehole radar velocity inversion using cokriging and cosimulation. *Journal of Applied Geophysics*, 57, 242 – 259.

GLOAGUEN, E., MARCOTTE, D., GIROUX, B., DUBREUIL-BOISCLAIR, C., CHOUTEAU, M. et AUBERTIN, M. (2007). Stochastic borehole radar velocity and attenuation tomographies using cokriging and cosimulation. *Journal of Applied Geophysics*, 62, 141 – 157.

HANSEN, T., JOURNEL, A., TARANTOLA, A. et MOSEGAARD, K. (2006). Linear inverse Gaussian theory and geostatistics. *Geophysics*, 71, R101.

LI, X. et CHOUTEAU, M. (1998). Three-dimensional gravity modeling In all Space. *Surveys in Geophysics*, 19, 339–368.

MATHERON, G. (1965). Les variables régionalisées et leur estimation. *Une Application de la Théorie des Functions Aléatories aux Sciences de la Nature. Masson, Paris.*

MYERS, D. (1982). Matrix formulation of co-kriging. *Mathematical Geology*, 14, 249–257.

NOWAK, W., TENKLEVE, S. et CIRPKA, O. (2003). Efficient computation of linearized cross-covariance and auto-covariance matrices of interdependent quantities. *Mathematical Geology*, 35, 53–66.

PICHÉ, M., GUHA, J. et DAIGNEAULT, R. (1993). Stratigraphic and structural aspects of the volcanic rocks of the Matagami mining camp, Quebec ; implications for the Norita ore deposit. *Economic Geology*, 88, 1542–1558.

PILKINGTON, M. (2006). Joint inversion of gravity and magnetic data for two-layer models. *Geophysics*, 71, L35.

RAO, D. et BABU, N. (1991). A rapid method for three-dimensional modeling of magnetic anomalies. *Geophysics*, 56, 1729.

SHAMSIPOUR, P., CHOUTEAU, M. et MARCOTTE, D. (2011). 3d stochastic inversion of magnetic data. *Journal of Applied Geophysics*, 73, 336–347.

SHAMSIPOUR, P., MARCOTTE, D., CHOUTEAU, M. et KEATING, P. (2010). 3D stochastic inversion of gravity data using cokriging and cosimulation. *Geophysics*, 75, I1–I10.

TARANTOLA, A. et VALETTE, B. (1982). Generalized nonlinear inverse problems solved using the least squares criterion. *Rev. Geophys. Space Phys*, 20, 219–232.

ZEYEN, H. et POUS, J. (1993). 3-D joint inversion of magnetic and gravimetric data with a priori information. *Geophysical Journal International*, 112, 244–244.

CHAPITRE 7

GENERAL DISCUSSION AND CONCLUSION

7.1 Conclusion

A 3D stochastic inversion method based on a geostatistical approach is presented for three-dimensional single and joint inversion of potential fields. The algorithm has the capability of inverting data on multiple supports. The aim of applying geostatistics is to provide quantitative descriptions of natural variables distributed in space or in time and space. The method fully integrates the physical relations between the properties (density and magnetic susceptibility) and the indirect observations (gravity and total magnetic field). Two modes of application are presented : estimation and simulation. In all the methods presented in this thesis, compact and stochastic synthetic models are investigated. The results show the ability of the methods to invert surface and borehole data simultaneously on multiple scale parameters.

A case study using ground measurements of total magnetic field and gravity data at the Perseverance mine (Quebec, Canada) is presented. The recovered 3D susceptibility and density model provides beneficial information that can be used to analyze the geology of massive sulfide for the domain under study.

7.2 Limitations of proposed methods

In a very large problem with large number of prisms, the required storage and computational costs to compute the model parameter covariance matrix are prohibitive. We have recommended using the method based on circulant embedding and the fast Fourier transform (FFT) for efficient calculation of the parameter covariance matrix . Noted, using the full covariance matrix is expensive both in computing time and memory. When dealing with small compact ore body such as massive sulphides, the range of the variogram is likely to be

small. Therefore, most elements of covariance matrices are zero and sparse matrix techniques can be used to solve the cokriging equations efficiently. Use of sparsity in cokriging system is shown in a simple example in Chapter 4.

Obtaining a good fit between the theoretical and experimental covariances by the v-v plot method is sometimes challenging. Nevertheless, it is possible to use geological knowledge in order to obtain at least crude estimates of the variances of each variables and of the ranges along the principal geologic directions. This could also dictate good starting parameter values for the LCM model. As for any optimization, it can be useful to consider various starting values to help identify the presence of local minimums. The adjustment is usually best done semi-automatically. The structure of LCM model (number and type of elementary structures) is selected first manually after a few trials with different elementary structures. Then, the LCM parameters are adjusted automatically and modified at the end, when judged necessary (e.g. unrealistic parameter values upon stopping criteria). The method accommodates white noise (observation errors) in the form of a nugget effect $\boldsymbol{C_0}$ matrix . Results are stable (as for any kriging or cokriging) in the presence of noise. When $\boldsymbol{C_0}$ is present in Eqs. 6.12 and 6.13, the computed gravity and magnetic field anomalies do not match perfectly the observed data, however the observed discrepancies are compatible with the noise level described by $\boldsymbol{C_0}$. Note that when $\boldsymbol{C_0}$ is set to zero, the computed gravity and magnetic field match perfectly the observed data (as long as there are more parameters in the model than observations), irrespective of the data being really noise-free or not. Conversely, when $\boldsymbol{C_0} \neq 0$, the computed gravity and magnetic field match the observed data more or less depending of the noise variance level. The v-v plot helps determinate the values of $\boldsymbol{C_0}$, but other knowledge like the expected level of noise for a given data acquisition could also be used to estimate this matrix.

7.3 Future Works

– Similar to gravity inversion, recovering susceptibilities in 3D magnetic inversion requires integration of many different data. These data mainly come from different sources with different volume supports (point and block support). We have started to develop a 3D

stochastic inversion method based on a geostatistical approach (cokriging) for three-dimensional inversion of magnetic data on multiple scale parameters using borehole and surface data to limit the resulting solution space. This project in collaboration with Xtrata zinc company is currently in progress.

– Investigating Bayesian inversion of geophysical data by Markov chain Monte Carlo (MCMC) sampling is one of our interests. We could apply geostatistical techniques for the acquisition of prior model information and then the MCMC method could be adopted to infer the characteristics of the marginal distributions of model parameters.
– The computing efficiency can be increased using sparse and circulant matrix methods for multiscale joint inversion. Covariance matrix of parameters is the largest matrix ($m \times m$, m number of parameters) in solving cokriging system equations. Using the full matrix is expensive both in computing time and memory. When dealing with small compact ore bodies such as massive sulphides, the range of the variogram is likely to be small. Therefore, most covariances are 0 and sparse matrix techniques can be used to solve efficiently the cokriging equations. Use of sparsity in cokriging system is shown in a simple example in Appendix 4.11. We can solve this problem using the method proposed by Nowak *et al.* (2003), which is based on circulant embedding and the fast Fourier transform (FFT). This method is useful and has lower computational complexity.
– We would like also to integrate the topography effect on 3D inversion of potential field. This can be done by defining multigrid or unstructured mesh.
– We plan to develop interfaces for the presented algorithms. Currently, the codes are available in C++, Python language and Matlab without visualizer.

REFERENCES

ADAM, E., MILKEREIT, B. et MARESCHAL, M. (1998). Seismic reflection and borehole geophysical investigations in the matagami mining camp. *Canadian Journal of Earth Sciences*, 35, 686–695.

ARMSTRONG, M. (1984). Common problems seen in variograms. *Mathematical Geology*, 16, 305–313.

ASLI, M., MARCOTTE, D. et CHOUTEAU, M. (2000). Direct inversion of gravity data by cokriging. W. Kleingeld et D. Krige, éditeurs, *6th International Geostatistics Congress, Cape town, South Africa*, Cape Town, South Africa. 64–73.

BHATTACHARYYA, B. (1964). Magnetic anomalies due to prism-shaped bodies with arbitrary polarization. *Geophysics*, 29, 517.

BLAKELY, R. (1995). *Potential Theory in Gravity and Magnetic Applications*. Cambridge University Press.

BOSCH, M. et MCGAUGHEY, J. (2001). Joint inversion of gravity and magnetic data under lithologic constraints. *The Leading Edge*, 20, 877–881.

BOSCH, M., MEZA, R., JIMÉNEZ, R. et HÖNIG, A. (2006). Joint gravity and magnetic inversion in 3D using Monte Carlo methods. *Geophysics*, 71, G153.

BOULANGER, O. (2004). *Modélisations et inversions tri-dimensionnelles en prospections gravimétrique et électrique*. Thèse de doctorat, École Polytechnique de Montréal.

BOULANGER, O. et CHOUTEAU, M. (2001). Constraints in 3D gravity inversion. *Geophysical Prospecting*, 49, 265 – 280.

CALVERT, A. et LI, Y. (1999). Seismic reflection imaging over a massive sulfide deposit at the Matagami mining camp, Québec. *Geophysics*, 64, 24–32.

CHASSERIAU, P. et CHOUTEAU, M. (2003). 3D gravity inversion using a model of parameter covariance. *Journal of Applied Geophysics*, 52, 59 – 74.

CHILÈS, J. et DELFINER, P. (1999). *Geostatistics : modeling spatial uncertainty*. Wiley.

DEUTSCH, C. et JOURNEL, A. (1998). *GSLIB : Geostatistical Software Library and User's Guide, 369 pp*. Oxford Univ. Press, New York.

FEDI, M. et RAPOLLA, A. (1999). 3-D inversion of gravity and magnetic data with depth resolution. *Geophysics*, 64, 452–460.

FRANKLIN, J. (1970). Well posed stochastic extensions of Ill posed linear problems. *J. Math*, 31, 682–716.

FREGOSO, E. et GALLARDO, L. (2009). Cross-gradients joint 3D inversion with applications to gravity and magnetic data. *Geophysics*, 74, L31.

GALLARDO-DELGADO, L., PEREZ-FLORES, M. et GÓMEZ-TREVIÑO, E. (2003). A versatile algorithm for joint 3D inversion of gravity and magnetic data. *Geophysics*, 68, 949–959.

GIROUX, B., GLOAGUEN, E. et CHOUTEAU, M. (2007). bh_tomo–a Matlab borehole georadar 2D tomography package. *Computers and Geosciences*, 33, 126–137.

GLOAGUEN, E., MARCOTTE, D., CHOUTEAU, M. et PERROUD, H. (2005). Borehole radar velocity inversion using cokriging and cosimulation. *Journal of Applied Geophysics*, 57, 242 – 259.

GLOAGUEN, E., MARCOTTE, D., GIROUX, B., DUBREUIL-BOISCLAIR, C., CHOUTEAU, M. et AUBERTIN, M. (2007). Stochastic borehole radar velocity and attenuation tomographies using cokriging and cosimulation. *Journal of Applied Geophysics*, 62, 141 – 157.

GOMEZ-HERNANDEZ, J., FROIDEVAUX, R. et BIVER, P. (2004). Exact conditioning to linear constraints in kriging and simulation. O. Leuangthong et C. V. Deutsch, éditeurs, *Gestatistics Banff 2004*, Springer, Berlin.

GREEN, W. (1975). Inversion of gravity profiles by use of a Backus-Gilbert approach. *Geophysics*, 40, 763–772.

HAÁZ, I. (1953). Relations between the potential of the attraction of the mass contained in a finite rectangular prism and its first and second derivatives. *Geophysical Transactions II*, 7, 57–66.

HANSEN, T., JOURNEL, A., TARANTOLA, A. et MOSEGAARD, K. (2006). Linear inverse Gaussian theory and geostatistics. *Geophysics*, 71, R101.

HANSEN, T. et MOSEGAARD, K. (2008). VISIM : Sequential simulation for linear inverse problems. *Computers and Geosciences*, 34, 53–76.

JOURNEL, A. (1999). Conditioning geostatistical operations to nonlinear volume averages. *Mathematical Geology*, 31, 931–953.

JOURNEL, A. et HUIJBREGTS, C. (1978). *Mining Geostatistics* . Academic Press, London.

LAST, B. et KUBIK, K. (1983). Compact gravity inversion. *Geophysics*, 48, 713–721.

LE RAVALEC, M., NOETINGER, B. et HU, L. (2000). The FFT Moving Average (FFT-MA) Generator : An Efficient Numerical Method for Generating and Conditioning Gaussian Simulations. *Mathematical Geology*, 32, 701–723.

LI, X. et CHOUTEAU, M. (1998). Three-dimensional gravity modeling In all Space. *Surveys in Geophysics*, 19, 339–368.

LI, Y. et OLDENBURG, D. (1996). 3-D inversion of magnetic data. *Geophysics*, 61, 394–408.

LI, Y. et OLDENBURG, D. (1998). 3-D inversion of gravity data. *Geophysics*, 63, 109–119.

LIU, Y. et JOURNEL, A. J. (2009). A package for geostatistical integration of coarse and fine scale data. *Computer and Geosciences*, 35, 527–547.

MARCOTTE, D., RIVEST, M. et PASQUIER, P.AND BOUZAGLOU, V. (2008). Simulation of hydraulic head fields compatible with a hydrogeological conceptual model. J. M. Ortiz et X. Emery, éditeurs, *Geostats 2008, Proceedings of the Eighth international Geostatistics Congress*, Santiago,Chile.

MATHERON, G. (1965). Les variables régionalisées et leur estimation. *Une Application de la Théorie des Functions Aléatories aux Sciences de la Nature. Masson, Paris.*

MENKE, W. (1989). *Geophysical Data Analysis : Discrete Inverse Theory*. Academic Press.

MONTAGNER, J. et JOBERT, N. (1988). Vectorial tomography-II. Application to the Indian Ocean. *Geophysical Journal International*, 94, 309–344.

MYERS, D. (1982). Matrix formulation of co-kriging. *Mathematical Geology*, 14, 249–257.

NOWAK, W., TENKLEVE, S. et CIRPKA, O. (2003). Efficient computation of linearized cross-covariance and auto-covariance matrices of interdependent quantities. *Mathematical Geology*, 35, 53–66.

PICHÉ, M., GUHA, J. et DAIGNEAULT, R. (1993). Stratigraphic and structural aspects of the volcanic rocks of the Matagami mining camp, Quebec ; implications for the Norita ore deposit. *Economic Geology*, 88, 1542–1558.

PILKINGTON, M. (1997). 3-D magnetic imaging using conjugate gradients. *Geophysics*, 62, 1132–1142.

PILKINGTON, M. (2006). Joint inversion of gravity and magnetic data for two-layer models. *Geophysics*, 71, L35.

RAO, D. et BABU, N. (1991). A rapid method for three-dimensional modeling of magnetic anomalies. *Geophysics*, 56, 1729.

SHAMSIPOUR, P., CHOUTEAU, M. et MARCOTTE, D. (2011). 3d stochastic inversion of magnetic data. *Journal of Applied Geophysics*, 73, 336–347.

SHAMSIPOUR, P., MARCOTTE, D. et CHOUTEAU, M. (2010a). 3D stochastic inversion of borehole and surface gravity data using Geostatistics. Capri, Italy.

SHAMSIPOUR, P., MARCOTTE, D., CHOUTEAU, M. et KEATING, P. (2010b). 3D stochastic inversion of gravity data using cokriging and cosimulation. *Geophysics*, 75, I1–I10.

TARANTOLA, A. et VALETTE, B. (1982). Generalized nonlinear inverse problems solved using the least squares criterion. *Rev. Geophys. Space Phys*, 20, 219–232.

ZEYEN, H. et POUS, J. (1993). 3-D joint inversion of magnetic and gravimetric data with a priori information. *Geophysical Journal International*, 112, 244–244.

APPENDIX A

3D STOCHASTIC INVERSION OF GRAVITY DATA USING COKRIGING AND COSIMULATION

A.1 Abstract

A new application based on geostatistical techniques of cokriging and conditional simulation is presented for the three-dimensional inversion of gravity data including geological constraints. The necessary gravity, density and gravity-density covariance matrices are estimated using the observed gravity data. Then, the densities are cokriged or simulated using the gravity data as the secondary variable. The model allows to include noise in the observations. The proposed method is applied to two different synthetic models : 1) a short dipping dyke ; 2) a stochastic distribution of densities. Then, some geological information is added as constraints to the cokriging system. The results show the ability of the method to integrate complex a priori information. Finally, the survey data of the Matagami mining camp is considered as a case study. The inversion method based on cokriging is applied to the residual anomaly in order to map the geology through the estimation of the density distribution in this region. The results of inversion and simulation methods are in good agreement with the surface geology of the survey region.

A.2 Introduction

In inverse problems, we want to use the measured data $\boldsymbol{d}$ to find the model parameters $\boldsymbol{m}$ characterizing some physical process, using a forward mapping operator (linear or nonlinear). For the gravity inversion, this operator is linear.

In 3D gravity inversion, there are different ways that the model $\boldsymbol{m}$ can be defined. One flexible way is to describe the model by a grid of prismatic cells. The subsurface is divided into prisms of known sizes and positions. The density contrasts are supposed constant within

each cell. The parameters to estimate are the cell densities.

By defining the gravity field using potential theorem (Blakely, 1995), there are no assumptions about the shape of the sources or distribution of density. Many equivalent density distributions below the surface will reproduce the known field at the surface (theoretical ambiguity) even when the surface field is known at every point. Besides, when the number of parameters is larger than the number of observations at the ground surface, the system does not provide enough information to determine uniquely all model parameters. In this situation, the problem is said to be underdetermined. As a result, although a solution that satisfies the observed data can easily be found, a problem of non-uniqueness still exists which is caused by the nature of the physics and the underdetermination of the problem. The non-uniqueness of solutions is further increased when one considers data uncertainty.

Many strategies can be used to deal with the non-uniqueness problem in gravity inversion. They all involve some kind of constraints or regularization (Gallardo-Delgado *et al.*, 2003) to limit the resulting solution space. Green (1975) used an appropriate weighting matrix to fix some of the parameters when geological or density information are available. Last et Kubik (1983) sought a compact solution with a minimum volume constraint. Smoothness or roughness of density distribution which control gradients of parameters in spatial directions are used in magnetic inversion by Pilkington (1997). Li et Oldenburg (1998) counteract the decreasing sensitivities of cells with depth by weighting them with an inverse function of depth. Another 3D inversion technique allowing definition of depth resolution is proposed by Fedi et Rapolla (1999). Prior information in the form of parameter covariances can be included (Tarantola et Valette, 1982). Montagner et Jobert (1988) used exponential covariance functions in which the rate of exponential decay determines the correlation length of the parameters.

Geostatistical methods in geophysical inversion were applied by Asli *et al.* (2000), Gloaguen *et al.* (2005, 2007), Giroux *et al.* (2007), Hansen *et al.* (2006), Hansen et Mosegaard (2008) and Gomez-Hernandez *et al.* (2004). Bosch et McGaughey (2001) and Bosch *et al.* (2006) also applied geostatistical constraints to gravity inversion using Monte Carlo techniques. In fact, linear stochastic inversion was first described by Franklin (1970) and then

popularized by Tarantola et Valette (1982). Chasseriau et Chouteau (2003) have done 3D inversion of gravity data using an a priori model of covariance. However, their method involved nonlinear constraints on density so they used an iterative approach (Tarantola et Valette, 1982). Asli *et al.* (2000) cokriged gravity anomalies to obtain cell densities. They showed how the covariance model can be adjusted to observed gravity data using some prior information to guide the choice of the model.

We assess uncertainty on the density inversions by using geostatistical conditional simulations. Simulations allow to identify stable features of the inverted fields. Simulations are also essential to estimate non-linear functions of the inverted fields like, for example, the maximum density gradient. Such quantity could indicate favorable exploration targets. Simulations allow to estimate high density gradients values and locations. There exist many efficient algorithms (Chilès et Delfiner, 1999) to simulate spatially structured models such as the Fast Fourier Transform Moving Average simulation (FFT-MA) (Le Ravalec *et al.*, 2000). In a Gaussian framework the simulations obtained are then post-conditioned to gravity data by using cokriging (Journel et Huijbregts, 1978). We show that density simulation ensures exact reproduction of gravity data, when observed without error, for any choice of the covariance model. This is due to the linear relationship between density and gravity. This property applies also for the case of non-linear averaging that can be approximated by a power average (Journel, 1999). In geophysics, Gloaguen *et al.* (2005) and Hansen *et al.* (2006) applied geostatistical simulation to inversion of radar data.

We build on (Asli *et al.*, 2000) approach. We extend their approach to assess uncertainty on the inversions by doing conditional simulations that enable to identify stable features of the inverted fields and to estimate non-linear functions like the maximum gradient. To the authors' knowledge, this is the first time conditional simulations are applied to gravity data.

We present the method for 3D stochastic inversion of gravity data using cokriging and cosimulation. First, we introduce the method of inversion by cokriging and cosimulation. Then, we use synthetic data sets from two different models to illustrate the application of the method. Finally the proposed method is applied to a data set collected over the Matagami

mining camp in Québec, Canada.

Theoretical overview

A.2.1 3D gravity modeling

The purpose of forward modeling is to compute the gravimetric response $\boldsymbol{g}$ at the surface due to a density distribution in the sub-surface $\boldsymbol{\rho}$. The most common method of evaluating the gravity from the density based on Newton's law is to break down the 3D domain into geometrically simple bodies having constant density. In our case, and for the sake of simplicity, the domain studied is divided into a finite number of rectangular prisms of constant density. Following the formula of Haáz (1953), the gravity caused at point of coordinates $\boldsymbol{x}_0 = (x_0, y_0, z_0)$ by a single prism b_l with density ρ_l is :

$$g(\boldsymbol{x}_0, b_l, \rho_l) = -\gamma\rho_l \sum_{i=1}^{2}\sum_{j=1}^{2}\sum_{k=1}^{2} \mu_{ijk} \left[x_i ln(y_j + r_{ijk}) + y_i ln(x_j + r_{ijk}) - z_k arctan(\frac{x_i y_j}{z_k r_{ijk}}) \right] \quad \text{(A.1)}$$

with,

$x_i = x_0 - \xi_i$, $y_j = y_0 - \eta_j$, $z_k = z_0 - \zeta_k$ $i, j, k = 1, 2$

$r_{ijk} = \sqrt{x_i^2 + y_j^2 + z_k^2}$

$\mu_{ijk} = (-1)^i(-1)^j(-1)^k$

ξ, η, ζ define the 8 corners of the prism b_l and γ is Newton's gravitational constant.

The response at point (x_0, y_0, z_0) is caused by the contribution of all m prisms making up the body and it is given by :

$$g(\boldsymbol{x}_0) = \sum_{l=1}^{m} g(\boldsymbol{x}_0, b_l, \rho_l) \quad \text{(A.2)}$$

Considering that there are n gravity observations and m rectangular prisms, the preceding relationship can also be written in the matrix form :

$$\boldsymbol{g}_{n\times 1} = \boldsymbol{G}_{n\times m}\boldsymbol{\rho}_{m\times 1} \quad \text{(A.3)}$$

with $\boldsymbol{G}$, the matrix of the geometric terms. When observation errors (e) are present, we have :

$$\boldsymbol{g}_{obs} = \boldsymbol{g} + \boldsymbol{e} \tag{A.4}$$

A.2.2 Cokriging

Cokriging (Myers, 1982) (Chilès et Delfiner, 1999) is a mathematical interpolation and extrapolation tool that uses the spatial correlation between the secondary variables and a primary variable to improve estimation of the primary variable at unsampled locations. The cokriging method gives weights to data so as to minimize the estimation variance (the cokriging variance). In this paper, the primary variable is density ($\boldsymbol{\rho}$, estimated by $\boldsymbol{\rho}^*$) and the secondary variable is gravity ($\boldsymbol{g}$). Assuming spatial homogeneity of the mean for the density and gravity field, we work with gravity and density contrasts, i.e., $E[\boldsymbol{\rho}] = E[\boldsymbol{g}] = 0$. The estimation variances are found on the diagonal of the following matrix (Myers, 1982) :

$$E((\boldsymbol{\rho} - \boldsymbol{\rho}^*)(\boldsymbol{\rho} - \boldsymbol{\rho}^*)^T) = \boldsymbol{C}_{\rho\rho} - \boldsymbol{C}_{g\rho}^T\boldsymbol{\Lambda} - \boldsymbol{\Lambda}^T\boldsymbol{C}_{g\rho} + \boldsymbol{\Lambda}^T\boldsymbol{C}_{gg}\boldsymbol{\Lambda}. \tag{A.5}$$

where $\boldsymbol{C}_{gg}$ is the gravity covariance matrix, $\boldsymbol{C}_{\rho\rho}$ is the density covariance matrix, $\boldsymbol{C}_{g\rho}$ is the cross covariance between gravity and density and $\boldsymbol{\Lambda}$ is the vector of weighting coefficients. Here $\boldsymbol{\rho}$ and $\boldsymbol{g}$ are multidimensional random variables and $\boldsymbol{\rho}^*$ is the estimated density defined on block support. Minimization of the above estimation variance yields the simple cokriging solution :

$$\boldsymbol{C}_{gg}\boldsymbol{\Lambda} = \boldsymbol{C}_{g\rho} \tag{A.6}$$

Finally, the estimate of densities are obtained from the gravity data using the optimal weights :

$$\boldsymbol{\rho}^* = \boldsymbol{\Lambda}^T\boldsymbol{g} \tag{A.7}$$

The vector of cokriging variances is obtained from :

$$\boldsymbol{\sigma}_{ck} = diag(\boldsymbol{C}_{\rho\rho} - \boldsymbol{\Lambda}^T \boldsymbol{C}_{g\rho}) \tag{A.8}$$

The off-diagonal elements represent the covariances between estimation errors. As densities are defined on a block basis, the density covariance model is also, directly, for blocks. Therefore, there is no need for lengthy and delicate numerical integration of a point density covariance function. In cases where the mean density is expected to vary spatially, an initial field for the density expectation must be provided and its associated gravity response subtracted from the observed data. The field for the local mean is assumed known without uncertainty. We are then back to gravity and density contrasts and the proposed methodology applies, except the density contrasts are now relative to the local mean density. This could be useful for example to remove, from gravity data, regional effects due to well known large geological units, or to impose a vertical density gradient on the solution.

A.2.3 Inversion by Cokriging

Based on equations A.3 and A.4, density and gravity covariance matrices are linearly related :

$$\boldsymbol{C}_{gg} = \boldsymbol{G}\boldsymbol{C}_{\rho\rho}\boldsymbol{G}^T + \boldsymbol{C}_0 \tag{A.9}$$

where $\boldsymbol{C}_0$ is the gravity error covariance matrix related to data errors ($\boldsymbol{e}$). This matrix is usually modeled as $\boldsymbol{C}_0 = C_0\boldsymbol{I}$ which assumes a homoscedastic uncorrelated noise. The scalar C_0 can be estimated from the data using standard gravity variograms or the V-V plot approach (Asli *et al.*, 2000) (see next section). The $\boldsymbol{G}\boldsymbol{C}_{\rho\rho}\boldsymbol{G}^T$ term is the covariance of the modeled gravity. We also have :

$$\boldsymbol{C}_{g\rho} = \boldsymbol{G}\boldsymbol{C}_{\rho\rho} \tag{A.10}$$

When the data are observed without error, i.e. $C_0 = 0$, we have the following property :

$$\boldsymbol{g}^* = \boldsymbol{G}\boldsymbol{\rho}^* = \boldsymbol{G}\boldsymbol{\Lambda}^T\boldsymbol{g} = \boldsymbol{G}(\boldsymbol{C}_{gg}^{-1}\boldsymbol{C}_{g\rho})^T\boldsymbol{g} = \boldsymbol{G}(\boldsymbol{G}\boldsymbol{C}_{\rho\rho})^T(\boldsymbol{G}\boldsymbol{C}_{\rho\rho}\boldsymbol{G}^T)^{-1}\boldsymbol{g} = \boldsymbol{g} \tag{A.11}$$

That is the gravity anomaly of the cokriged density is equal to the observed gravity anomaly.

The model covariance is obtained using the V-V plot method. Once an acceptable model covariance function is obtained, the model parameter field is cokriged using the gravity data and any available known model data. Note that including constraints is straightforward. Here we suppose that we have two kinds of constraints ; fixed densities $\boldsymbol{\rho}_F$ of some cells and known gradients ($\boldsymbol{gr}$) between two adjacent cells in the x, y, z directions. Using the above constraints, the estimate for densities is obtained using a similar cokriging system as before, but, here we have two more secondary variables. The estimation variance is minimized with respect to the weights $\boldsymbol{\Lambda}$, $\boldsymbol{\Gamma}$, $\boldsymbol{\Omega}$. The simple cokriging system is given by :

$$\begin{bmatrix} \boldsymbol{C}_{g,g} & \boldsymbol{C}_{g,\rho_F} & \boldsymbol{C}_{g,gr} \\ \boldsymbol{C}_{\rho_F,g} & \boldsymbol{C}_{\rho_F,\rho_F} & \boldsymbol{C}_{\rho_F,gr} \\ \boldsymbol{C}_{gr,g} & \boldsymbol{C}_{gr,\rho_F} & \boldsymbol{C}_{gr,gr} \end{bmatrix} \begin{bmatrix} \boldsymbol{\Lambda} \\ \boldsymbol{\Gamma} \\ \boldsymbol{\Omega} \end{bmatrix} = \begin{bmatrix} \boldsymbol{C}_{g,\rho} \\ \boldsymbol{C}_{\rho_F,\rho} \\ \boldsymbol{C}_{gr,\rho} \end{bmatrix} \tag{A.12}$$

$$\boldsymbol{\rho}^* = \boldsymbol{\Lambda}^T\boldsymbol{g} + \boldsymbol{\Gamma}^T\boldsymbol{\rho}_F + \boldsymbol{\Omega}^T\boldsymbol{gr} \tag{A.13}$$

The vector of cokriging variances is obtained from :

$$\boldsymbol{\sigma}_{ck} = diag(\boldsymbol{C}_{\rho\rho} - \tilde{\boldsymbol{\Lambda}}^T\tilde{\boldsymbol{C}}_{g\rho}) \tag{A.14}$$

where : $\tilde{\boldsymbol{\Lambda}}^T = [\boldsymbol{\Lambda}^T, \ \boldsymbol{\Gamma}^T, \ \boldsymbol{\Omega}^T]$ and $\tilde{\boldsymbol{C}}_{g\rho}$ is the right member in equation A.12.

The inverse matrix calculation can be done by singular value decomposition (SVD). This method is preferred to the conjugate gradient algorithm (CGA) used by Li et Oldenburg (1998) and Boulanger et Chouteau (2001), because it is numerically stable and it is a standard tool for small inverse problems. However, for very large problems, preconditioned CGA is needed.

A.2.4 Model covariance estimation

If we assume working on density contrast, i.e. $E[\boldsymbol{\rho}] = 0$ and $E[\boldsymbol{g}] = 0$, the observed data covariance matrix can be written as :

$$\boldsymbol{C}_{gg-exp} = \boldsymbol{g}_{obs}.\boldsymbol{g}_{obs}^{T} \tag{A.15}$$

The covariances $\boldsymbol{C}_{gg}$ and $\boldsymbol{C}_{g\rho}$ are not stationary even on a horizontal plane due to the limited lateral extension of the underlying density model. The non-stationary nature of the gravity-gravity and gravity-density covariances presents a problem for statistical inference. Thus, traditional estimators such as variogram cannot be used directly, and the model parameters for density covariance must, themselves, be estimated by inversion. We used the V-V plot approach of Asli *et al.* (2000) and Gloaguen *et al.* (2005) which enable immediate generalization to the non-stationary case. The algorithm for V-V plot is as follows :

1. Assume an initial model for the density covariance $\boldsymbol{C}_{\rho\rho}$.
2. Calculate the matrices $\boldsymbol{C}_{gg-exp}$ from equation A.15 and $\boldsymbol{C}_{gg-th}$ from equation A.9 where subscripts *exp* and *th* stand for experimental and theoretical respectively.
3. Transform both matrices into vectors $\boldsymbol{v}_{th}$ and $\boldsymbol{v}_{exp}$.
4. Sort $\boldsymbol{v}_{th}$ in decreasing order and apply the same ordering to $\boldsymbol{v}_{exp}$.
5. Bin the vectors $\boldsymbol{v}_{th}$ and $\boldsymbol{v}_{exp}$ in N_{lag} lags and compute the mean for each lag. ($\overline{\boldsymbol{v}}_{th}[i]$ and $\overline{\boldsymbol{v}}_{exp}[i]$)
6. Minimize the mean absolute error (MAE) between $\boldsymbol{v}_{th}$ and $\boldsymbol{v}_{exp}$ with the relation $MAE = \frac{1}{N_{tot}} \sum_{i=1}^{N_{lag}} N_i \left| \overline{\boldsymbol{v}}_{th}[i] - \overline{\boldsymbol{v}}_{exp}[i] \right|$ by modifying the model covariance $\boldsymbol{C}_{\rho\rho}$, ($N_i$ is the number of pairs for lag_i and N_{tot}=$\sum_{i=1}^{N_{lag}} N_i$).

In the V-V plot approach, bining is useful to downweight the influence of extreme pairs in the fitting. It also allows for a better visualization of the fit much alike for standard variogram modeling. Working on all individual pairs (variogram cloud), provides noticeably unstable values for the estimated parameters of the variogram model (Armstrong, 1984).

For minimization we used a simplex method of optimization (Nelder-Mead algorithm). All the fits were then critically examined visually and, when deemed unsatisfactory, improved by trial and error. Visual inspection of the V-V plot can be used to check the good fit at small structural distances, leading eventually to modification to the fitted model, much like with classical variogram fitting procedure. A simple test illustrating the correctness of the V-V plot approach is shown in Appendix A.10.

The initial density covariance model (or variogram model $\gamma(h)$ as, for stationary field, $C(h) = C(0) - \gamma(h)$) can be tailored to available geological information. If we lack this information, we can get a first estimate by using the covariance of minimum length solution (Menke, 1989) :

$$\boldsymbol{C}_{\rho\rho} = \boldsymbol{G}^T(\boldsymbol{g}\boldsymbol{g}^T)^{-1}\boldsymbol{C}_{gg}(\boldsymbol{G}^T(\boldsymbol{g}\boldsymbol{g}^T)^{-1})^T \tag{A.16}$$

Where $\boldsymbol{C}_{gg}$ could be obtained from gravity data. This will provide a very smooth initial model. Also we can use the dimension of our prisms as minimum ranges for the density variogram in the three directions (Chasseriau et Chouteau, 2003).

A.2.5 Cosimulation

Inversion using cokriging gives a smooth estimate of the density model. Sometimes it is desirable and useful to obtain various reasonable solutions in order to see the variability that can be expected from the density covariance model adopted. This can be achieved using geostatistical simulation algorithms rather than cokriging. The method of post conditioning by kriging was first proposed by Journel et Huijbregts (1978) and extended to cokriging by Myers (1982). It was applied by Gloaguen *et al.* (2005) for inversion of borehole radar velocity.

The FFT-MA algorithm (Le Ravalec *et al.*, 2000) is a fast simulation algorithm for generating regular grid non-conditional Gaussian stationary fields. It is necessary to post-condition the simulation by cokriging. First, the cokriging of densities $\boldsymbol{\rho}^*$ with measured gravity data $\boldsymbol{g}$ is performed. Then, for each realization $\boldsymbol{\rho}_s$, the gravity data, $\boldsymbol{g}_s$, are computed and an observation error is added when required (Marcotte *et al.*, 2008). Keeping the same cokriging

weights, cokriging of the densities $\boldsymbol{\rho}_s^*$ with $\boldsymbol{g}_s$ is performed. Finally, the conditional simulated densities $\boldsymbol{\rho_{cs}}$ are :

$$\boldsymbol{\rho}_{cs} = \boldsymbol{\rho}^* + (\boldsymbol{\rho}_s - \boldsymbol{\rho}_s^*) \tag{A.17}$$

where $\boldsymbol{\rho}_{cs}$ has the desired prior covariance. Using the conditional simulation approach, we can produce many statistically equivalent density models. As with cokriging, when the gravity covariances have zero nugget effect (no observation error), the measured and the computed gravity data of each conditional simulation are identical. As we know, $\boldsymbol{G\rho}^* = \boldsymbol{g}$ and $\boldsymbol{G\rho}_s^* = \boldsymbol{G\rho}_s = \boldsymbol{g}_s$. Then, using equation A.17, we have :

$$\boldsymbol{G\rho}_{cs} = \boldsymbol{g} + (\boldsymbol{g}_s - \boldsymbol{g}_s) = \boldsymbol{g} \tag{A.18}$$

A.3 Modelled data

We apply the proposed method based on cokriging and cosimulation on two sets of synthetic data : a dipping dyke and a stochastic density model.

A.4 Dipping dyke

We use a simple 45^o dipping short dyke with uniform density contrast 1500 kg/m^3 with respect to an homogeneous background (see Figure A.1). We select this model (Chasseriau et Chouteau (2003) ; Li et Oldenburg (1998)) to test the performance of the proposed method to resolve depth, anisotropy and dip. The 3D domain is divided into $22 \times 22 \times 22 = 10648$ cubic prisms with edge length of 0.1 km. The range of gravity values is from 0.2028 mGal to 2.0306 mGal. We assume there is no noise in the gravity data, meaning $C_0 = 0$.

Because we know the true density of the synthetic model, we can compute and fit directly the density variogram along and across the dyke. We fit an exponential model with $C_0 = 0$, sill $C = 32000$ (kg/m^3)^2 and ranges 1.5, 0.2 and 0.23 km along dyke direction and across dyke directions respectively (geometric anisotropy). In real applications where the density is unknown everywhere, we must fit the variogram based on the gravity data using the me-

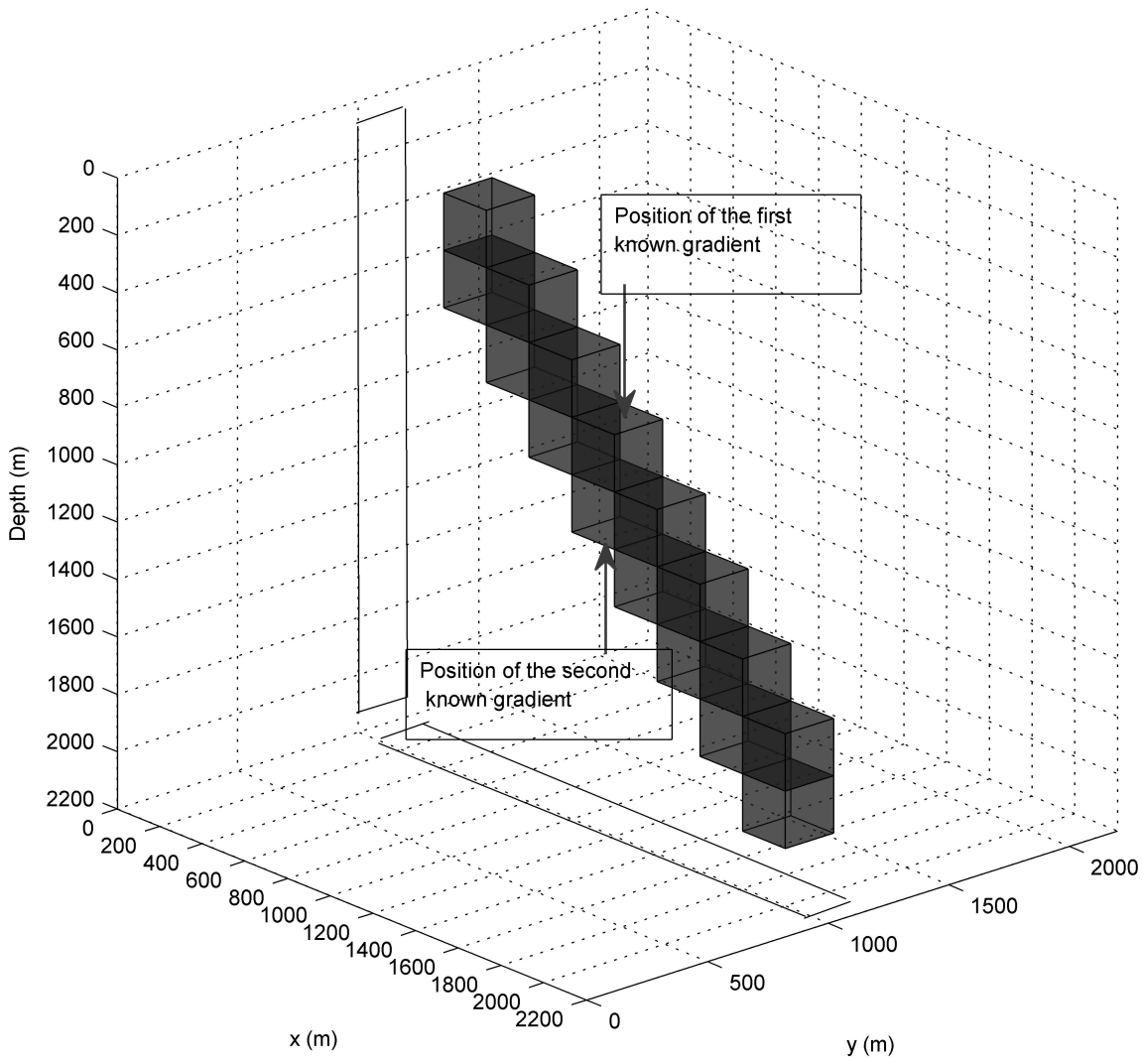

Figure A.1 Model of dipping dyke ($\boldsymbol{\rho}$ = 1500 kg/m^3) in homogeneous background. The locations of known gradients are also shown.

thod described in the preceding sections. It is also admissible to include as much as possible geological information in the fitting procedure, for example by including the model anisotropies along known geological directions. The modeled density covariance function obtained this time from the gravity data is exponential with ranges 1.5, 0.2 and 0.2 km along dyke direction and across dyke directions respectively. Density nugget effect is $C_0 = 62$ $(\text{kg/m}^3)^2$ and sill is $C = 19000$ $(\text{kg/m}^3)^2$. Note how the estimated parameters are close to parameters obtained upon direct fit of the experimental variogram of known densities.

Using the density variogram model, we calculate $\boldsymbol{C}_{\rho\rho}$, $\boldsymbol{C}_{g\rho}$ and $\boldsymbol{C}_{gg}$ covariance matrices needed for cokriging and estimate $\boldsymbol{\rho}^*$ as in equation A.7. The estimated density distribution at section $y = 1.1$ km and $x = 800$ m is shown in Figure A.2(a) and (c) respectively. Figure A.2 (b) is the solution with known gradients between blocks as constraints (see Figure A.1). We see that cokriging (a, b), and to a lesser extent simulations (d to f), recovers well the location and shape of the synthetic model, basically due to the anisotropy identified in the covariance model. However, except for the case with the known density contrasts (b), which effectively reaches the imposed 1500 kg/m^3 density contrast, all the contrasts appear weaker than in the model. Nevertheless, all solutions reproduce perfectly the gravity data as there was no observation error in the gravity data.

Note that using the same density covariance matrix obtained from V-V plot in the linear method of Tarantola et Valette (1982) does give the same results as cokriging. The formal equivalence between cokriging and least squares inversion is well known (e.g. Chasseriau et Chouteau (2003) and Boulanger (2004)). The main difference between the two approaches is that for cokriging the density covariance model is estimated directly from gravity data and prior information (V-V plot approach), whereas in the linear approach the density covariance model is specified as a prior.

A.5 Synthetic Data generated by stochastic method

Densities for $1 \times 1 \times 0.2$ km prisms were generated by non-conditional LU simulation using a spherical variogram model with $C = 60000$ $(\text{kg/m}^3)^2$, $a_{h,45}$=5 km, $a_{h,135}$=9 km, $a_{vert} = 4$ km

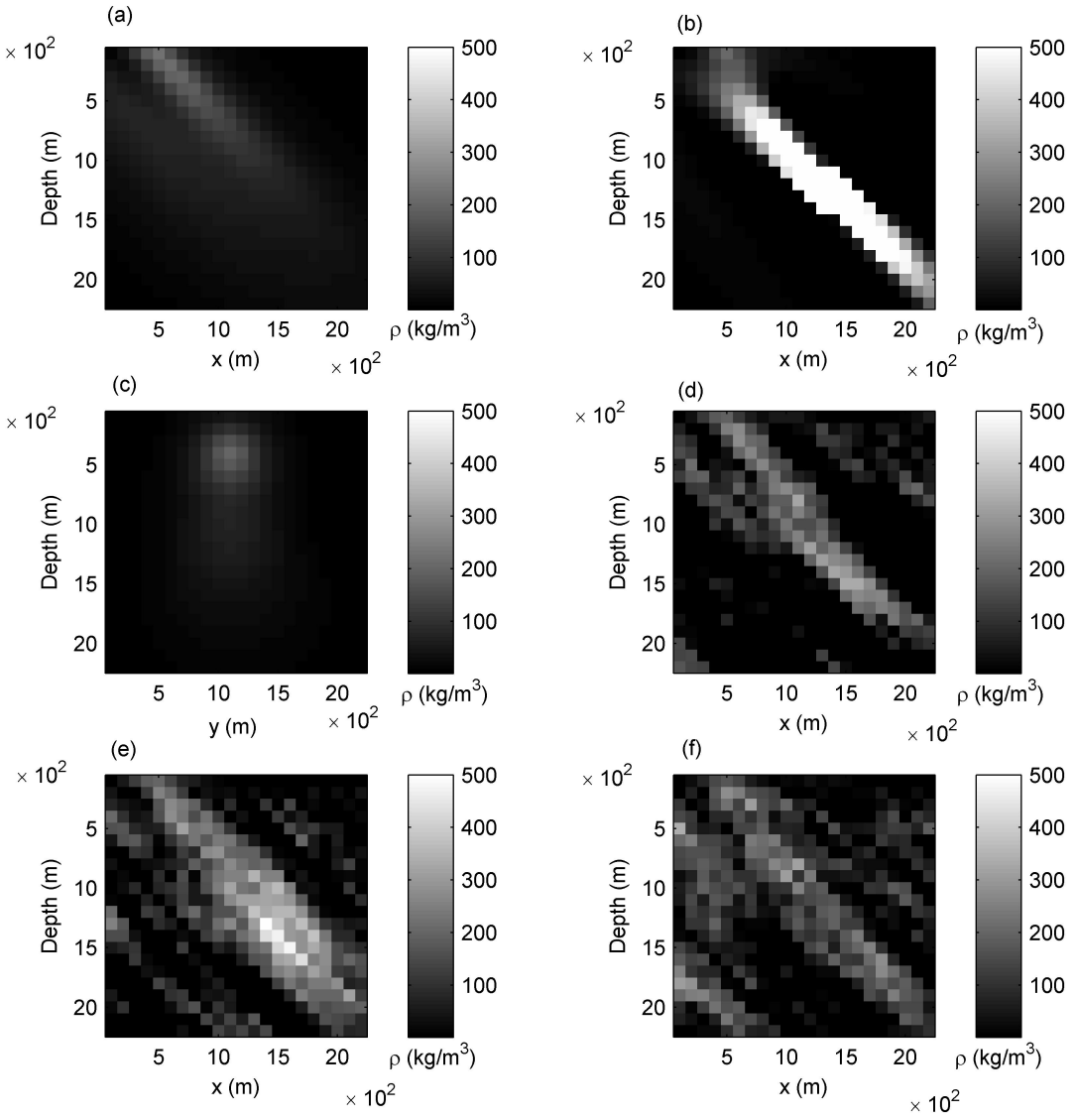

Figure A.2 (a) Estimated density distribution at section $y = 1100$ m using inversion by cokriging. (b) Estimated density distribution at section $y = 1100$ m using inversion by cokriging with constraints (known gradients). (c) Estimated density distribution at section $x = 800$ m using inversion by cokriging. (d), (e), (f) Three realizations of simulation.

where C is the variogram sill, and $a_{h,45}$, $a_{h,135}$, a_{vert} are the variogram ranges along horizontal directions 45^o and 135^o and vertical direction respectively. The 3D domain is divided into $11 \times 11 \times 21 = 2541$ cubic prisms. Using density values, we calculate the synthetic gravity data using equation $\boldsymbol{g} = \boldsymbol{G\rho}$, where, $\boldsymbol{G}$ is the matrix of geometric terms that are calculated using equation A.3. Again, we suppose that gravity data without error are observed at the center of the top face of the surface prisms (n =121). From now on, we assume the generated gravity are known and we invert them in order to estimate the density distribution.

A.5.1 Inversion of synthetic data

Using the V-V plot method with $N_{lag} = 100$, we adjust the density covariance matrix $\boldsymbol{C}_{\rho\rho}$ such that experimental and theoretical variograms become similar. The adjusted density variogram model is spherical with $C = 90000$ $(\text{kg/m}^3)^2$ and $a_{h,45} = 6.9$ km, $a_{h,135} = 8.9$ km, $a_{vert} = 4$ km, values close to those of the parameters used to simulate the densities.

A.5.2 Inversion on synthetic data using constraints

We now assume that there are 5 vertical boreholes in our domain and we know the densities along these boreholes. We assume this information allows us to estimate perfectly the density of all the prisms crossed by the boreholes. The 5 boreholes are located at locations $(x = 2, y = 2)$ km, $(x = 2, y = 8)$ km, $(x = 5, y = 5)$ km, $(x = 8, y = 2)$ km, $(x = 8, y = 8)$ km. So, we know the densities of $5 \times 21 = 105$ prisms and we use these additional data in the cokriging.

The section of synthetic densities at $y = 5000$ m is shown in Figure A.3 (b). Inversions by cokriging (c), and cokriging with 4 (d) and 5 (e) boreholes as constraints are shown. In (f) the inversion is done with the 5 boreholes but from noisy gravity data with error variance of 5 mgal^2. We see that cokriging gets more accurate as we include more density measurements. Nevertheless all solutions appear smoother than the real model. Comparing (f) to (e), we see that the solution is similar, indicating that cokriging is robust to data errors.

By FFT-MA, we generate 100 conditional simulated density distributions. Two realiza-

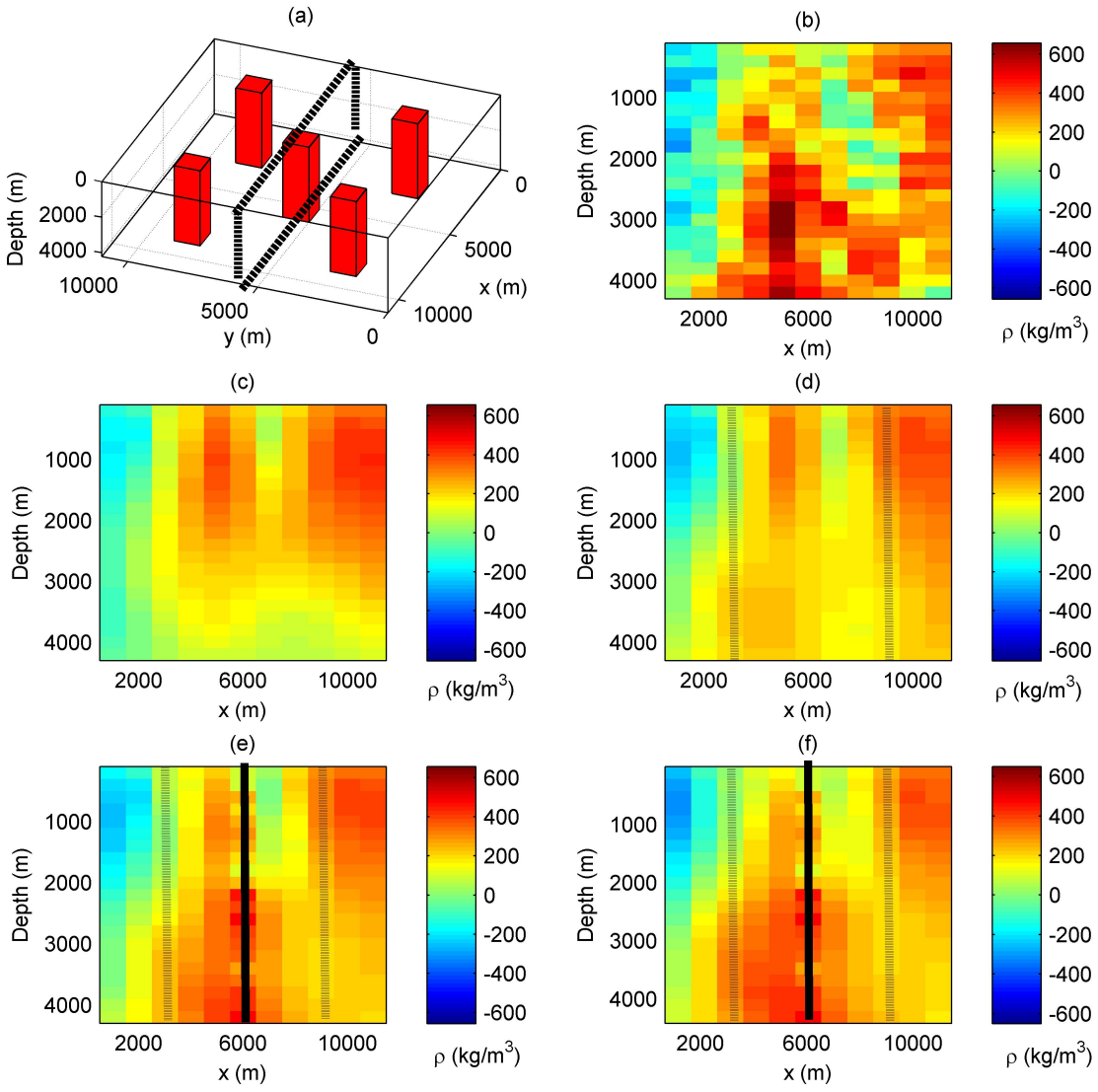

Figure A.3 (a) Borehole locations, (b) Synthetic density, (c to f) Inverted density by cokriging, at section $y = 5000$ m, (c) without constraints, (d) with 4 boreholes, (e) with 5 boreholes, (f) with 5 boreholes and from gravity data with error (C_0=5 mgal^2). Solid line is for borehole in the section, dashed lines are for boreholes in parallel sections.

tions of conditional simulated densities are selected at random. The conditional densities without constraints and with constraints (5 boreholes) at section $y = 5000$ m are shown in Figure A.4 (a to d). We see that by adding constraints, the correlation between the conditional simulated densities and the input densities is increased. Figure A.4 (e) shows the data misfit variance distribution obtained for 100 inversions when data have errors of variance 5 mgal^2. As expected, we recover the assumed data error variance.

The mean densities of the synthetic model, cokriged model with constraints and simulated model with constraints are all similar (between $112.4 - 116.5$ kg/m^3). The cokriging estimate is actually the mean of the posterior Gaussian distributions. However, the standard deviation of the cokriged solution is only 185 kg/m^3 compared to 225 and 224.8 kg/m^3 respectively for the synthetic model and the simulated model. The difference in standard deviations is due to the smoothing effect of cokriging (Chilès et Delfiner, 1999).

Figure A.5 (a) shows the cokriging standard deviation at the section $y = 5000$ m. Figure A.5 (b) shows the maps of the probability that the density falls below 300 kg/m^3 obtained from 100 conditional simulations. The probability map shown here is a transfer function which can also be obtained from cokriging estimates and variance (under Gaussian hypothesis) as it depends on a single prism at a time. However, simulations are essential for more complex transfer functions. One example is the maximum density gradient norm which can be a good indicator of a lithological contact. Maximum density gradient norm over each realization is computed. The histogram is shown in A.5 (c) and the mean is compared with maximum gradient computed by cokriging. It is shown that cokriging underestimates severely the maximum gradient norm.

In this section, only known densities were used as constraints. Adding other constraints such as known gradients can be done the same way as it was done in the dipping dyke example.

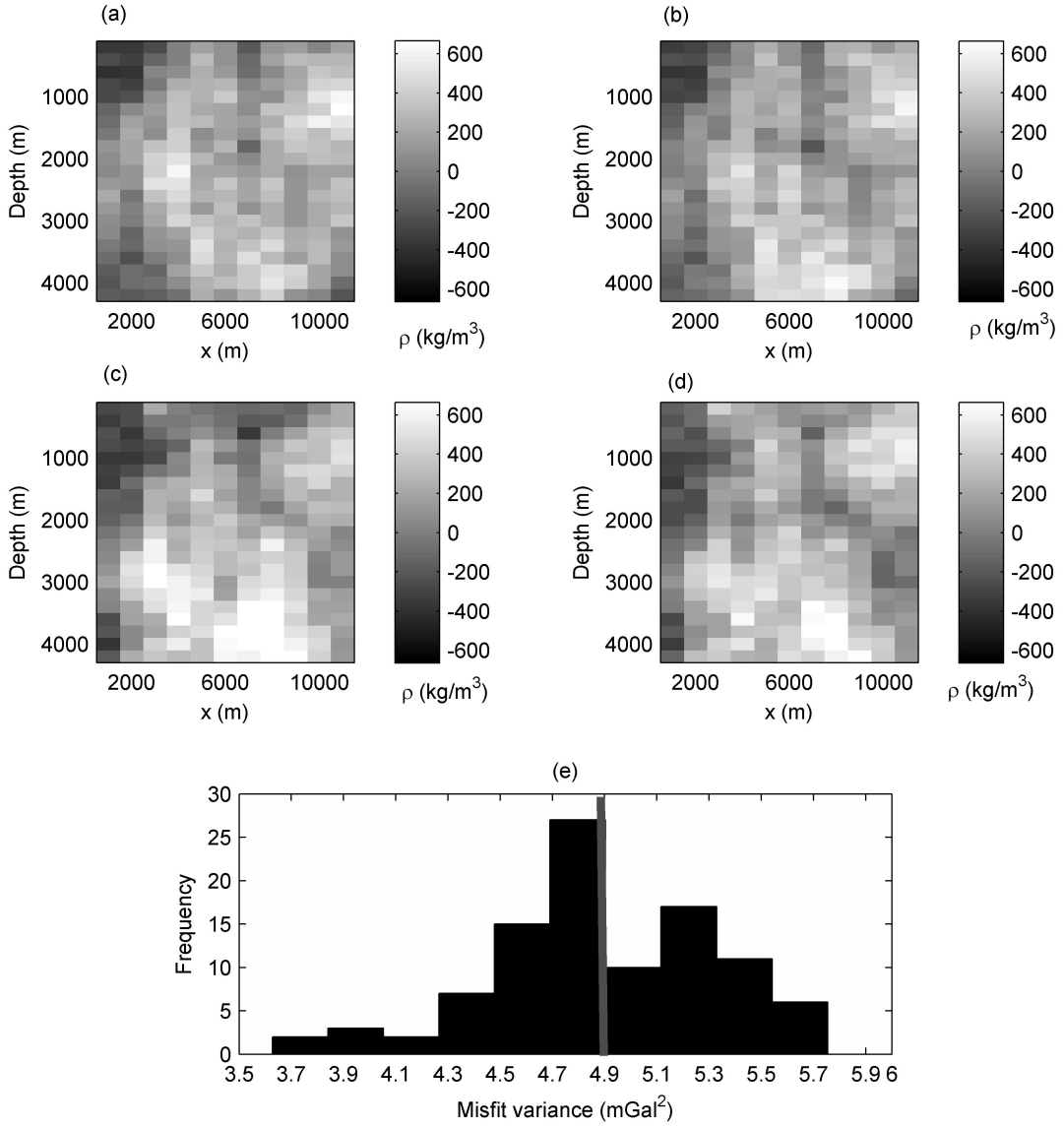

Figure A.4 (a to d), Four density realizations obtained from gravity data without error, (a) and (c) without constraints, (b) and (d) with constraints (5 boreholes). (e) Histogram of data misfit variances (from 100 realizations) when an error of variance 5 mgal^2 is added on gravity data. Red vertical line is the mean of misfit variances. All the figures are at section $y = 5000$ m. Synthetic density shown in Figure A.3 (b).

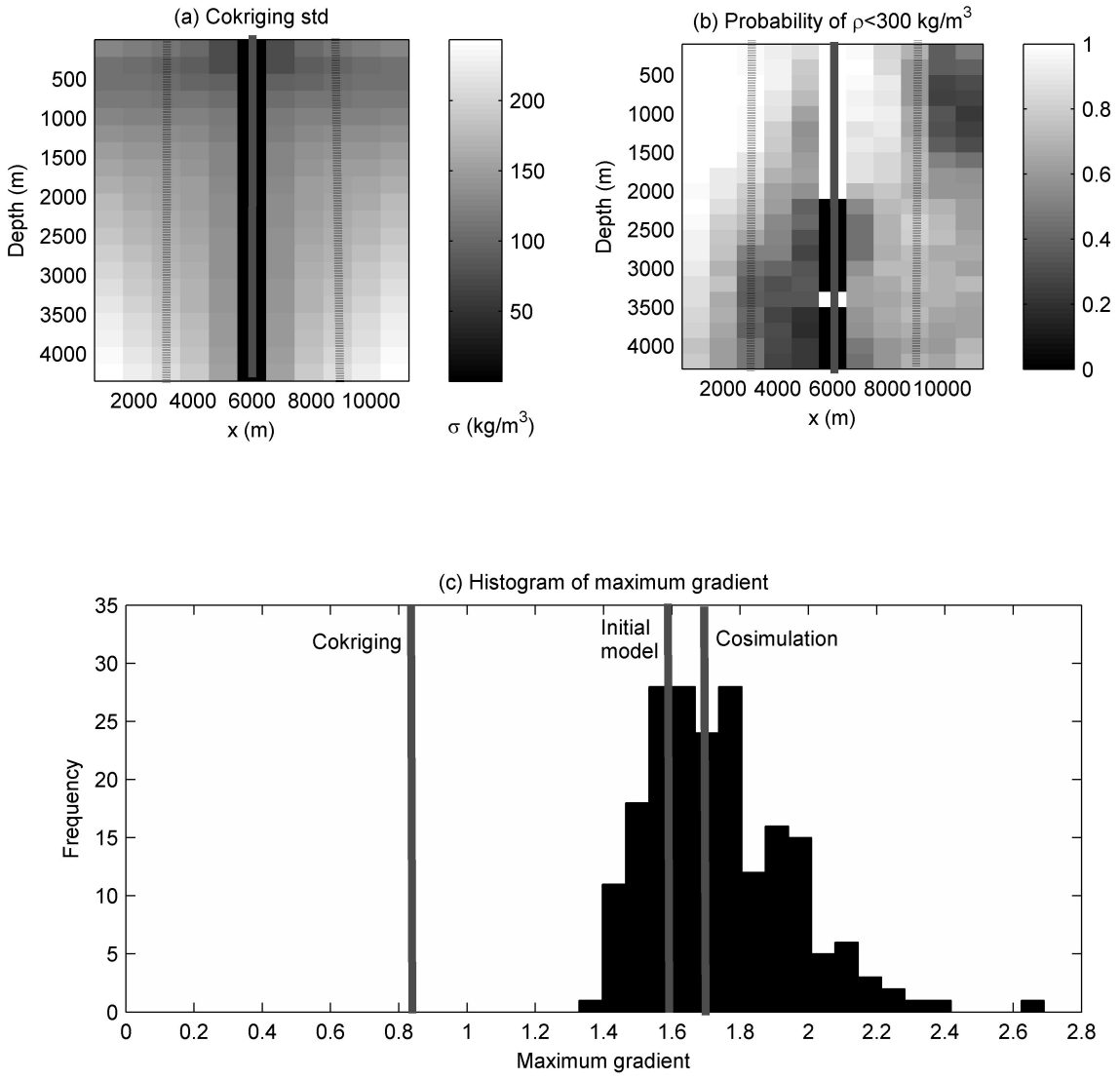

Figure A.5 (a) Cokriging standard deviation at section $y = 5000$ m, (b) Probability of $\boldsymbol{\rho} < 300$ kg/m^3 at section $y = 5000$ m, (c) Histogram of maximum gradients. Maximum gradient of initial model and of cokriging, and mean of maximum gradient of cosimulation realizations, are indicated.

A.6 Application to Survey Data

The study area is located in the Matagami region in Quebec, Canada. The area of the gravity survey extends from -77° 11′ to -77° 36′ latitude and from 49° 38′ to 49° 49′ longitude. 1880 gravimetric measurements with about a 600 m spacing were collected in 2007 for the entire studied region.

Many volcanogenic massive sulfide (VMS) deposits have been identified at the contacts of bimodal volcanic sequences in the Archean-age Abitibi greenstone belt. The Matagami volcanic complex of northern Abitibi belt is formed by two major phases of volcanism (Piché *et al.*, 1993). The end of the volcanic initial phase produced rhyolites of the Watson Lake Group. The beginning of the late volcanic phase formed the basaltic Wabassee Group. A cherty, sulphidic chemical sediment known as the Key Tuffite marks the contact and discontinuity between the two groups. This thin horizon ($0.6 - 6$ m) is the primary exploration target because it hosts most of the ore bodies discovered in the area (Calvert et Li, 1999). Exploration of the Key Tuffite by systematic drilling is very expensive especially with increasing depth (up to 1600 m), thus use of geophysical methods can be a very efficient solution. The Key Tuffite is too thin to be resolved by this gravity survey, but the important issue is that the Key Tuffite is located at the contact between the mafic Wabassee Group and the felsic Watson Lake Group. The mafic Wabassee Group has a high density, so it produces gravity highs. On other hand, the felsic Watson Lake Group (rhyolite) has a low density, so it produces gravity lows. The geological setting of the studied area is shown in Figure A.6.

The study area is covered by overburden of glacial origin consisting of clay, sand, gravel and till of variable thickness from 0 to 60 m. Most of this information is deduced from EM methods surveyed by Xtrata Zinc. The contribution of overburden was removed from the measured gravity data. The gravity caused by overburden was between 0 to 3 mGal. However, in many locations, the gravity caused by overburden was small (below 1 mGal).

The gravity data were corrected for drift, free air and latitude to yield the Bouguer anomaly. The regional anomaly is obtained by upward continuation to 10 km of the Bouguer

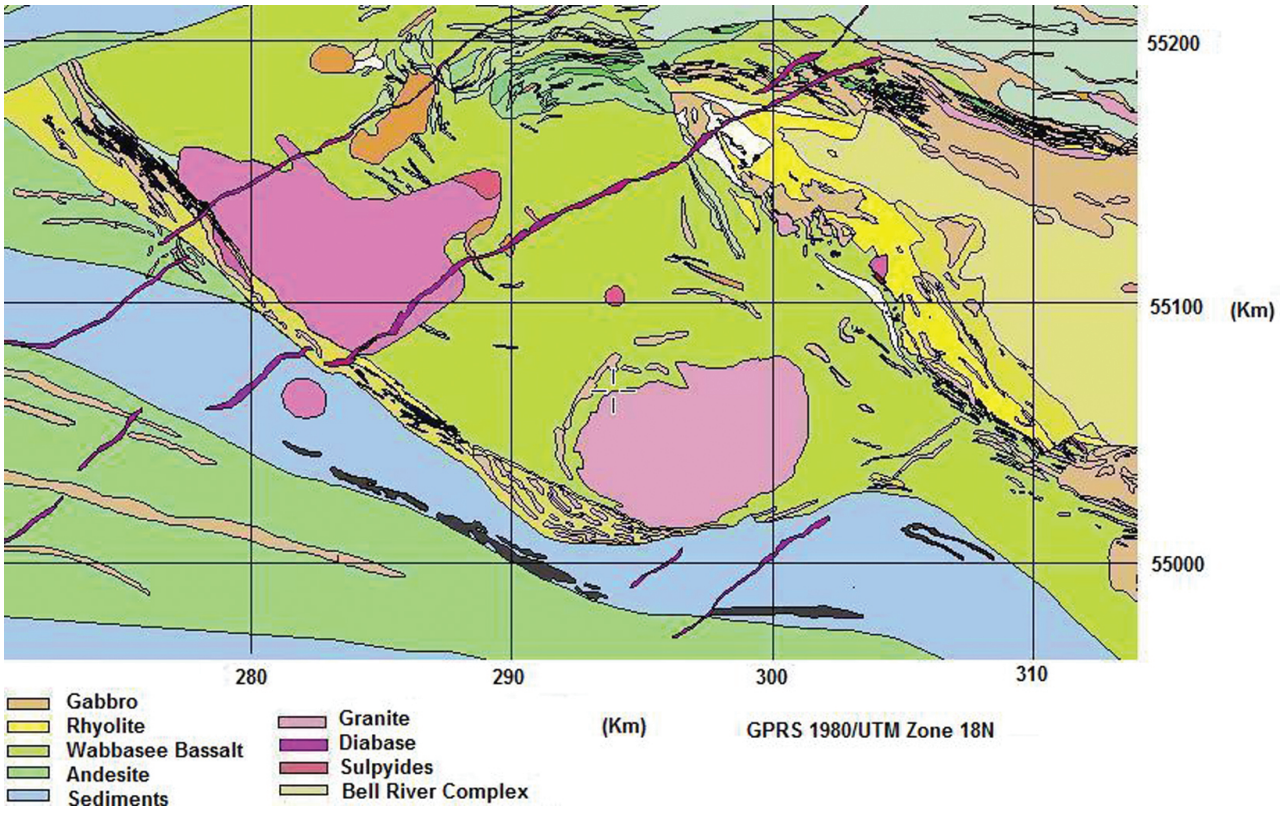

Figure A.6 Geological setting of the studied area. Adapted from Xstrata Zinc and Donner Metals.

anomaly in order to invert data on a grid reaching 5 km of depth. Subtracting the regional from the Bouguer anomaly results in the residual anomaly (Figure A.7) ranging between -8.7 to 9.2 mGal.

A.6.1 Inversion by Cokriging

Knowing the residual anomalies from the previous section, we use inversion by cokriging to estimate the density model. We use the gravity residuals to calculate the experimental gravity covariance matrix. The inversion domain is divided into $n_x = 99$ by $n_y = 38$ by $n_z = 10$ cubes of dimension $500 \times 500 \times 500$ m. So, the whole domain is $49.5 \times 19 \times 5$ km, the total number of prisms is $m = 37620$ and the total number of gravity data is 2061.

The adjusted density variogram model using V-V plot method is anisotropic and spherical with $C_0 = 105$ $(\text{kg/m}^3)^2$, sill $C = 5500$ $(\text{kg/m}^3)^2$ and ranges $a_{h,45} = 6.5$ km, $a_{h,135} = 7.5$ km and $a_{vert} = 5$ km. The covariance vectors $\boldsymbol{v}_{exp}$ and $\boldsymbol{v}_{th}$ are shown in Figure A.8.

The estimated densities by cokriging are actually density contrasts. Therefore, a density of 2650 kg/m^3 is added as the mean to the contrasts estimated by cokriging. The estimated density distribution are shown in Figures A.9 and A.10. Comparing these figures with the geology setting of the study area reveals an agreement with the geology on the surface. We can see that two granitic intrusions have been recovered by inversion. Also, different densities corresponding to mafic and felsic rocks can be recognized from each other. As expected, the mean density contrast converges to zero in the left hand part of the domain where there is no data.

Two sections of the estimated densities at $y = 5515000$ m and $z = 1000$ m are presented in Figure A.10. It shows that the structure of the studied area matches well with the geological settings.

We separate inverted densities in two different groups. First, we consider the densities between 2700 and 3000 kg/m^3 which are representative of Wabassee group (mafic). Likewise, densities between 2300 and 2640 kg/m^3 are representative of felsic rock. Figure A.11 (a, b, c) shows three realizations selected at random of co-simulated densities at section $y = 5515000$

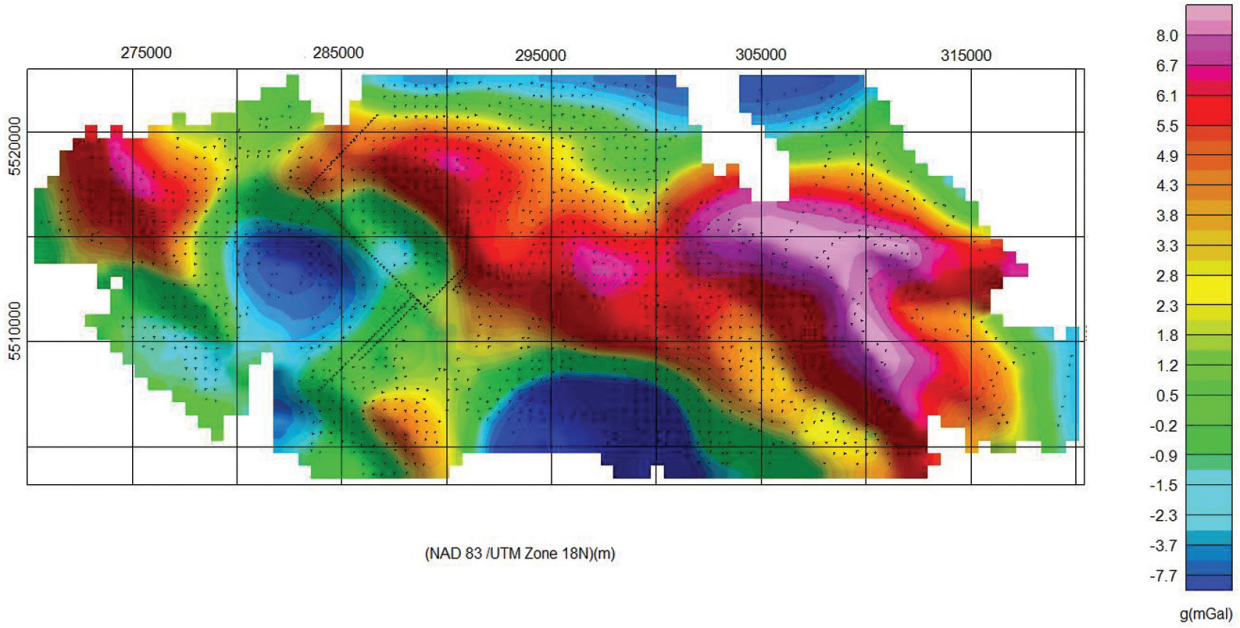

Figure A.7 Residual anomaly obtained from upward continuation to 10 km of Bouguer anomaly.

m along with the probability map of $2700 < \boldsymbol{\rho} < 3000$ kg/m^3 (d) and the histogram of maximum density gradient norm (e). As we saw in the synthetic case, we expect the maximum gradient in the real field to be closer to the cosimulation than cokriging. Note that a few realizations have their maximum gradient lesser than the one found with cokriging. Although each realization is expected to show globally more variations than the cokriged solution, it can happen that some realizations appear smoother locally, around a given location, than cokriging.

A.7 Discussion

The proposed non-iterative inversion method based on cokriging and cosimulation is computationally efficient as practical solutions exist for large problems. The algorithm is stable and robust in the presence of data noise. It enables to incorporate easily any known density values or known density gradients.

Cokriging provides one smooth solution to the underdetermined problem, while cosimula-

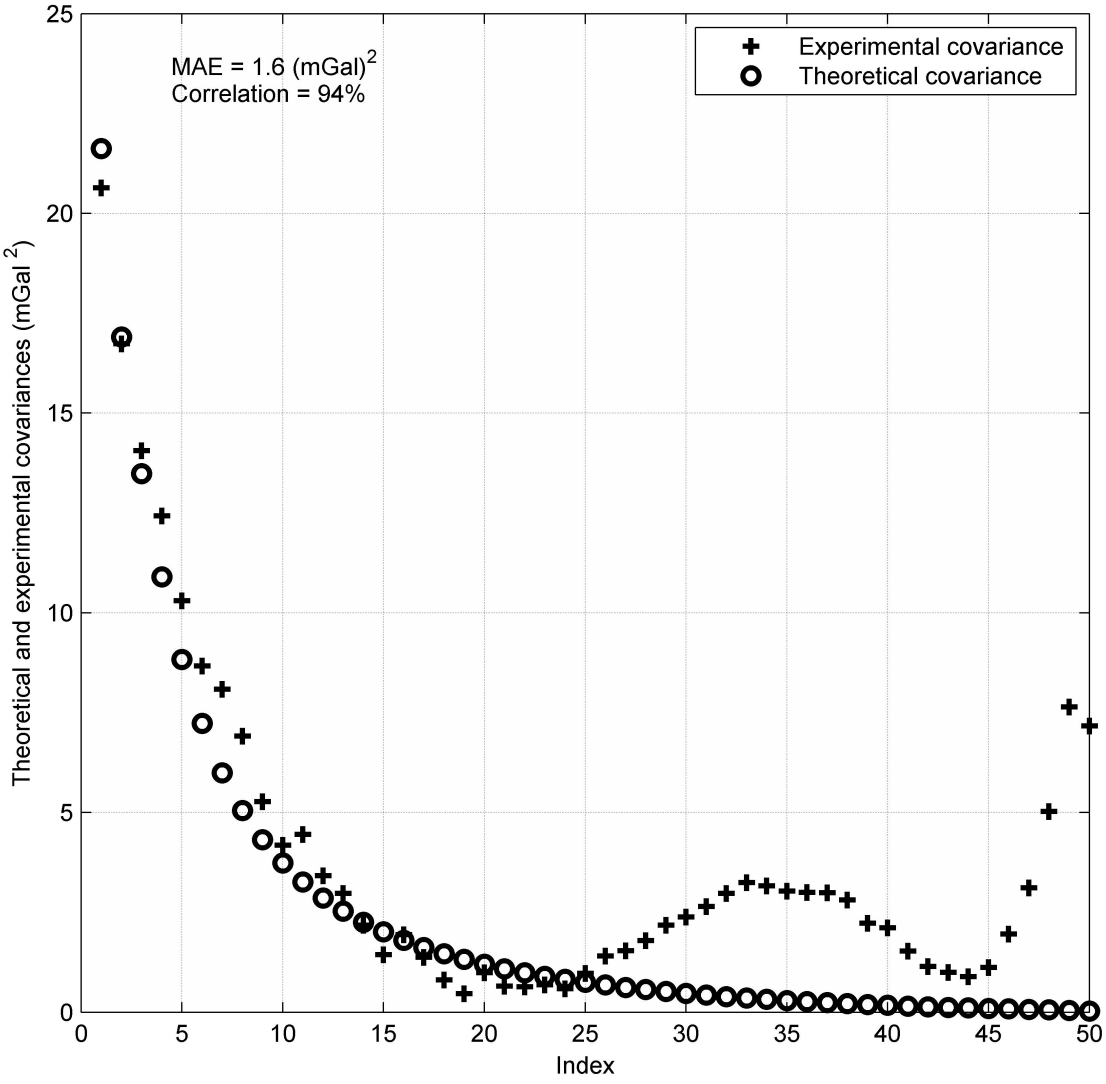

Figure A.8 Fit of the experimental and theoretical gravity covariance matrices. The x axes is the index of bins. Density covariance model : anisotropic and spherical with $C_0 = 105$ $(\text{kg/m}^3)^2$, $C = 5500$ $(\text{kg/m}^3)^2$ and $a_{45} = 6500$ m, $a_{135} = 7500$ m and $a_{vert} = 5000$ m.

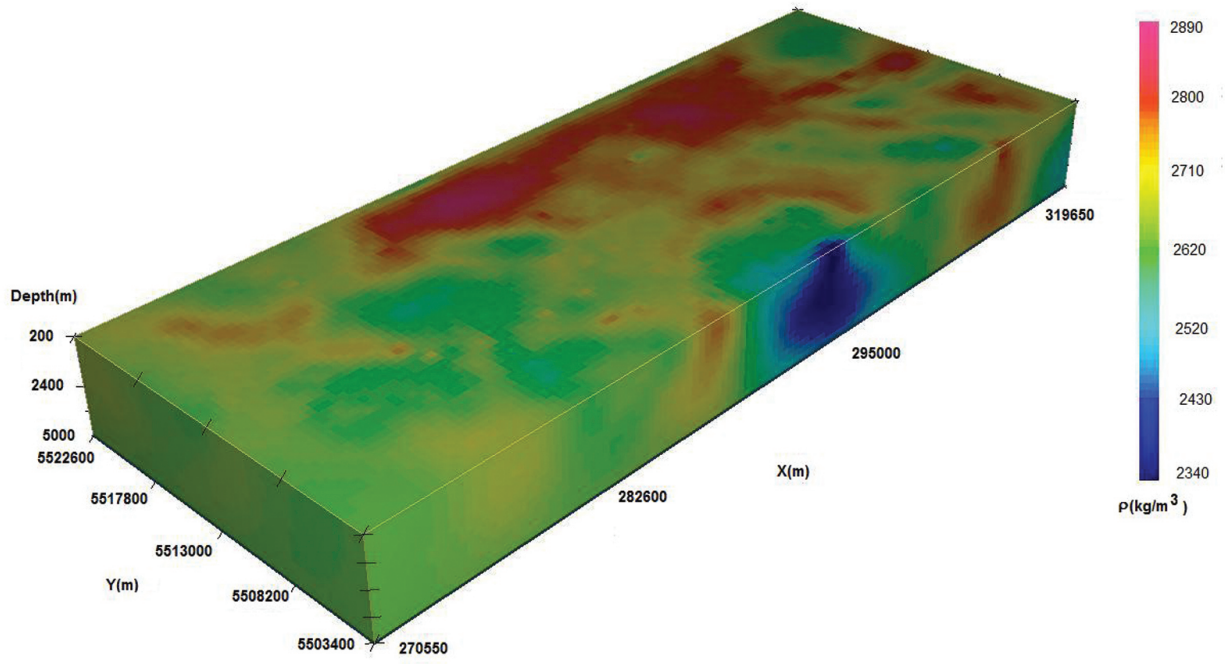

Figure A.9 3D estimated density distribution using inversion by cokriging.

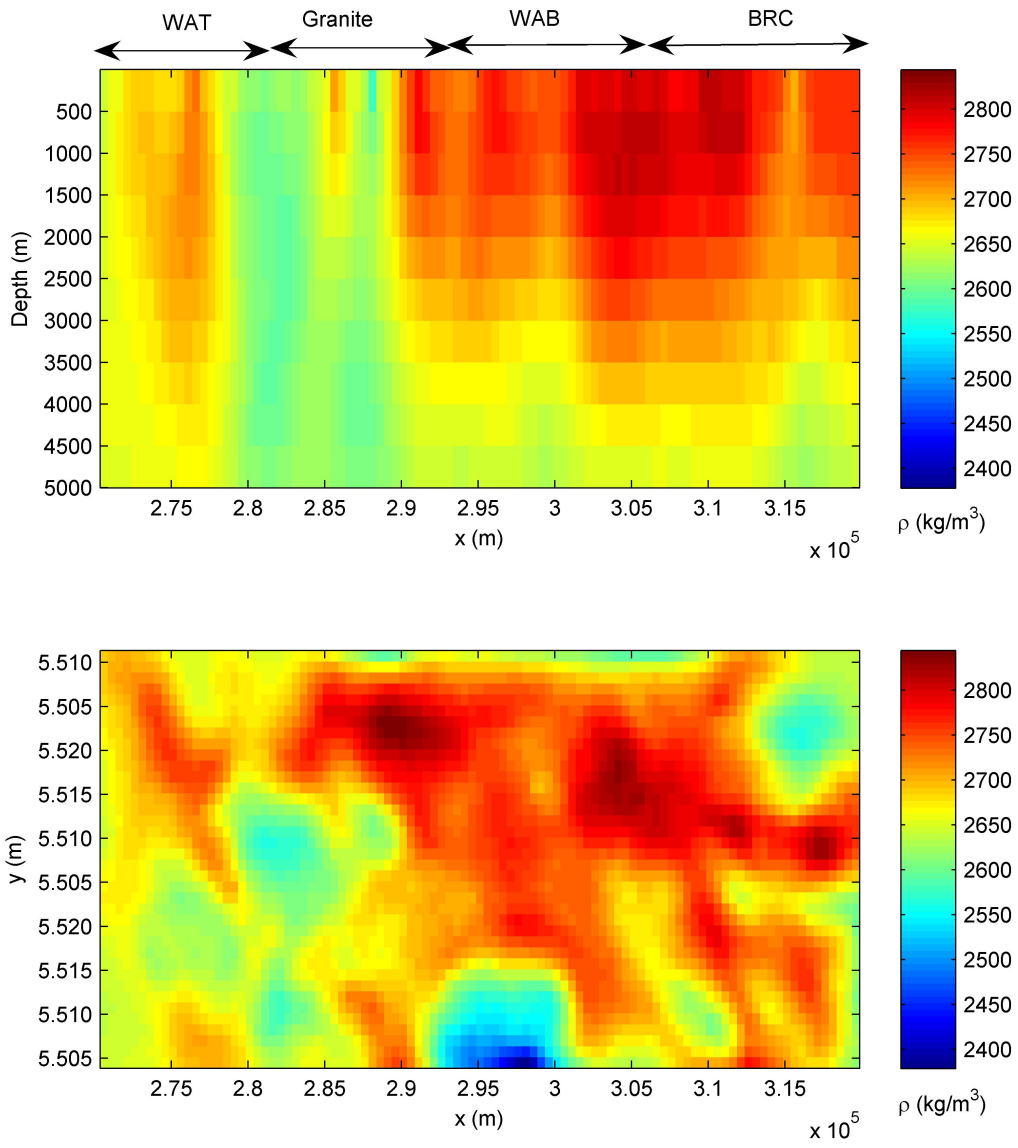

Figure A.10 The estimated densities at sections $y = 5515000$ m and $z = 1000$ m using inversion by cokriging. WAT : Watson Group (rhyolite), WAB : Wabassee group (basalt), BRC : Bell River Complex.

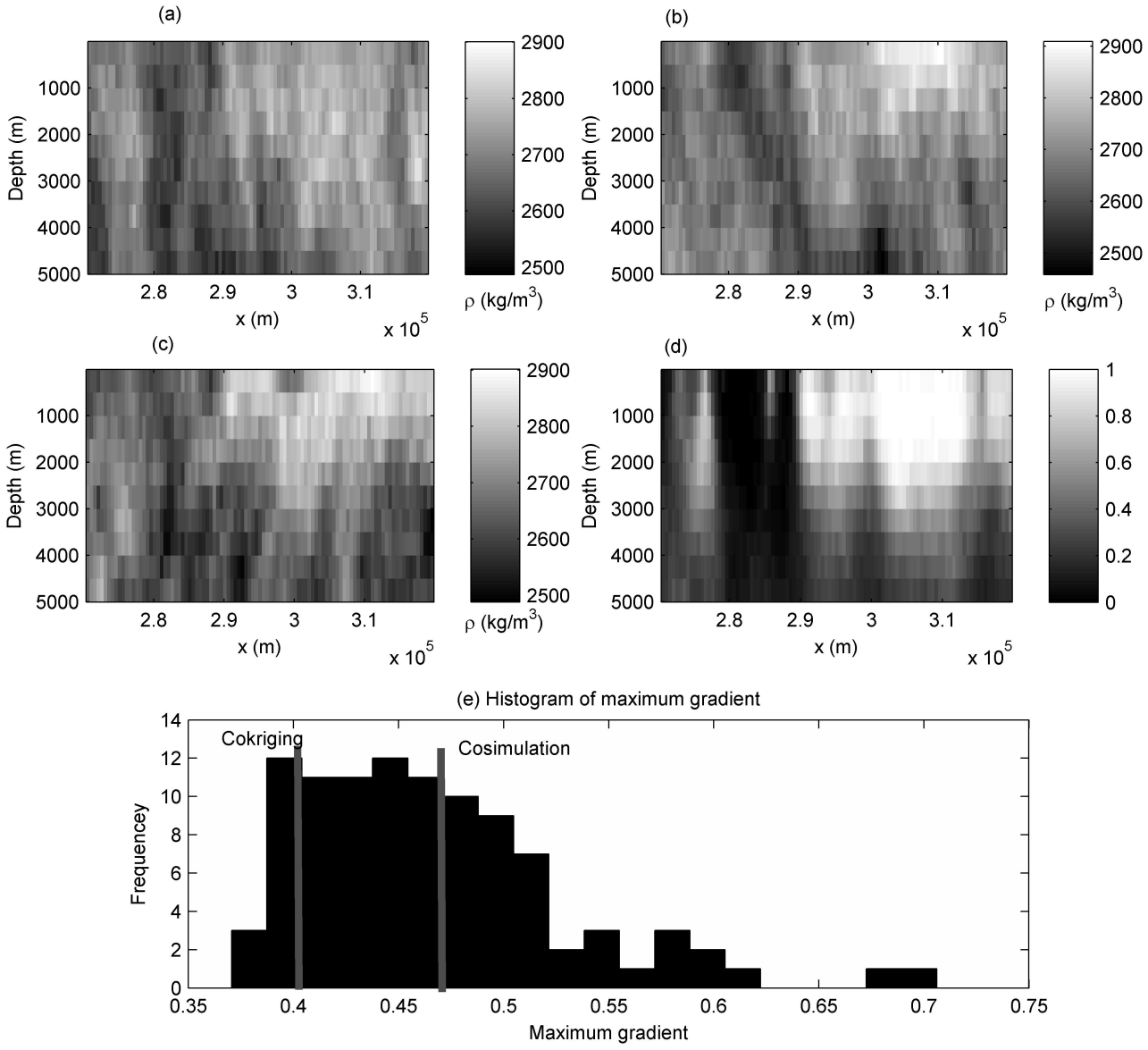

Figure A.11 (a-c) Cosimulated Densities (three realizations selected at random), (d) Probability map of $2700 < \boldsymbol{\rho} < 3000$ kg/m^3. All the figures are from section $y = 5515000$ m. (e) Histogram of maximum gradients. Density maximum gradient of cokriging and mean of maximum gradient of cosimulation realizations indicated.

tion provides a set of equally possible solutions, aimed at reproducing the spatial variability of the true density field. One important use of simulation is to generate scenarios as input for non-linear transfer function applied on the field. An illustrative example is the maximum density gradient norm. It was shown that simulations enable, because they reproduce the variability of the field, to better estimate the gradient norm than cokriging. Suppose for example a density gradient of 0.5 is deemed necessary to define a valuable exploration target. The cokriging solution does not find any target. On the other hand, although most realizations do not find exploration target, a few ones do. Hence, areas most frequently identified in the realizations with gradients above 0.5 would constitute high-priority targets.

The effect of increasing the amount of information using constraints was illustrated. It improved the estimation of density distribution especially at greater depths.

Obtaining a good fit between the theoretical and experimental covariances is sometimes challenging. Nevertheless, it is possible to obtain at least crude estimates of the sill and the ranges along principal geological directions. It is also possible to validate prior covariance model deduced from geological knowledge. For large systems one idea is to discretize the field initially with much larger blocks to find covariance at this scale. Often, it is relatively easy to deduce the approximate covariance model for smaller blocks.

In the case study, the number of prisms m is large. Therefore, the required storage and computational costs to compute $\boldsymbol{C}_{g\rho}$ and $\boldsymbol{C}_{gg}$ are prohibitive. We can solve this problem using the method proposed by Nowak *et al.* (2003), which is based on circulant embedding and the fast Fourier transform (FFT). This method is useful and has lower computational complexity. This approach works best when gravity data are located on a regular grid (not necessarily full), and the density covariance is isotropic.

The choice of the FFT-MA and post-conditioning by cokriging is justified by important advantages over alternative simulation methods like the sequential Gaussian simulation (SGS) (Deutsch et Journel, 1998). Besides being noticeably faster, the main advantage is that the density field can be simulated simultaneously over all the prisms using all the gravity data and known densities. Therefore, provided the required covariances are computed using Equa-

tions A.9 and A.10, and assuming there is no observation error, the exact reproduction of gravity data by all the realizations is ensured. This is not possible with SGS, for realistic models, as the cokriging system will be too large using all the density prisms of the model. Dropping prisms to work with local neighborhood, as is done in SGS, will inevitably results in deviations of the simulated gravity field compared to observed gravity data, even when gravity is observed without error.

A.8 Conclusion

We presented an application of the inversion method based on a geostatistical approach (cokriging) for three dimensional inversion of gravity data including geological constraints. We extended the approach to cosimulation of densities. Simulation results were shown helpful to better estimate non-linear functions of the inverted densities, like the maximum density gradient found in a given area. We showed on synthetic models the value of adding constraints to cokriging or cosimulation to improve the accuracy of density estimation/simulation. The use of known gradients and densities as constraints can be useful in the mining industry wherever 3D information is available from boreholes. We applied the proposed method on real data from Matagami area where the results of inversion prove in agreement with the known geology.

This method can be extended to other 2D and 3D geophysical linear inversion methods.

A.9 ACKNOWLEDGMENTS

The authors wish to thank Research Affiliate Program (RAP) and the Geological Survey of Canada contribution 20080670 for their financial support. We wish to express sincere thanks to Michel Allard from Xstrata Zinc for his guidance and support. We also thank University of British Columbia for providing 'MeshTools3D' to visualize the 3D image. We thank the reviewers for numerous constructive comments that helped to improve the manuscript.

A.10 Appendix ; A simple test on the V-V plot approach

We test the V-V plot for the zero-mean, 1D, stationary case. Five hundred points with a Gaussian variogram showing C_0=0.3, C=0.7 and effective range 35 are simulated by FFT-MA. The theoretical and experimental variograms between each pair of simulated points are computed. Pairs with equal theoretical variogram values are regrouped and averaged to obtain the V-V plot. Figure A.12 shows the V-V plots obtained for 100 different realizations (left), the average V-V plot (middle) and the histograms of the estimated parameters (right) obtained using a non-linear regression between experimental and theoretical covariance values, for each realization, together with the true parameter value used in the simulation (red line). The results do not show the presence of bias for the model parameter estimates. Similar

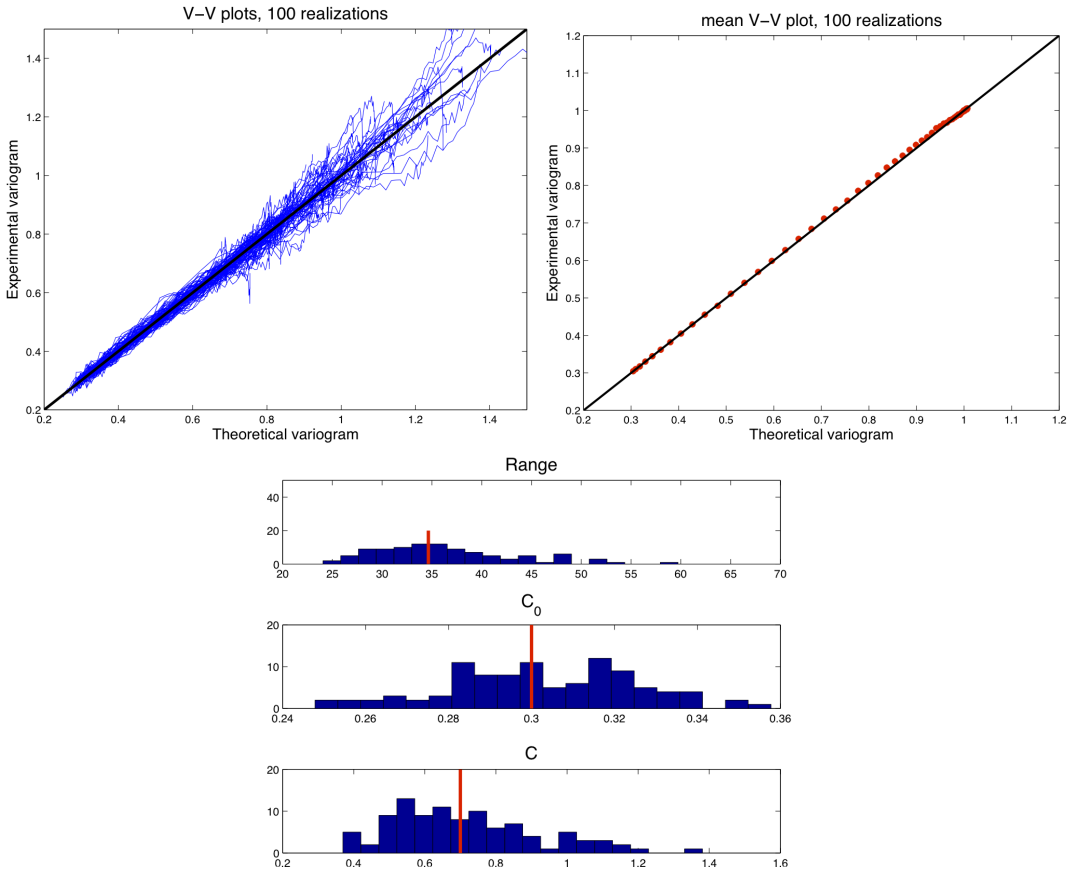

Figure A.12 Test of the V-V plot approach

results were obtained with an exponential variogram model. Note that for visualization, an

alternative representation of the V-V plot is to show both the experimental and theoretical variogram values as a function of the distance between points (in the stationary case) or as a function of a lag index (in the non-stationary case, as done with gravity data). This choice of visualization has no effect on the estimated parameters.

APPENDIX B

BLOCK KRIGING

B.1 Block kriging

In order to integrate data of different scales, we must consider different supports simultaneously in the kriging system. The major assumption is that the initial density information is at the point support level and block data are calculated as averages of the point support. Suppose, we require a block estimate meaning an estimate of the average value of the density within a certain area. In order to find this estimate, our certain area can be discretized into small prisms and then the individual prism estimates are averaged over the area. We refer to the small prisms as points and larger areas as blocks. This procedure may be computationally expensive, because for each block estimate we require to perform kriging for all the points inside the block. However, it is possible to construct and solve only one kriging system for each block estimate Chilès et Delfiner (1999) using block kriging.

We first explain the point kriging and then extend it to the block kriging. In order to find the density value of a point at x_0 using sample values at s points (x_1, x_2, ..., x_s), we solve the following matrix equation :

$$\begin{bmatrix} \boldsymbol{C}_{1,1} & \boldsymbol{C}_{1,2} & \cdots & \boldsymbol{C}_{1,s} \\ \boldsymbol{C}_{2,1} & \boldsymbol{C}_{2,2} & \cdots & \boldsymbol{C}_{2,s} \\ \vdots & \vdots & \ddots & \vdots \\ \boldsymbol{C}_{s,1} & \boldsymbol{C}_{s,2} & \cdots & \boldsymbol{C}_{s,s} \end{bmatrix} \begin{bmatrix} \boldsymbol{\lambda}_1 \\ \boldsymbol{\lambda}_2 \\ \vdots \\ \boldsymbol{\lambda}_s \end{bmatrix} = \begin{bmatrix} \boldsymbol{C}_{1,0} \\ \boldsymbol{C}_{2,0} \\ \vdots \\ \boldsymbol{C}_{s,0} \end{bmatrix} \tag{B.1}$$

where $\boldsymbol{C}_{i,j}$ is the covariance between densities at points x_i and x_j. The estimate at point x_0 will be :

$$\boldsymbol{\rho}^*(x_0) = \sum_{i=1}^{s} \boldsymbol{\lambda}_i \boldsymbol{\rho}(x_i). \tag{B.2}$$

Now, suppose we need to estimate the mean value of density over a certain area (block), rather than at a point. The mean value of a random function over a local area is simply the average of all the point random variables inside that area. The mean value of density over a block of volume v is

$$\boldsymbol{\rho}_v = \frac{1}{|v|} \sum_{j|x_j \in v} \boldsymbol{\rho}(x_j). \tag{B.3}$$

Now, we try to modify the point kriging system given in Eq. B.1 for block estimation. The right member matrix has nothing to do with the location at which the estimation is required and therefore it does not need to be changed. We only need to change the vector in the right hand side of the equality. It consists of covariance values between densities at the sample locations and the density at the location that we are trying to estimate. They are point-to-point covariances. For block estimation, they need to be changed to point to block covariances and can be calculated as follows :

$$\begin{aligned}
&\hat{\boldsymbol{C}}_{i,v} = Cov(\boldsymbol{\rho}_v, \boldsymbol{\rho}(x_i)) = E(\boldsymbol{\rho}_v \boldsymbol{\rho}(x_i)) - E(\boldsymbol{\rho}_v)E(\boldsymbol{\rho}(x_i)) \\
&= E(\frac{1}{|v|} \sum_{j|x_j \in v} \boldsymbol{\rho}(x_j)\boldsymbol{\rho}(x_i)) - E(\frac{1}{|v|} \sum_{j|x_j \in v} \boldsymbol{\rho}(x_j))E(\boldsymbol{\rho}(x_i)) \\
&= \frac{1}{|v|} \sum_{j|x_j \in v} \{E(\boldsymbol{\rho}(x_i)\boldsymbol{\rho}(x_j)) - E(\boldsymbol{\rho}(x_i))E(\boldsymbol{\rho}(x_j))\} \\
&= \frac{1}{|v|} \sum_{j|x_j \in v} Cov(\boldsymbol{\rho}(x_i), \boldsymbol{\rho}(x_j)) = \frac{1}{|v|} \sum_{j|x_j \in v} \boldsymbol{C}_{i,j}.
\end{aligned} \tag{B.4}$$

Therefore, for block kriging and estimating the density value of block v, the following matrix system should be solved :

$$\begin{bmatrix} \boldsymbol{C}_{1,1} & \boldsymbol{C}_{1,2} & \cdots & \boldsymbol{C}_{1,s} \\ \boldsymbol{C}_{2,1} & \boldsymbol{C}_{2,2} & \cdots & \boldsymbol{C}_{2,s} \\ \vdots & \vdots & \ddots & \vdots \\ \boldsymbol{C}_{s,1} & \boldsymbol{C}_{s,2} & \cdots & \boldsymbol{C}_{s,s} \end{bmatrix} \begin{bmatrix} \hat{\boldsymbol{\lambda}}_1 \\ \hat{\boldsymbol{\lambda}}_2 \\ \vdots \\ \hat{\boldsymbol{\lambda}}_s \end{bmatrix} = \begin{bmatrix} \hat{\boldsymbol{C}}_{1,v} \\ \hat{\boldsymbol{C}}_{2,v} \\ \vdots \\ \hat{\boldsymbol{C}}_{s,v} \end{bmatrix}. \tag{B.5}$$

The mean value of density at block v is

$$\boldsymbol{\rho}_v = \sum_{i=1}^{s} \hat{\boldsymbol{\lambda}}_i \boldsymbol{\rho}(x_i). \tag{B.6}$$

The block kriging variance is given by

$$\boldsymbol{\sigma}_{bk}^2 = \hat{\boldsymbol{C}}_{v,v} - \sum_{i=1}^{s} \hat{\boldsymbol{\lambda}}_i \hat{\boldsymbol{C}}_{i,v} \tag{B.7}$$

where $\hat{\boldsymbol{C}}_{v,v}$ is the average covariance between pairs of points in block v :

$$\hat{\boldsymbol{C}}_{v,v} = \frac{1}{|v|^2} \sum_{i|x_i \in v} \sum_{j|x_j \in v} \boldsymbol{C}_{i,j}. \tag{B.8}$$

In block kriging, in order to estimate the mean density value of a block, we only need to solve one kriging system. The calculation of the point to block covariances involves slightly more computation than the calculation of the point to point covariances.